SIZE-BY-SIZE OPTIMIZATION OF DRY GRAVITY SEPARATION USING A 3-INCH KNELSON CONCENTARTOR

Meng Zhou

Department of Mining and Materials Engineering

McGill University

Montreal, Quebec, Canada

April, 2016

A Thesis Submitted to the Faculty of Graduate studies and Research in Partial Fulfilment of the Requirements for the Degree of Master of Engineering

ABSTRACT

Enhanced gravity, or centrifugal, separators have revolutionised gold processing over the past decades, significantly increasing the recovery of fine (-106 µm) free gold. The Knelson Concentrator, one of the most commonly used centrifugal concentrators, has become the predominant unit for primary gold recovery by gravity. However, its application potential does have limitations. One of the main drawbacks of the Knelson Concentrator is the large volume of water required. With water becoming an ever increasingly important "commodity", reducing the usage of water is of great importance, both from an environmental and a financial point of view.

A modified laboratory scale 7.5 cm Knelson Concentrator was used to investigate the potential of dry gravity separation, with air used to replace the water as the fluidising medium. A methodology based on the use of a synthetic feed (mixture of tungsten and quartz to mimic a gold ore) was designed to study the performance of the dry Knelson. The Response Surface Method and Central Composite Design techniques were used to design the experiments and to model the results, with the experimental variables being the motor power (related to increase gravitational acceleration), air fluidising pressure and the solids feed rate.

Size-by-size analysis was conducted, with the concentrate grade and recovery of tungsten from silica determined. Results indicate that motor power and air fluidising pressure are the two most important factors affecting the grade and recovery. For all feed sizes studied, when the feed is fine, a higher motor power was needed to achieve a maximum recovery. The maximum tungsten recovery drops significantly when the feed size is <53 µm compared to the coarse sizes.

The mono size fractions studied could be separated into three size fractions. -425+300 µm, -300+212 µm and -212+150 µm are consider as one mono coarse size fraction; -150+106 µm, -106+75 µm and -75+53 µm are consider as one mono middle size fraction; and -53 µm is considered to be the fine size fraction. The optimized values for the concentration with the highest recovery of motor power, solid feed rate and air fluidizing pressure are 30%, 200 g/min and 10 psi, respectively for coarse size fraction; for middle size fraction, the optimized values for the concentration with the highest recovery of motor power, solid feed rate and air fluidizing pressure are 50%, 160 g/min and 11 psi; for fine size fraction, the optimized values for the concentration with the highest recovery of motor power, solid feed rate and air fluidizing pressure are 65%, 200 g/min and 11 psi.

RÉSUMÉ

Les séparateurs a gravité améliorer, ou centrifuge, ont révolutionné le traitement de l'or au cours des dernières décades, augmentant significativement la récupération de l'or natif fin (-106 μm). Le concentrateur Knelson, un des concentrateurs centrifuges les plus couramment utilisé, est devenu l'unité prédominante pour la récupération de l'or primaire par gravité. Cependant, son potentiel d'application a des limites. L'un des principaux inconvénients du concentrateur Knelson est le grand volume d'eau requis. Tandis que l'eau est transformée d'une «marchandise» toujours plus importante, la réduction de la consommation d'eau est d'une grande importance, à partir d'environnement et d'un point de vue financier.

Un concentrateur Knelson modifiée à l'échelle du laboratoire 7.5 cm a été utilisé pour étudier le potentiel de séparation par gravité à sec, avec de l'utilisation d'air pour remplacer l'eau comme moyen de fluidification. Une méthode basée d'une charge synthétique (mélange de tungstène et de quartz pour imiter un minerai d'or) a été conçu pour étudier les performances de la Knelson sec. La méthode Réponse de la méthode de Surface et les Techniques de conception Composite centrale ont été utilisés pour concevoir les expériences et de modéliser les résultats, avec les variables expérimentales étant la puissance du moteur (liés à augmenter l'accélération gravitationnelle), la pression de l'air de fluidification et le taux d'alimentation de solides.

L'analyse de taille par taille a été réalisée, avec le teneur de concentré et le rendement du tungstène à partir de silice déterminée. Les résultats indiquent que la puissance du moteur et la pression de fluidisation d'air sont les deux facteurs les plus importants qui affectent la qualité et la récupération. Pour toutes les tailles d'alimentation étudiée, lorsque la charge est de granulométrie fine, une puissance motrice supérieure était nécessaire pour parvenir à un rendement maximal. La récupération de tungstène maximale diminue considérablement lorsque la taille de charge est < 53 μm par rapport à la taille grossière.

Les fractions de taille de mono étudiés peuvent être séparées en trois fractions granulométriques. -425+300 μm, -300+212 μm et -212+150 μm sont considèrent comme une fraction mono grossière de la taille; -150+106 μm, -106+75 μm et -75+53 μm sont considèrent comme une fraction mono de taille moyenne; et -53 μm est considérée comme la fraction granulométrie fine. Les valeurs optimisées pour enrichissement avec la plus grande récupération de la puissance du

moteur, taux d'alimentation solide et la pression d’air de fluidisation sont de 30%, 200 g/min et 10 psi, respectivement pour la fraction de la taille grossière; pour la fraction de taille moyenne, les valeurs optimisées pour la enrichissement avec la plus grande récupération de la puissance du moteur, taux d'alimentation solide et la pression d’air de fluidisation sont de 50%, 160 g/min et 11 psi; pour la fraction granulométrique fine, les valeurs optimisées pour la enrichissement avec la plus grande récupération de la puissance du moteur, taux d'alimentation solide et la pression d’air de fluidisation sont de 65%, 200 g/min et 11 psi.

ACKNOWLEGEMENTS

I would like to offer my sincerest thanks to my supervisor, Professor and Dr. Kristian E. Waters, for his intelligence and wisdom. His high scientific standards and excellent advice never failed to bring out the best in me and my research. I am also grateful to him for his trust.

I want to thank Dr. Kökkılıç Ozan, for his erudite knowledge in centrifugal separation and design of experiment, patient direction in my research work, as well as his wise advice and kind help while writing the thesis and publications. A special thanks to Mr. Raymond Langlois for his effective help in offering me all the training of the relative experimental equipment and his kind help for the research.

I appreciate the full understanding and support from my family members, as well as my girlfriend. Thanks to all of my other colleagues from Mineral Processing Group, for their friendly help and cooperation during my stay at McGill University.

This research would not have been completed without the financial support from Natural Science and Engineering Research Council of Canada (NSERC) in conjunction with: SGS Canada Inc.; Shell Canada; Barrick Gold Corp; COREM; Teck Resources Ltd.; Vale Base Metals; CheMIQA; and XPS Consulting and Technical Services, a Glencore company.

Table of Contents

List of Figures

List of Tables

CHAPTER 1: INTRODUCTION

Mineral processing, also known as ore dressing, ore beneficiation, mineral dressing, or milling, follows mining and prepares the ore for extraction of the valuable metal in the case of metallic ores, or to produce a commercial end product as in the case of minerals such as potash (soluble salts of potassium) and coal (Finch and Wills, 2015). The twentieth century saw the development of mineral processing as an important profession in its own right, and certainly without it the concentration of many ores, and particularly the metalliferous ores, would be hopelessly uneconomic (Wills and Atkinson, 1991).

Gravity concentration is the separation of minerals based upon the difference in density. Techniques of gravity concentration have been around for millennia. In recent years, mining companies have renewed interest in gravity systems due to increasing costs of flotation reagents, the relative simplicity of gravity processes, and the fact that they produce comparatively little environmental impact. Gravity concentration remain the main concentrating methods for iron and tungsten ores and are used extensively for treating tin ores, coal, gold, beach sands, and many industrial minerals.

1.1. Knelson Concentrator

The Knelson concentrator, one of the most common enhanced gravity separators, is essentially a vertical axis bowl-type centrifugal concentrator that uses a fluidized bed to concentrate the fine size material. The bowl consists of a conical inner shell, with a series of riffles, attached to a rotating outer shell. Feed material, most commonly cyclone underflow or ball mill discharge, is introduced through a central tube as slurry into the rapidly rotating bowl, which generates an artificially enhanced gravity field. This produces a significantly increased sedimentation velocity differential, so enhanced gravity separators can process fine particles with high separation efficiency. A theoretical centrifugal acceleration of around 60-100 G causes the feed solids to fill the inter-riffle spaces from bottom to top. Once the riffles are full of solids, the sorting stage starts, where heavy/dense material displaces the light material and as a result the heavy minerals are trapped in the inter-riffle spaces to become the concentrate while the lighter minerals are carried by water to the top of the unit as tailings. The sorting is achieved by the fluidization of the bed in the riffle, allowing for the substitution of dense particles for those of a lower density. The fluidization is by water injected through holes in the riffles. This fluidization water must be strong enough to inhibit severe compaction of the heavy mineral bed due to the strong centrifugal force (Knelson and Edwards, 1990, Knelson, 1992, Laplante, 1993, Luttrell *et al*., 1995, Laplante *et al*., 1999).

Even though Knelson Concentrators have achieved a quality product with high recovery and good separation efficiency, they still have some disadvantages. One of the drawbacks of these separators as they currently operate is the volume of water required. At a laboratory scale, processing 24 kg of ore can consume approximately 300 litres of water (Laplante *et al*., 1995a,b). This is becoming a serious problem globally due to water scarcity, in areas such as Australia, Chile, and China. Secondly, because of the very fine suspended particles in the water, wet beneficiation processes require waste water treatment and water recovery processes such as filters, centrifuges and thickeners, which will increase the capital costs and the operating costs. Dry processes avoid the problems associated with treatment and storage of process waste water (Dwari and Rao, 2007, Sahu *et al*., 2009, MacPherson and Galvin, 2010, Firdaus *et al*., 2012, Oshitani *et al*., 2010, 2011, 2013a,b, Yang *et al*., 2013, Wang *et al*., 2013). With environmental costs becoming more apparent, and the lack of water becoming a critical issue in mining areas with drought due to global warming, efforts to reduce the water usage are important (MacPherson and Galvin, 2010, MacPherson *et al*., 2010, 2011, Oshitani *et al*., 2010, 2011, 2013a,b, Greenwood *et al*., 2013, Kökkılıç *et al*., 2015).

1.2. Objectives of the Study

In this research work, a series of experiments and statistical analyses of the performance of dry processing using a laboratory scale Knelson Concentrator were conducted. The research work was designed to:

a. Investigate the potential use of the Knelson Concentrator as a dry method of gravity concentration

b. Determine the optimum operating conditions for a synthetic ore (mimicking a gold ore) size-by-size

c. Modelling and optimization of the dry Knelson process size-by-size

1.3. Structure of the Thesis

This thesis consists of four chapters.

Chapter 1 introduces briefly the background, objectives of the research project and then the structures of the thesis.

Chapter 2 reviews the history of the gravity concentration; the prior application and research on gravity concentrators, including the Knelson Concentrator, and the experimental design that will be used for thesis experiments.

Chapter 3 shows the experimental materials and set-up for a series of dry Knelson tests on synthetic ores, as well as the methodology.

Chapter 4 presents the results and the statistical analysis of the dry Knelson process size-by-size.

In Chapter 5, conclusions based on the thesis experiments are drawn.

CHAPTER 2: LITERATURE REVIEW

2.1. Development and application of gravity concentration

2.1.1. History of gravity concentration

Gravity concentration, which can be defined as the separation of minerals by methods utilizing differences between their specific gravities or densities, has a long history. Records show that ancient Chinese, Egyptian and Greek civilizations used this method to recover gold, silver, tin, and copper to provide arms and finance (Turner, 1991). The basis of the ancients' technology was the sluice, which has remained as an important means of separating minerals to the present day.

The earliest methods of gravity concentration were developed to deal with easily processed alluvial and fluvial mineral deposits using human labour and flowing water as the energy sources needed to facilitate a separation. The ores were fed into a trench or natural channel, then a stream or part of the flow of a river was redirected to wash over the bed of minerals removing the lighter particles and leaving the heavy particles trapped. The heavy particles were then hand panned to upgrade the heavy mineral concentrate.

Some ores from outcrops or underground operations were selectively mined and then handpicked before being processed in sluices. Large numbers of workers were required for these processes, with few changes in the following centuries. Ores were still broken by hand, and the sluice remained the dominant methods of concentration.

In the fifteenth century, Europe renewed interest in the waterwheel that had first been utilized in ancient China. Figure 2.1 shows the application of waterwheel driving a mine hoist, taken from "De Re Metallica" written by Agricola. This book illustrated all aspects of mining from exploration to finished product. It was the definitive work of the Medieval age, and maintained this position of excellence until the industrial revolution in the eighteenth century.

The mining industry was transformed by the invention of the steam engine in late eighteenth century. Steam driven pumps made it possible to dewater deeper mines and steam hoists enabled the ore to be hoisted to surface rapidly; steam driven stamps made it possible to crush hard ores.

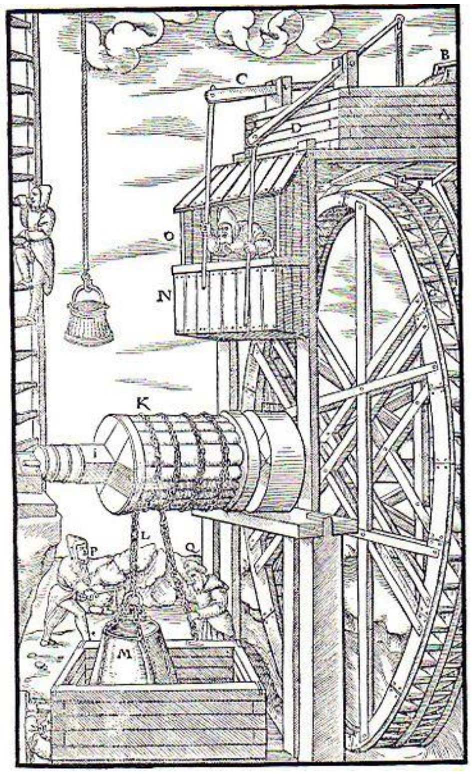

Figure 2.1 Waterwheel powering a mine hoist in De re Metallica (Agricola, 1556)

Gravity concentration declined in importance in the first half of the twentieth century due to the development of the froth-flotation process, which allows for the selective treatment of low-grade complex ores. However, gravity concentration remained the main concentrating methods for a number of ores, including iron, coal, tin and tungsten (Turner 1991).

In recent years, industry's renewed interest in gravity systems is in part due to the increasing costs of flotation reagent and environmental concerns. Modern gravity techniques have been developed including centrifugal concentration and dry gravity concentration. These methods have been proven efficient for recovering the fine particles with several advantages compared to the conventional gravity concentration.

2.1.2. Single G force gravity concentrators

Gravity concentration is widely used due to several advantages such as low capital and operating costs, high efficiency and with the lack of chemicals and excessive heating requirements which means it is environment-friendly. Gravity concentration is utilized in different modern forms such as pinched sluices, jigs, spirals and shaking tables. It is widely used for the coal mine, alluvial tin, iron, lead/zinc, gold, platinum, diamonds, barite and tungsten ores.

Jigging is one of the older gravity concentration methods which have been in use for over a century. The basic principle of a conventional jig is illustrated in Figure 2.2. An open tank filled with water, a thick bed of coarse and heavy particles (ragging) resting on a jig screen. The bed is fluidized with the pulsated water up and down by plunger. The feed material enters at the top, moving across the ragging. The heavy particles go through the screen and settle down as the concentrate and the light particles go to the tailings with the water flow. The concentrate is removed from the bottom (Haldar, 2013).

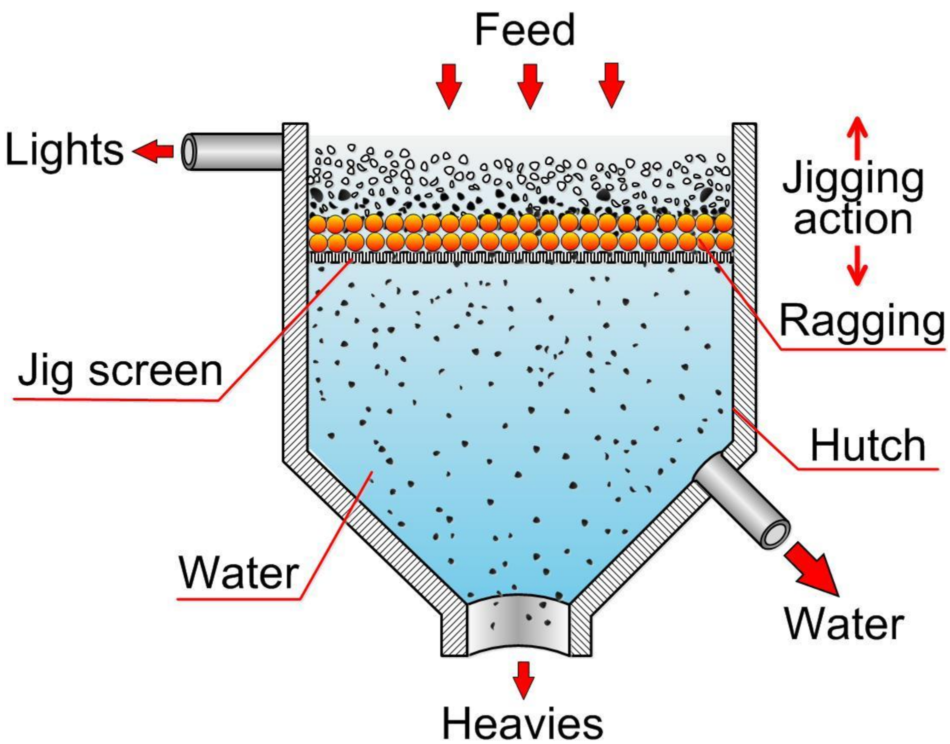

Figure 2.2 Basic construction of Jig concentrator (Wills and Finch, 2016)

The pinched sluice is a 60-90 cm long inclined slope made of wood, aluminum, steel or fiberglass. The channel is about 25 cm wide at the start of feeding part and 3 cm wide at the discharge end. A slurry contains particles of different densities flows over the channel. The feed enters the sluice as the particles flow through the sluice. The gravitational and frictional force were imparted on the particles. The materials squeeze into the narrow discharge area (pinching), dilation of the bed occurs due to the pinching with heavier particle migrating to the bottom and lighter particles to the top. Near the end of the sluice, the minerals are separated by a splitter as shown in Figure 2.3 (Haldar, 2013).

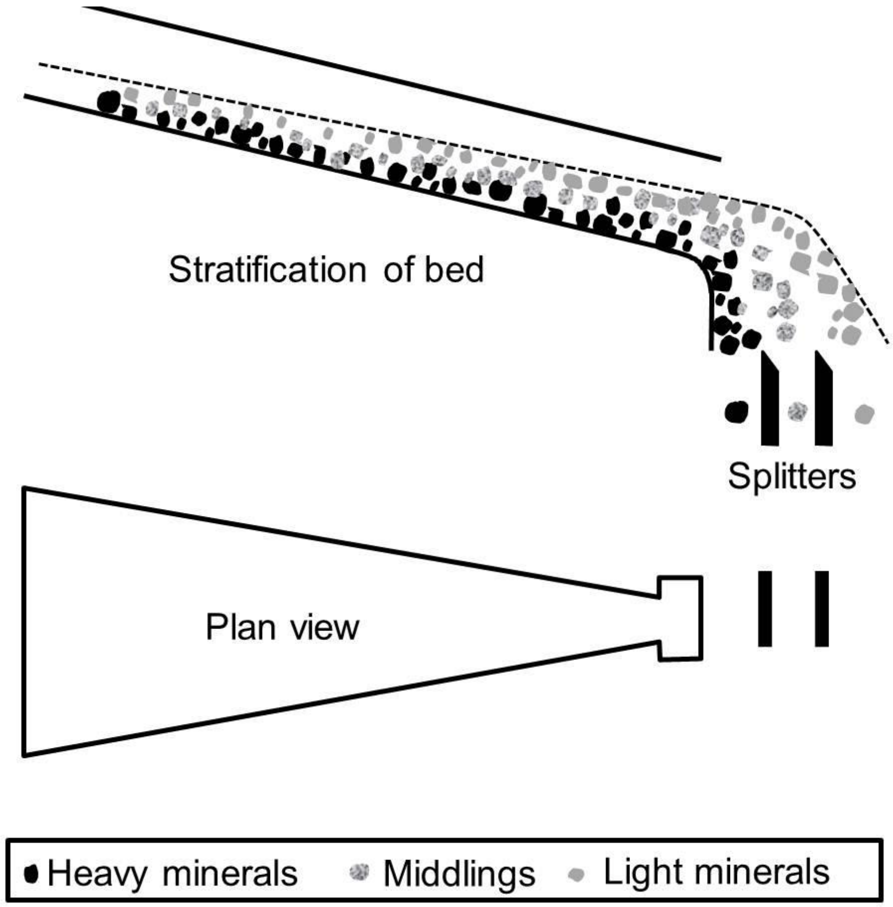

Figure 2.3 Diagram illustrates the basic principle of a pinched sluice concentrator (Wills and Finch, 2016)

The spiral as shown in Figure 2.5, an inclined trough wrapped around a central column, is a modern high-capacity and low-cost gravity concentration device. It works on the basis of gravitational forces imparted on particles of different densities. Spirals may have a wash water channel and a series of concentrate removal ports placed at regular intervals along the spiral. Separation is achieved by stratification of material caused by a complex combined effect of centrifugal acceleration, differential settling and heavy particle migration through the bed to the inner part of the conduit as shown in Figure 2.4. The most extensive application is treatment of heavy mineral beach sand consisting of minerals such as monazite, ilmenite, rutile, zircon and garnet. It is also widely used to upgrade chromite concentrates (Tripathy and Murthy, 2012 and

Haldar, 2013). The early spiral models were used before the development of trays and cones. These models were usually made of cast iron or cast cement and required wash water. Light-weight materials such as fiberglass and polyurethane were introduced while through profiles and concentrate cutters were modified. Wash water has been eliminated in most applications with the improvements in trough profiles in the early 1980s. Significant increases in both feed capacity and separation efficiency have been realized.

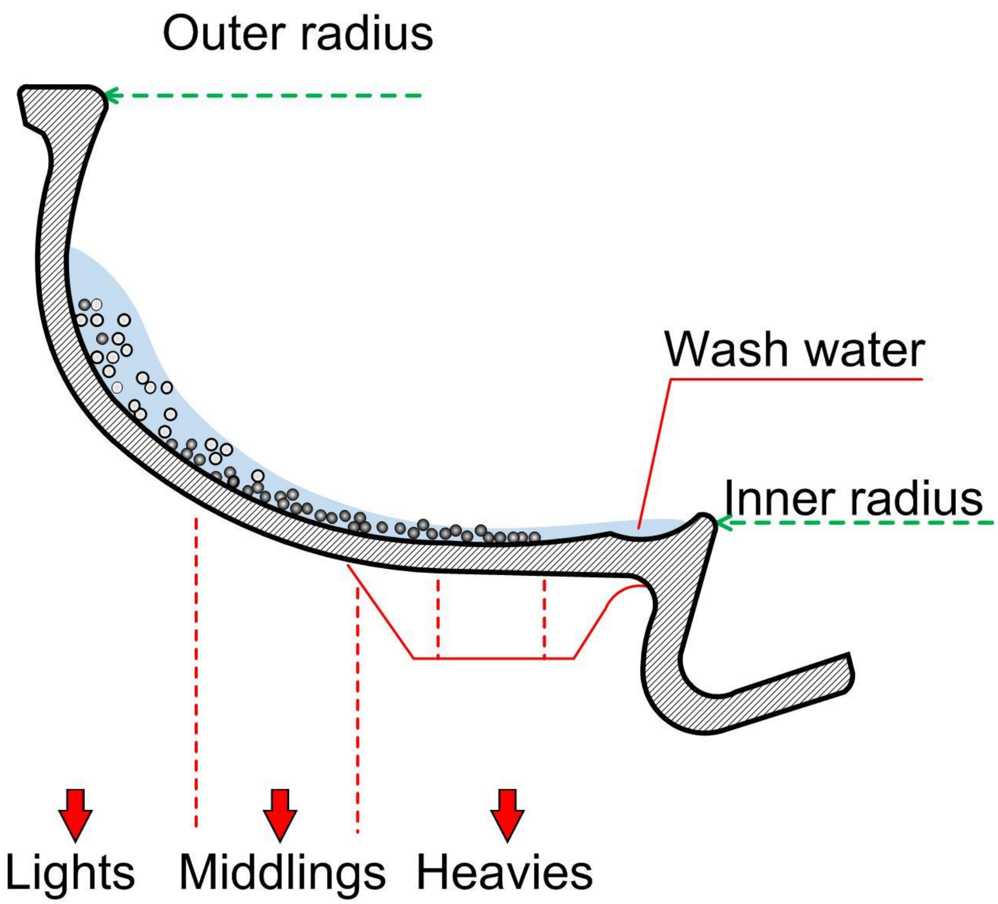

Figure 2.4 Cross section of spiral stream (Wills and Finch, 2016)

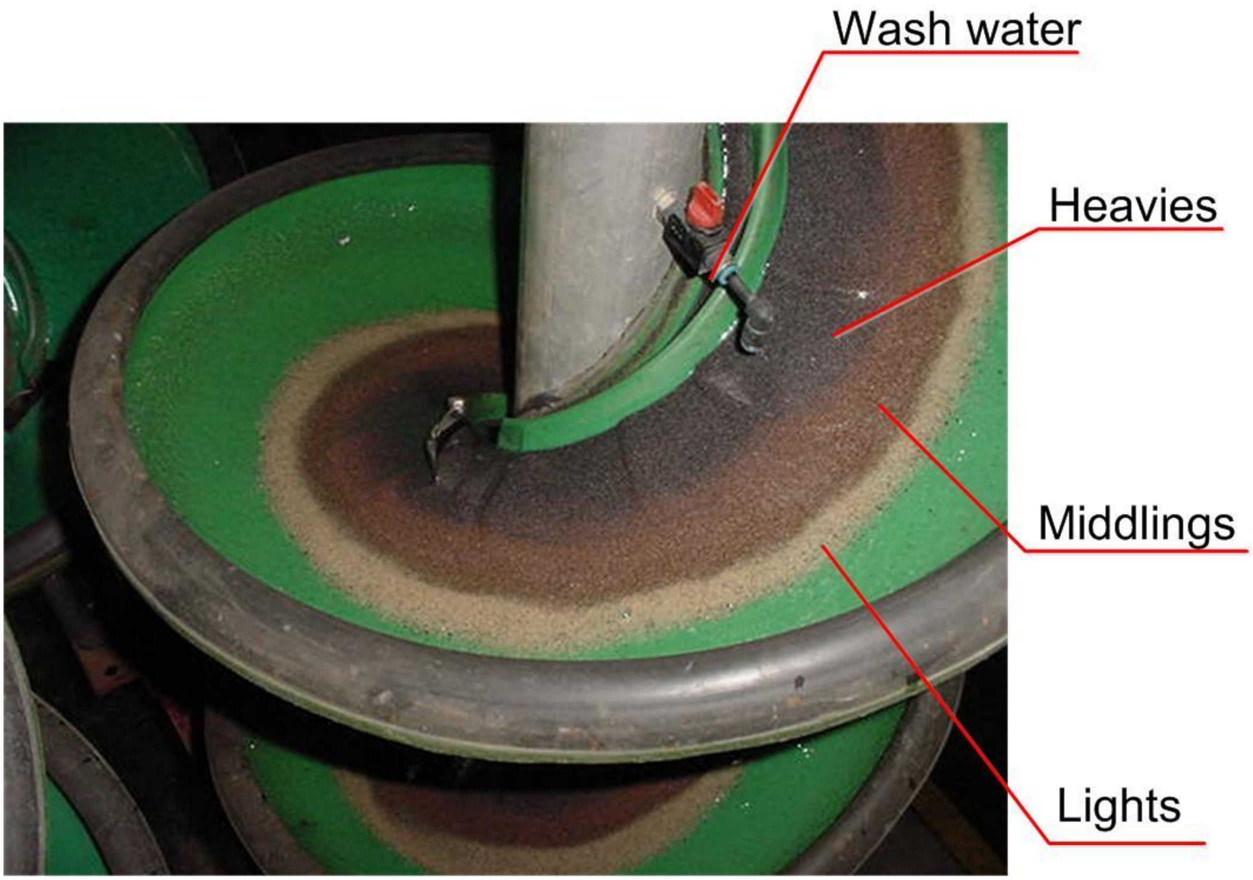

Figure 2.5 Example of stratification across a spiral trough (Wills and Finch, 2016)

Shaking tables (Figure 2.6) are another form of gravity separator that have been in use for a long time, consisting of a sloping deck or multi-deck with a rifled surface. Shaking tables are often used for cleaning due to the low capacity. For a shaking table, the principle of separation is the motion of particles according to specific gravity and size moving in a slurry across an inclined table. The table oscillates backwards and forwards essentially at right angles to the slope. The riffles hold back the particles that are closest to the deck. This motion and configuration cause the fine high specific gravity particles to migrate closest to the deck. They are carried along by the riffles to be discharged uppermost from the table. The low specific gravity coarser particles move or remain closer to the surface of the slurry and ride over the riffles, discharging over the lowest edge of the table (Haldar, 2013).

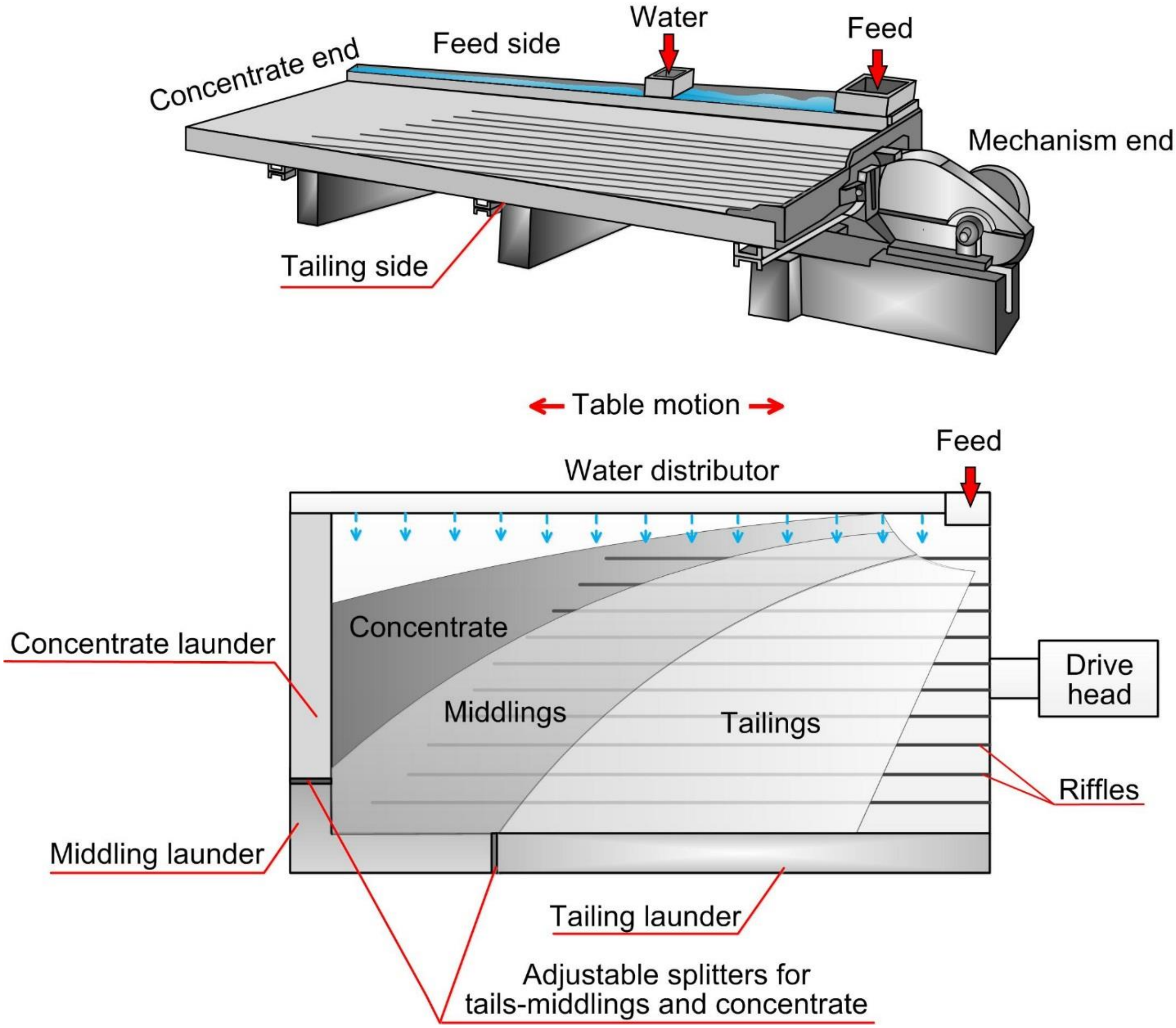

Figure 2.6 Diagram of shaking table (Wills and Finch, 2016)

Gravity concentration has been used for the beneficiation of minerals for centuries. But there is little change in the methods used from 500 B.C. to 1550 A.D. Some of these methods, such as the sluice and the hand pan, are still used to this day. The discovery and utilization of new sources of energy, first water power, then steam and finally electricity has led to improvements in the methods.

Gravity concentrators listed above are very efficient when the mineral particles are well liberated and of large sizes. Both efficiency and throughput fall rapidly with decreases in particle size. Gravity concentrators above still have a limitation of not being able to recover the fine gravity recoverable gold (less than 100 µm) or gold associated with sulphides. These limitations resulted in the development of alternative technologies, such as flotation, CIP processing and heap leaching. However, the use of chemical reagents cause environmental hazards and increase the capital and operating costs intensively (Turner, 1991, Luttrell *et al*., 1995, Laplante and Spiller, 2002, Falconer, 2003, Oruç *et al*., 2010, El-Midany and Ibrahim, 2011). There has been a continuous search with centuries' efforts to find new methods for the recovery of fine particles.

2.1.3. Centrifugal gravity concentrators

The application of an increased centrifugal acceleration has made it possible to separate fine particles. The early centrifugal technology can be described as the idea of using centrifugal acceleration to lift liquids. The first centrifugal device known in the history of mineral processing was a centrifugal pump which operated in a copper mine in Portugal in the fifth century (Lazarkiewicz, 1965).

The advantage of centrifugal separators lies in the fact that the settling velocity, which with gravitational separators for fine particles revolves from 10^{-9} – 10^{-4} m/s, increases 500–30,000 times (Axelsson and Madsen, 2008). The increased settling velocity reduces the particle settling time, in the rotor of separator, which results in smaller separator dimensions, at the same capacity, in comparison with conventional gravitational separators.

The Hendy concentrator was one of the earliest forms of centrifugal concentrators employed in California, patented in 1868 (Rose, 1898; Louis, 1894). It consisted of shallow cast-iron pan, 1.2 m or 1.8m in diameter, supported by a vertical shaft in the centre, rotated by bevel gear. The pulp was fed into the pan near the periphery; the heavy particles were driven outwards by centrifugal force as a consequence of a rapid oscillating motion given by the revolution of a craft shaft. The light particles were discharged into the circular basin and were removed by opening discharge gates at intervals.

The Ainlay bowl (Taggart, 1945), which had been used to a limited extent on doodlebugs and small placer operations before 1945, was an embryonic form of some contemporary advanced centrifugal concentrators. This device was a vertical bowl-shaped basin, 30 to 90 cm diameter at the rim, rubber-riffled on the inner surface. The peripheral speed at the bowl rim could be up to about 300 m/min. The slurry was fed into the bowl. The material moved around upward toward the bowl periphery under the influence of centrifugal force; gold was caught between the riffles and the overlying lighter sand passed on upward and over the rim. The gold concentrate was washed out of the bowl at intervals by shutting off feed.

With the rapid development of technology, many new centrifugal concentrators have been developed. The advent of new materials and electronic technology made it possible centrifugal concentrators with features such as high centrifugal acceleration and capacity allied with high efficiency. As a result, centrifugal concentration has been increasingly used for the processing of various materials, in particular ores, and resulted in renewed interest in this field. The centrifuges are already used or potentially suitable for a variety of industrial applications. Several modern centrifugal concentrator are presented below.

The Kelsey jig is the best-known centrifugal jig based on the principle similar to the conventional jig. They are operated at a much higher centrifugal “G” force, which allows the separation of fine (several micrometre in diameter) and more similar specific gravity particles. The Kelsey jig is a Harz jig placed vertically in a centrifugal field. It has a number of concentrate hutches and incorporates a side pulsing mechanism, rotated by a spin drive (Beniuk *et al*., 1994).

The Kelsey centrifugal jig is fed down a fixed central pipe, and the feed slurry is distributed at the bottom of the bowl which flows upwards over the surface of the ragging bed supported by a cylindrical screen. The screen is spun coaxially with the rotor, and pressurized water is introduced into a series of hutches behind the screen. Water is pulsed through the ragging bed which helps in stratifying the feed as well as dilating the ragging bed. Particles with specific gravity greater than or equal to the bed of the ragging material will pass through the ragging bed. The principles of the differential acceleration hindered settling and interstitial trickling hold as in conventional jigging. The differential acceleration rates are substantially enhanced by the higher apparent gravitational forces arising out of the rotation. The denser particles pass through the internal screen to underflow hutches and then through spigots to an underflow launder. The lighter particles are swept away by the rising flow and are discharged over a ragging retention ring into the overflow launder as shown in Figure 2.7.

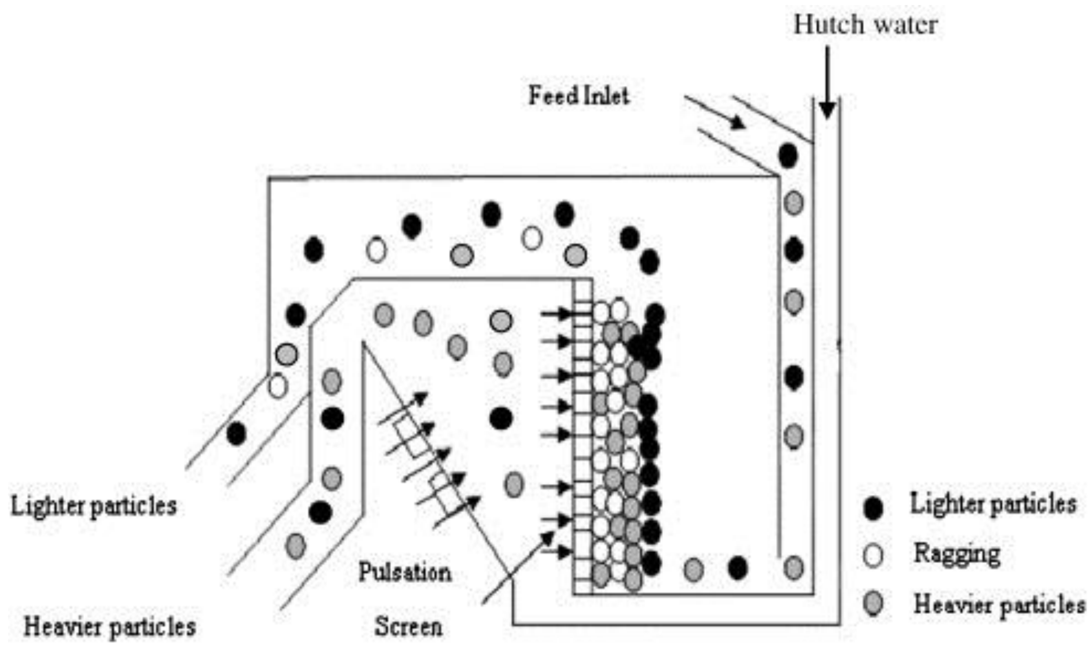

Figure 2.7 Partial cross-section of the Kelsey centrifugal jig (Singh and Das, 2013)

The centrifugal acceleration generated by the centrifugal jig can be as high as 100 times that of Earth's natural gravity (Brewis, 1995), resulting in increased particles separation efficiency, especially for fine sizes below 40 µm. Another advantage of this unit is its ability for continuous operation since both concentrate and tailing are continuous discharged. The Kelsey jig is widely used to recover minerals such as fine cassiterite, tantalite, hematite and tungsten (Brewis, 1995; Wyslouzil, 1990 and Tucker, 1995).

The Falcon concentrator is a vertical axis fluidized bed enhanced gravity concentrator, which separates minerals by density. It is a new type of centrifuge without the addition of counter flow water and operating at a very high speed, allowing the centrifugal force employed on a particle up to 300 G's. It is a widely used for concentrating various minerals including coal, gold and celestite (Lins *et al*., 1992; Honaker *et al*., 1996; Oruç *et al*., 2010 and El-Midany and Ibrahim, 2011).

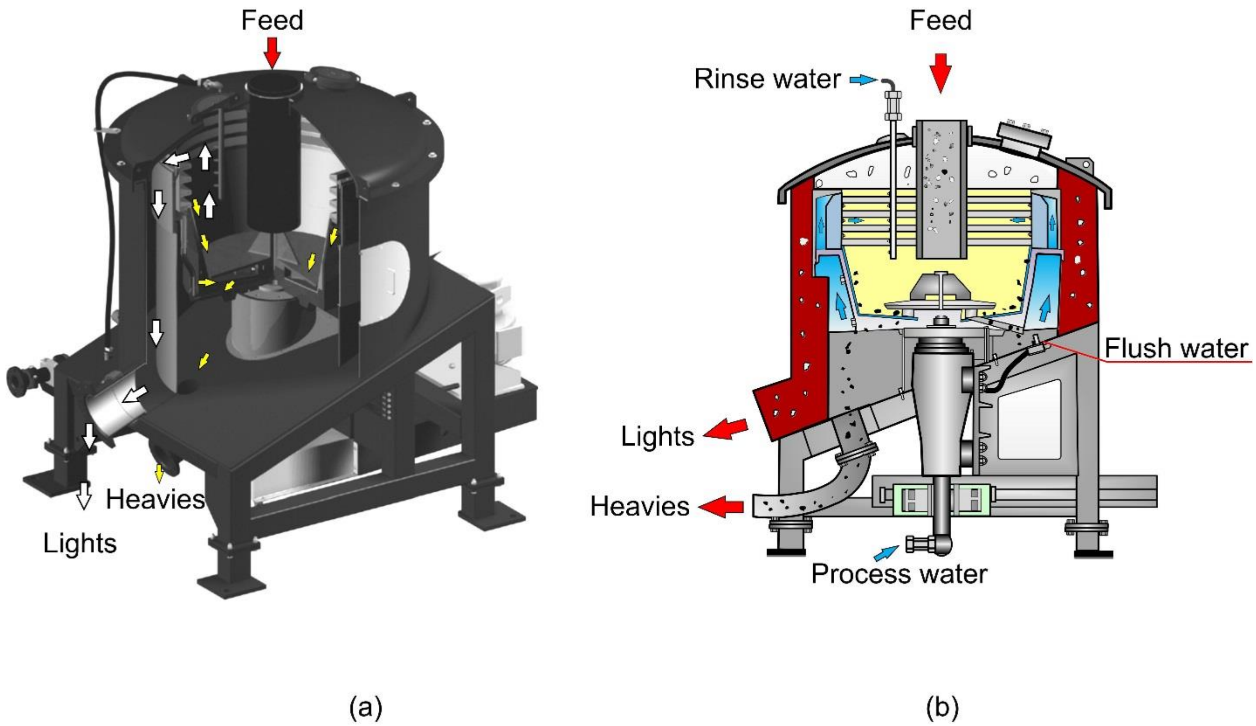

Figure 2.8 Falcon SB Concentrator: (a) cutaway view and (b) flow of feed and products (Wills and Finch, 2016)

Figure 2.8 shows the working principle of the Falcon SB concentrator. Feed material as a slurry enters the base of high-speed rotating rotor bowl through a central feed pipe. The impeller at the very base of the rotor evenly distributes the slurry to the internal wall and provides an initial acceleration. The centrifugal force can be up to 300 G's. The heavy particles settle rapidly on the lower wall of the rotor, and most of them migrate into the riffles. The concentrate is fluidized and cleaned by back-injection water. Lighter particles are washed out of the bowl due to their lower specific gravity or small size. When a concentration cycle is done, and the centrifuge and injection water are shut down, the concentrate is flushed into the concentrate launder. In the case of laboratory tests, the concentrate inside the bowl is rinsed into a pan after removing the rotor bowl.

There are three models of Falcon concentrators provided by Sepro Mineral Systems. Each concentrator has a specialized purpose dependent on the mining application and stage of recovery. All models rely on a high-speed rotating bowl to create high gravitational force. Falcon C Models are typically used in mineral recovery applications that require a higher mass yield to mineral concentrate when compared with Falcon SB Gravity Concentrators. SB Models are

"Semi-Batch" Gravity Concentrators as they continually accept feed during the run cycle and produce mineral concentrate during periodic rinse cycles. UF model gravity concentrators are known as "Ultrafine" concentrators because they are used as an effective way to economically recover and upgrade particles as fine as three microns. Ultrafine mineral recovery has been a mining industry goal for many years (Kroll-Rabotin *et al*., 2010).

Multi-gravity separator (MGS) is very promising for processing fine particles as a gravity based separator. It achieves very fine mineral separation based on a combination of conventional shaking table and the centrifuge.

Figure 2.9 shows the schematic diagram of the MGS reported by Finch and Wills (2016). The MGS is based on the combined effects of centrifugal acceleration and forces acting on a conventional table. MGS may be considered as a cylindrical version of a conventional shaking table. Separation of different density particles occurs inside the drum surface. A shaking to-and-fro motion (in the direction of material flow) similar to the motion in a conventional shaking table is imparted to the drum. The amplitude and shake frequency of the drum motion are adjusted according to the size of the material to be processed. In general, for coarser size feeds, higher amplitudes are needed, and for finer size feeds higher frequency results in good separation. The settled bed of heavy particles is continuously scraped into the concentrate launder (positioned at the feed end) with the help of a spiral scraping assembly. Efficient rejection of entrapped lighter material from the heavies takes place with the wash water added on the stratified bed near the heavies' discharge end. The washed lighter material reports continuously through the tailing launder positioned opposite to the feed end. Due to several chances of bed dilation and contraction before the heavies' discharge, which is being caused by the cyclic process of scraping and water washing. The concentration in MGS occurs mostly based on relative densities of particles.

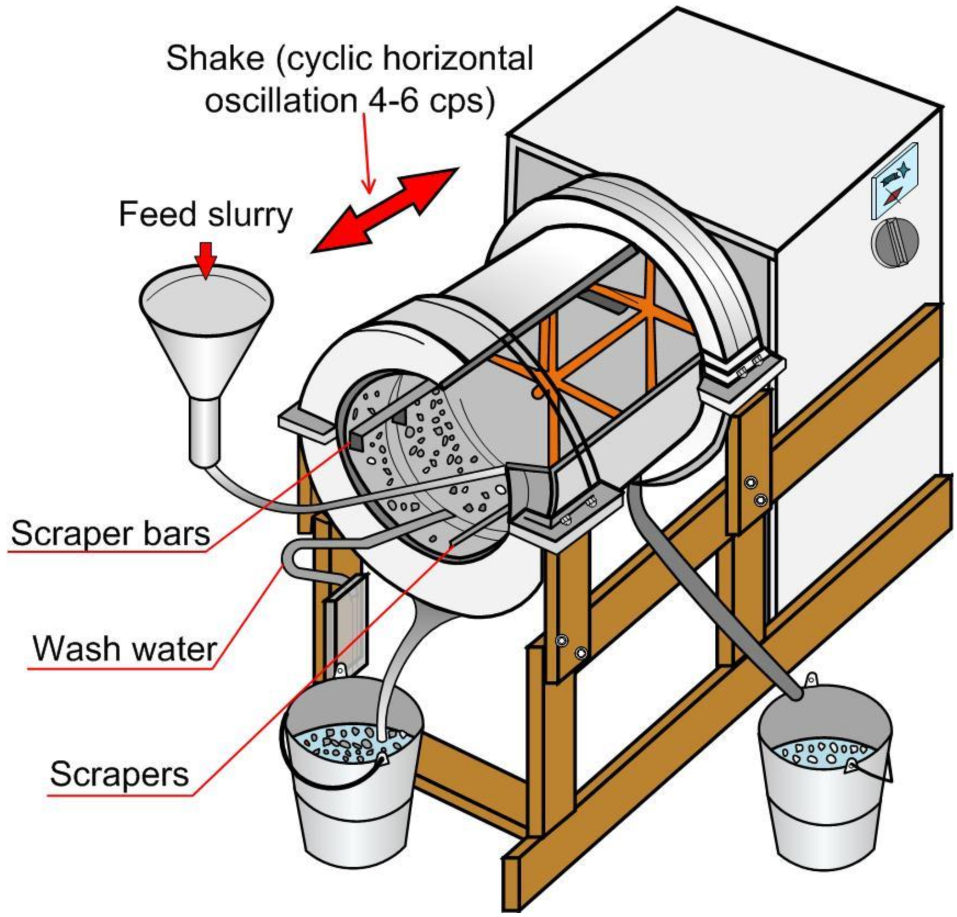

Figure 2.9 Schematic diagram of the MGS (Wills and Finch, 2016)

The MGS has been proven to be a very effective gravity concentrator for recovering fine minerals. Chan *et al*. (1991) conducted gravity tests with a plant scale MGS to treat fine cassiterite, chromite, celestite and magnetite. The performance was compared with conventional devices such as shaking table and spiral. The results showed that the MGS could achieve better recoveries in treatment of very fine materials. Traore *et al*. (1995) used a synthetic ore made up of ferrosilicon and quartz and a natural tungsten ore to carry out a comparative performance study between the MGS and a fine table. They pointed out that the MGS appeared to obtain better results than the fine table, particularly for particles below 20 µm. Burt *et al*. (1995) reported that the Mozley MGS was superior in treatment of tantalum slimes with a size typically 45% below 12 microns. In addition, research work showed that the MGS could reject some 75-85% of the pyritic sulphur from seam coal (Brewis, 1995).

The Knelson concentrator is one of the most common enhanced centrifugal concentrators. In 1978, the first prototype of Knelson concentrator was patented by Byron Knelson in Canada as an innovative centrifugal separator. The Knelson concentrator is a vertical axis bowl-type and high-speed centrifuge that employs centrifugal force on particles in a slurry against a fluidizing water flow. It has "V" shaped riffles, the diameter increases from the bottom to top as shown in Figure 2.10. Fluidizing water comes through the holes around the outside surface of each ring. The feed slurry enters through the tube and flows down to the bottom of the concentrate cone. Centrifugal force created by the high-speed rotation will drive the slurry outward to the cone wall. Solids start to fill the riffles from the very bottom. Once every ring reaches its capacity, a concentrating bed is established. Figure 2.10 also shows the cross section of the concentrate bed in a blown up ring. Fluidizing Water injected from the holes fluidizes this bed, the heavier particles displaced the lighter ones and trapped in the riffles as concentrate. This fluidization water must be strong enough to inhibit severe compaction of the heavy mineral bed due to the strong centrifugal force (Knelson and Edwards, 1990, Knelson, 1992, Laplante, 1993, Luttrell *et al*., 1995, Laplante *et al*., 1999). Lighter particles are carried out by the water flow to the top of the unit as tailings.

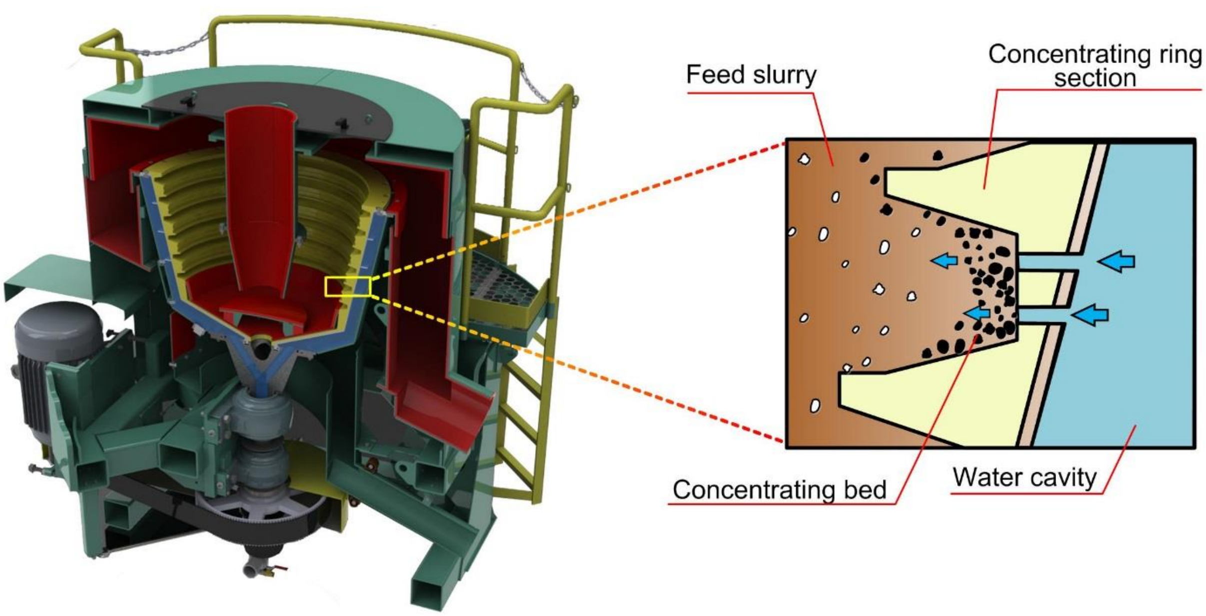

Figure 2.10 Knelson Concentrator cutaway; and cross-section of concentrate bed (Wills and Finch, 2016)

When the concentrating ends, the flush cycle is initiated, and the rotor power is shut off. The fluidizing water valve is opened for several seconds after the rotor stops completely. The water will flow into each ring to wash out the concentrates. Then concentrates flush out to the bottom of the concentrate cone and into the concentrate launder as shown in Figure 2.11.

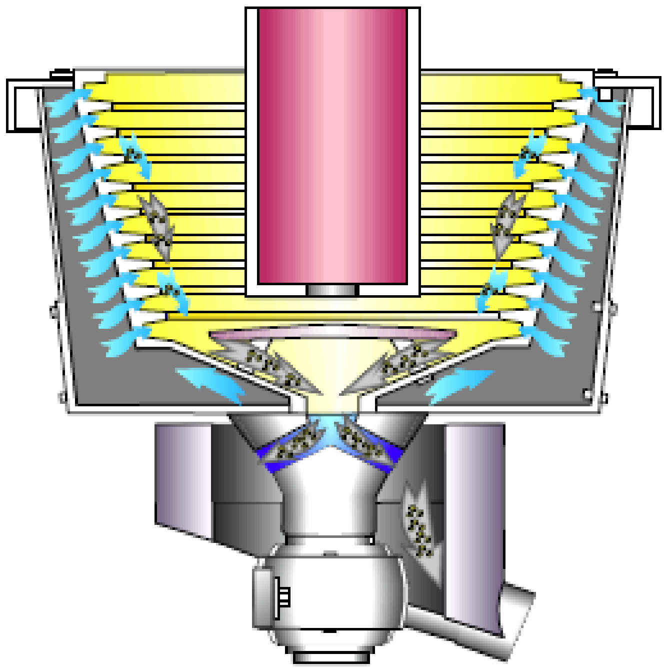

Figure 2.11 Flush circle of a Knelson concentrator (Söderlund and Johansson, 2005)

The 3” laboratory scale Knelson concentrator, shown in Figure 2.12 was developed in response to the mineral processing industry demands for a laboratory version of the Knelson batch concentrator. The gravity recoverable gold (GRG) test conducted by laboratory scale Knelson concentrator has now become the industry standard around the world (Laplante and Spiller, 2002 and Laplante and Dunne, 2002). It has also been extensively applied in the field as a reliable and accurate method of quickly reducing the volume of heavy mineral samples into very small quantities of highly enriched concentrates. These concentrates can be inexpensively transported from the field to the laboratory for further analysis.

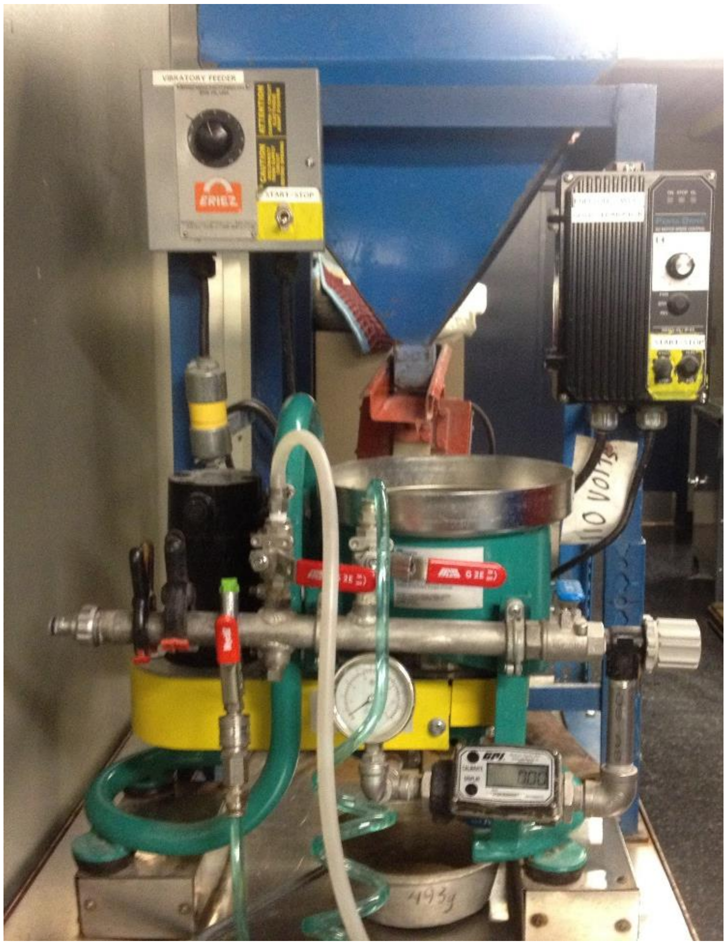

Figure 2.12 A 3" laboratory Knelson Concentrator

Even though centrifugal gravity separators have achieved a quality product with high recovery and good separation efficiency, they have some disadvantages. One of the drawbacks of these separators is they currently operate on a wet basis. A large volume of water is required during the operation. At the laboratory scale, processing 24 kg of ore can consume approximately 300 litres of water (Laplante *et al*., 1995a,b). Wet beneficiation processes require waste water treatment as the very fine suspended particles in the water. Water recovery processes such as filters, centrifuges and thickeners increase the capital costs and the operating costs.

The water supply in many remote mining locations is increasingly unreliable, such as Australia, Chile and China, the availability of water is scarce (Oshitani *et al*., 2010). Thus, there are growing pressures to minimize water consumption, and even dry processing is under consideration.

2.2. Dry gravity separation in mineral processing

During the gravity separation process, particles are separated based on the difference in density. In wet processing, the separation takes place in a water-based suspension. The water as a medium is a large factor in securing the differential movement between particles, which eventually results in separation (Dodbiba *et al*., 2002). When the medium is replaced by air, such separation is termed dry gravity separation or more commonly as air or pneumatic separation (Truscott, 1923).

In the past, dry separation has been considered to be less efficient than water based processing (Lockhart, 1984), hence this option has largely been overlooked, and therefore not developed. With the growing need to operate in dry locations, there has been renewed interest in advancing this area. Even if the separation efficiency of dry processing is lower than that obtained by wet processing, the overall economics of dry processing could still be advantageous.

Generally speaking, dry gravity separation has the attraction of low capital and operating cost that together with the lack of water, chemicals and drying requirements means it is environmentally friendly (Falconer, 2003).

Recent research has focused on the development of new mineral processing methods in order to reduce the water consumption in mineral processing. These new methods are of great importance especially in areas with drought due to global warming; hence, development of dry separations to replace the commonly used wet separations is in great demand.

Dry gravity separation is not a recent development, since many patents can be found dating back as far as 1850. They cover early attempts to separate materials of various densities or shapes by means of air (Arms, 1924).

There are a number of studies that show successful use of gravity based dry processing of coal cleaning (Dwari and Rao, 2007; Sampaio *et al*., 2008; Macpherson and Galvin, 2010; Macpherson *et al*., 2010, 2011; Yang *et al*., 2013 and Wang *et al*., 2013), iron (Oshitani *et al*., 2010, 2011, 2013a,b), copper (Franks *et al*., 2013) and tungsten (Greenwood *et al*., 2013). These methods include devices such as air jigs, air tables, fluidized separator and Knelson concentrator.

Air jigs have been commercialized and applied in many countries, particularly in the coal cleaning industry. In the gravity based dry processing, stratification of coal is achieved through fluidizing and pulsating air, vibration and an oscillating deck in dry separators. Figure 2.13 shows a semi-pilot scale Allair Jig (Allmineral, Germany) which consists of feed, separation (jigging) and powder filtering units. The fresh run of mine (ROM) coals were fed into a manual feed chute associated with belt conveyor and accumulated in the second feed chute where the feed rate was controlled by the stargates. Following the stratification of the feed in jigging cell by the fluidizing air from the fluidizing and pulsed air production and distribution mechanism towards the bottom part, the lighter coal particles are floated and discharged automatically from the channel while the discharge of the dense materials through separated channel is controlled by the stargates by varying the rotational speeds. During stratification, a limited amount of powder is ventilated by the filter unit through the ventilation pipe. During the stratification, the operational conditions are adjusted by the control panel (Boylu, 2014).

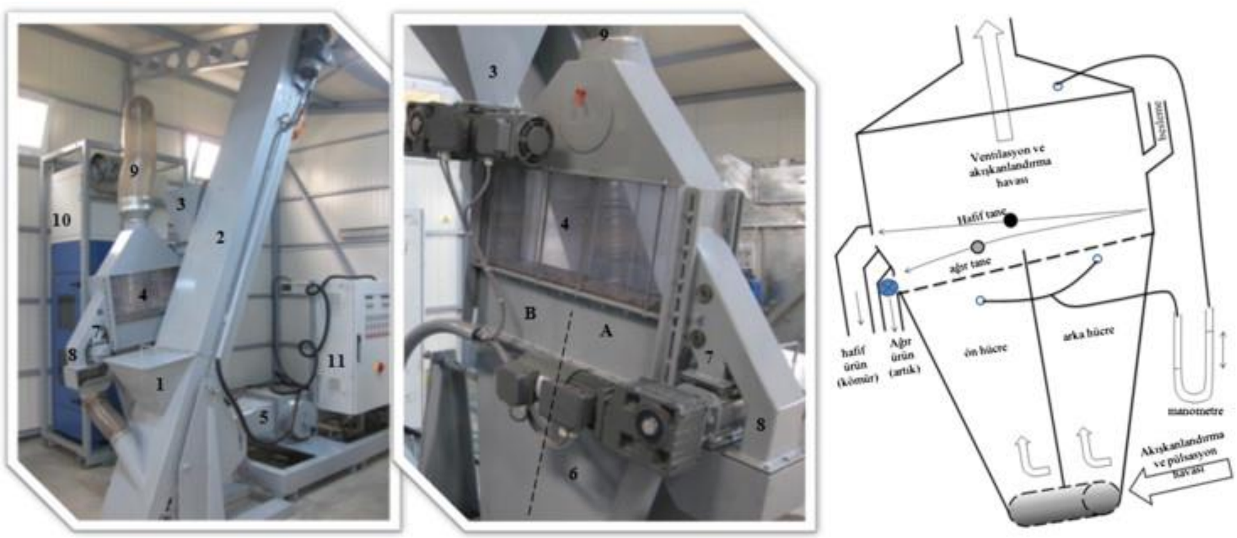

Figure 2.13 Lab Scale Allair Jig facility and cross-sectional view of the jigging cell (Boylu, 2014)

The air table is one form of the dry gravity separators that are similar in principle to their wet gravity separation counterparts. The air table consists of a hopper, a vibrating feeder, a porous deck powered by an eccentric drive to impart the longitudinal vibration, and an electric fan located below the porous deck to generate the upward airflow at a controlled value of superficial velocity, with a laboratory-scale air table is shown in Figure 2.14. A collecting bin is arranged alongside the discharge end of the separator. It consists of two compartments separated by a splitter. The left-hand compartment collects the so-called low-density fraction, whereas the right-hand compartment collects the high-density fraction.

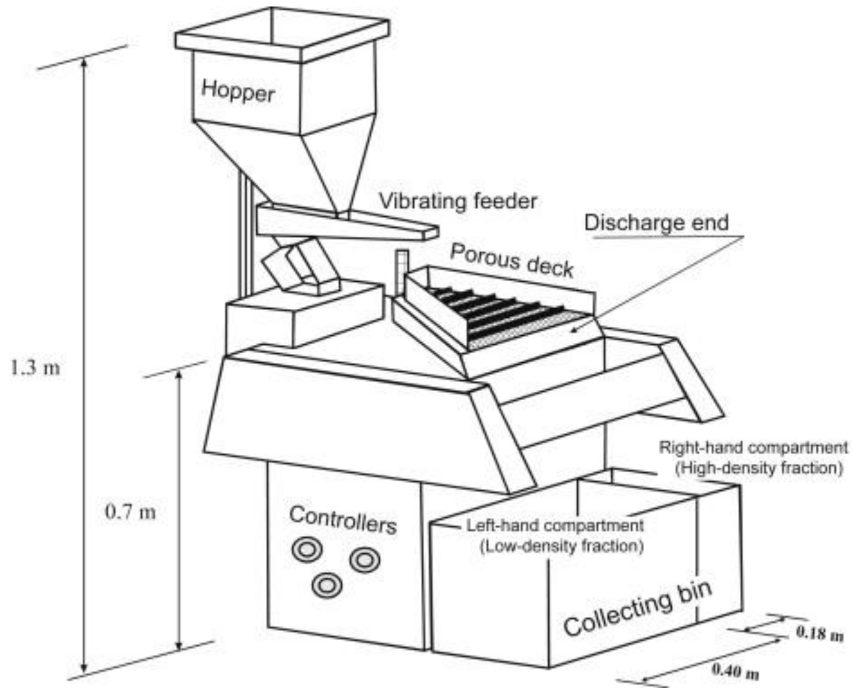

Figure 2.14 Schematic design of the laboratory scale air table (Dodbiba and Fujita, 2015)

The basic principles of air tabling hardly differ from those of wet tabling. In operation, particles of the same size are initially discharged from the hopper, and then are fed by the vibrating feeder onto the deck of the air table, creating an uniform bed over its surface. The eccentric drive vibrates the deck in a side-to-side motion, along the direction of riffles, at a frequency with corresponding stroke length. Simultaneously, the electric fan blows air upward through the porous deck at a superficial velocity.

The longitudinal vibration and airflow spread and lift the bed of particles on the surface of the deck; then, as the bed falls, it is expanded and fluidized. This stratifies the material according to density, causing the high-density particles to settle on the deck and contact its surface while the low-density particles to float on top of the high-density ones. As the eccentric drive vibrates the deck using a slow forward stroke and a rapid return, the high-density particles move along the deck between the riffles, uphill the end slope α towards the higher side as shown in Figure 2.15.

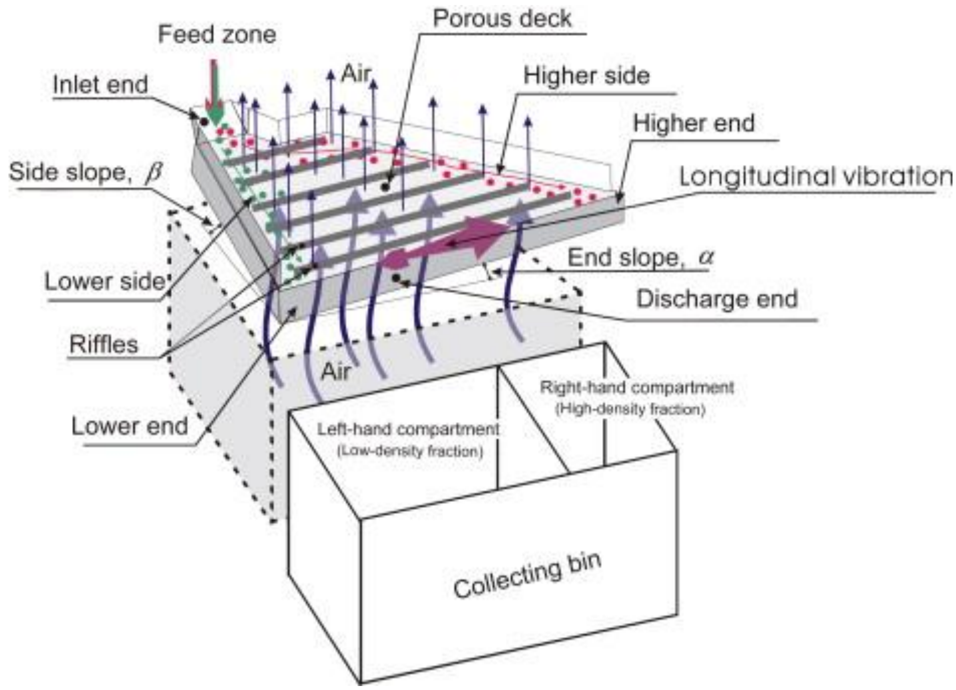

Figure 2.15 Schematic diagram illustrating the principle of separation by air table (Dodbiba and Fujita, 2015)

Subsequently, the high-density particles flow off the deck through the higher side, which channels them downward to the discharge end, and then drop into the right-hand compartment of collecting bin. The low-density particles, which remain fluidized, drift downhill in the direction of the deck's inclination due to gravity and are discharged from the deck at its lower end. The low-density fraction is then collected in the left-hand compartment of the collecting bin (Dodbiba and Fujita, 2015).

Air tables or pneumatic tables (Knapp, 1953), more than any other dry gravity separation devices, have found their major applications particularly in food industry as they were originally developed for seed separation (Burt, 1984 and Jaman, 1985). However, air tables have also an important use in treatment of heavy minerals sand deposit (Hudson, 1962 and Canning, 1980), in cleaning of coal (Appleyard, 1931, McCulloch *et al*., 1950 and Llewellyn, 1977), in upgrading of tungsten (Osborn, 1927), and in other applications where the water is at a premium (Sivamohan and Forssberg, 1985).

The fluidized bed separator is widely used for cleaning coal (Mak *et al*., 2008 and Sahu *et al*., 2009). Recently, it found its applications of treating iron and copper ores (Oshitani *et al*., 2010, 2011, 2013a,b and Franks *et al*., 2013). Figure 2.16 shows a picture of the dry dense medium continuous separator and a schematic drawing of the feeding and recovering devices. The fluidized bed section is 1600 mm long × 400 mm wide. The iron ore to be separated was fed at the middle to left side. The floaters are conveyed toward the right side of the fluidized bed surface by device A, and recovered by device B (rotating basket). The sinkers are conveyed toward the left side at the bottom and recovered by device C. The floaters and sinkers are treated by a trommel to remove the slight amount of fluidized media attached on the ore's surface. The recovered fluidized media is returned to the fluid bed automatically (Oshitani *et al*., 2013a).

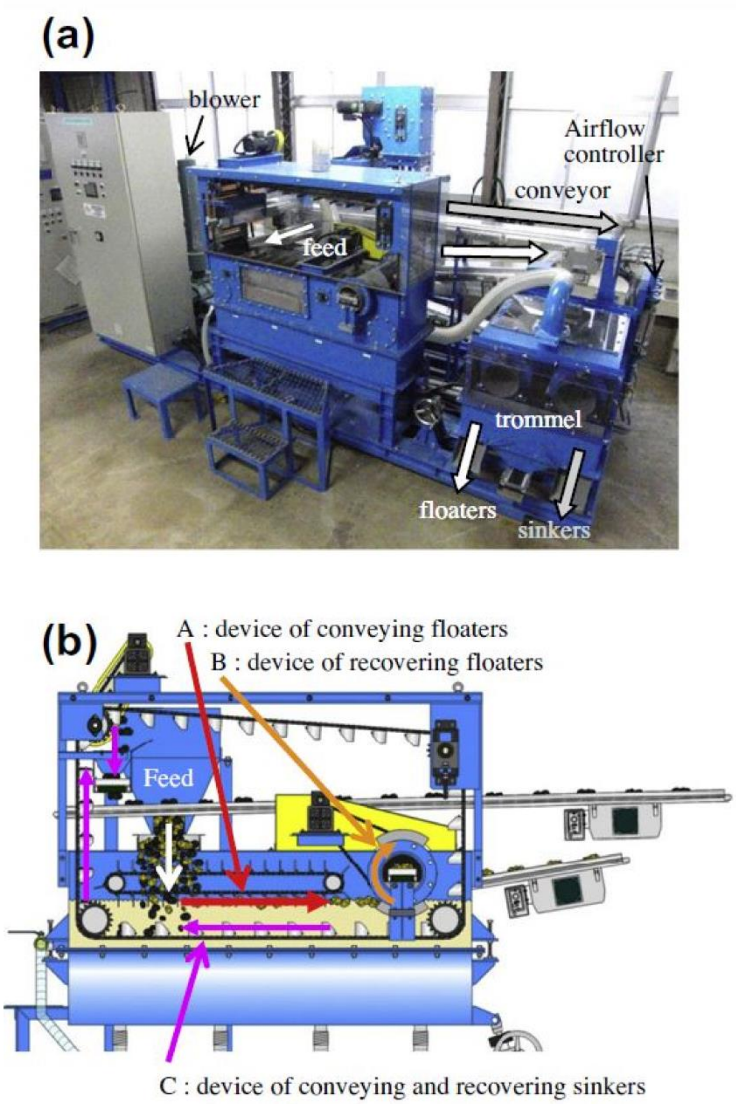

Figure 2.16 (a) A picture of the continuous separator and (b) the schematic drawing of feeding and recovering (Oshitani *et al*., 2013a)

Iron ore is an important raw material to make steel. Demand for iron ore will increase due to the growth of developing countries, in particular Asian countries. Conventional wet dense medium separation requires significant quantities of water. The dry dense medium separation of iron ore by using a gas-solid fluidized bed has been reported (Oshitani *et al*., 2010, 2011, 2013a,b). Iron ore can be efficiently separated at target set points within the range about 2500 to 4200 kg m3 with probable errors of approximately 0.03. The float-sink separation is affected by the size of the ore particles. The degree of the separation depends on the air velocity. The separation of copper ores by using a float/sink method in a dry dense-medium using a fluidized bed with air as the fluidizing medium has been investigated (Franks *et al*., 2013). The separation point density and the separation efficiency, characterized by the probable error, can be controlled by changing the amount of different density sand particles in the medium mixture and the fluidization air velocity. It has been shown that separation point densities between about 2200 and 3700 kg/m^3 with probable errors typically in the range of 0.01 to 0.06 can be obtained. Ores with particles in the size range of between about 10 and 25 mm can be treated. Depending on the ore mass–density distribution and copper-density distribution, between about 20 to more than 40% of the low-density ore could potentially be rejected prior to wet grinding with little loss of valuable copper.

The Knelson Concentrator, one of the popularly used centrifugal concentrators, has recently been shown to have potential for dry processing. Greenwood *et al*. (2013) first reported their research on dry Knelson. In the experimental study, air was used as the fluidising medium in order to separate tungsten from quartz in a synthetic ore (1% w/w tungsten), which was used to mimic a gold ore. A tungsten concentrate of 6.32% tungsten grade was produced with 78.5% recovery, introducing the possibility of operating a Knelson Concentrator on a dry basis.

The concentrate of each test was processed using a laboratory Mozley shaking table to separate the tungsten from the quartz completely. After being dried, the tungsten recovery and concentrate grade were calculated. Table 2.1 shows the results of tungsten recovery and concentrate grade for both wet and dry processing. Table 2.2 shows the results of tungsten recovery by size.

For this thesis study, it was decided to conduct modelling and optimisation on a size-by-size basis to expand the work introduced by Greendwood *et al*. and to gain a better understanding over the separation mechanism of the dry Knelson process at a lab scale.

Table 2.1 Tungsten recovery and concentrate grade (Greenwood *et al*., 2013)

Operating conditions	Tungsten recovery (%)		Concentrate grade (%)	
	Average	Standard deviation	Average	Standard deviation
Wet	94.92	0.87	30.96	0.20
Dry – 2 psi	78.53	6.40	6.32	0.91
Dry – 3 psi	69.90	0.90	15.57	0.83

Table 2.2 Size-by-size recovery of tungsten (Greenwood *et al*., 2013)

Size fraction (μm)	Wet processing (%)		Dry processing 2 psi (%)		Dry processing 3 psi (%)	
	Average	Standard deviation	Average	Standard deviation	Average	Standard deviation
−1180 + 300	98.22	0.31	82.37	5.85	56.95	2.44
−300 + 106	96.19	0.33	73.55	8.37	74.14	2.17
−106 + 38	90.45	3.16	82.00	6.04	79.45	2.81
−38	91.62	1.69	71.43	12.14	57.36	1.34

2.3. Design of Experiments

2.3.1. Introduction to design of experiments

Design of experiments (DOE) or experimental design is a formal mathematical tool and an efficient procedure for systematically planning and conducting scientific experiments and investigating the relationship between input and output factors. Multiple input factors are considered and controlled simultaneously to ensure that the effects on the output response are causal and statistically significant (Montgomery, 2004 & 2009, Ryan, 2007).

There are several DOE vocabulary that need to be defined:

- Factor (independent variable) - A controllable process, design or experimental variable to be tested (the *x*'s)
- Response (dependent variable) - The output or result (the *y*'s)

- Level - Specific value of the factor in the experimental run
- Design - Group of experimental runs to be performed and then statistically analyzed
- Run - One experimental test. A design is a series of runs.
- Repeats - Running the test again right away, taking an average that helps one to analyze for measurement error
- Replicates - Running the same experimental conditions more than once, rebuilding all conditions. Providing a measure of process error. Do not run sequentially if possible.
- Randomization - Running experiments in a random order to avoid the effects of lurking variables.

In order to obtain an appropriate design and analysis, three principles are suggested by Fisher (1966) in performing the experiment: randomization; local control (also called blocking); and replications. These can be explained as follows.

- Randomization is a process that collects all sources of variation affecting the treatment effects except those due to treatment itself. The randomization tends to reduce the confounding of uncontrolled factors and controlled factors. It is very important in experimental analysis because it is required to have a valid estimation of random error.
- Local control or blocking is a technique that is used to segregate an uncontrolled but known variation in an experiment not associated with the treatment effect. The blocking should be designed to have maximum variation among blocks (heterogeneous between blocks) but to have minimum variation with blocks (homogeneous within blocks).
- Replication refers to the replication of a treatment combination. It is needed for a specific degree of precision for measuring treatment effects. The reader should be aware that replications are not multiple readings. Replication requirements are stringent: to assure a proper replication, experimenters must reset every condition in the experiment. If the treatment combinations are not reset, the errors in the multiple readings are not independent. This, in turn, leads to the violation of the randomization principle.

DOE is used to determine which factors or variables and interactions are significant in contributing to the effect being measured, and those variables and interactions that are insignificant and do not contribute to either a particular product property or processing condition.

It can be used for solving any technical problem when you want to fully understand the response to different process variables that can be changed or controlled during the experimentation.

2.3.2. Advantages and limitations of DOE

The advantages of using experimental designs are obvious. The benefits can be described as follows:

- Achieve results in a short time with minimum experiment
- Identify important factors (screening test)
- Determine relationship between inputs and outputs
- Determine interaction between input factors
- Predict response for any combination of factors using only empirical results
- Find best operating conditions (optimum condition)

DOE also has its limitations:

- Before designing and conducting an experiment, one should use simulations of proposed experiments in order to determine which statistical design of experiments approach will identify the correct model from the experimental data with an acceptable degree of confidence.
- The model estimation performance is sensitive to the relative importance of the effects in the model, with balanced magnitudes of effects yielding the best model estimates.
- Data generated by first-order models usually resulted in a better capability of the statistical analysis. If any second-order quadratic interactions are present in the model, the statistical analysis often fails to identify the right model by either overfitting or under fitting.
- The proposed mathematical model sometimes does not match the practical case.

2.3.3. Experimental design types

There are two most important experimental designs: factorial design and response surface. Each design is used in specific situations to gather information from a particular set of independent variables (Montgomery, 2009).

2.3.3.1. Factorial design

Factorial design is used to screen process and/or product variables to determine which factors are significant in controlling the process. Normally, factorial designs are two-level designs, meaning a high and low value for each factor is used to determine whether an effect is present. Fractional factorial designs reduce the experimentation required and also decrease the information that can be obtained about potential interactions between independent variables in the experimental space. As the independent variables increase, the experiments required to understand which factors and interactions are significantly increasing.

2.3.3.2. Response surface design

Response surface designs are used after several independent variables have been identified and one wants a better description of their curvature and interactions in the experimental space. Response surface experiments, unlike factorial design, show curvature. It is explained in detail in the section 2.4.

Experimental design methods have been used in many areas, such as chemistry and chemical engineering (Djoudi *et al*., 2007), textiles (Torrades *et al*., 2011), the food industry (Chen and Parlar, 2013), manufacturing (Campatelli *et al*., 2014), biotechnology (Popa *et al*., 2007), civil Engineering (Hamzah *et al*., 2013), pharmaceutical industries (Kincl *et al*., 2005), oil industry (Cavalcante *et al*., 2010), education, psychology (Montgomery, 2009) and applied to modelling process parameters in mineral processing systems (Coulter and Subasinghe, 2005, Aslan 2007, Aslan, 2008, Tripathy and Murthy, 2012, Boylu, 2013).

2.4. Response Surface Method

2.4.1. Response surface methodology

Experimentation plays an important role in science, engineering, and industry. Experimentation is an application of treatments to experimental units, and then a measurement of one or more responses. It is a part of scientific method. It requires observing and gathering information about how processes and systems work. In an experiment, input (x's) transform into an output that has one or more observable response variables (y). Therefore, useful results and conclusions can be drawn by experiment. In order to obtain an objective conclusion an experimenter needs to plan and design the experiment, and analyze the results.

As an important subject in the statistical design of experiments, the Response Surface Methodology (RSM) is a collection of mathematical and statistical techniques useful for the modeling and analysis of problems in which a response of interest is influenced by several variables and the objective is to optimize this response (Montgomery, 2009). When treatments are from a continuous range of values, then a Response Surface Methodology is useful for developing, improving, and optimizing the response variable.

The design procedure of RSM is as follows (Gunaraj and Murugan, 1999):

i. Designing of a series of experiments for adequate and reliable measurement of the response of interest
ii. Developing a mathematical model of the second order response surface with the best fittings
iii. Finding the optimal set of experimental parameters that produce a maximum or minimum value of response.
iv. Reporting the direct and interactive effects of process parameters through two and three dimensional plots

If all variables are assumed to be measurable, the response surface can be express as follows:

$$y = f(x_1, x_2, x_3, \dots, x_k) \quad \textbf{(2.1)}$$

Y is the output of the system, and x_i are the variables (factors). The goal is to optimize the response variable y. It is assumed that the independent variable are continuous and controllable by experiments with negligible errors.

In most RSM problems, the true response function *f* is unknown. It is required to find a suitable approximation for the true functional relationship between independent variables and the response surface. In order to develop a proper approximation for *f*, the experimenter usually starts with a low-order polynomial in some small region. If the response can be defined by a linear function of independent variables, then the approximating function is a first-order model. If there is a curvature in the response surface, then a higher degree polynomial should be used. The approximating function is called a second-order model.

In general all RSM problems use either one or the mixture of the both of these models. In each model, the levels of each factor are independent of the levels of other factors. In order to get the most efficient result in the approximation of polynomials the proper experimental design must be used to collect data.

2.4.2. Designs fitting first-order models

First-order model is used to describe the flat surfaces that may or may not be tilted. This model is not suitable for analyzing maximum, minimum, and ridge lines. The first-order model approximation of the function *f* is reasonable when *f* is not too curved in that region and the region is not too big. First-order model is assumed to be an adequate approximation of true surface in a small region of the *x*'s (Montgomery 2009).

The class of first-order designs includes the full 2^k factorial designs and fractional of 2^k factorial designs, which do not have their main effects aliased with each other. 2^k factorial designs without replication or fractional of 2^k factorial designs does not provide with enough responses to estimate error. In practice, measurements are made at the center of the design to ensure that the error can be estimated in RSM.

The class of orthogonal designs called the simplex designs can also be used to fit first-order models. A regular sides figure with k+1 vertices is called a simplex. For instance, if two factors are investigated only, an equilateral triangle as shown in Figure 2.17 can be used; for three factors, the corresponding figure is the regular tetrahedron. Normally when the number factors is more than three, higher degree polynomial models will be used.

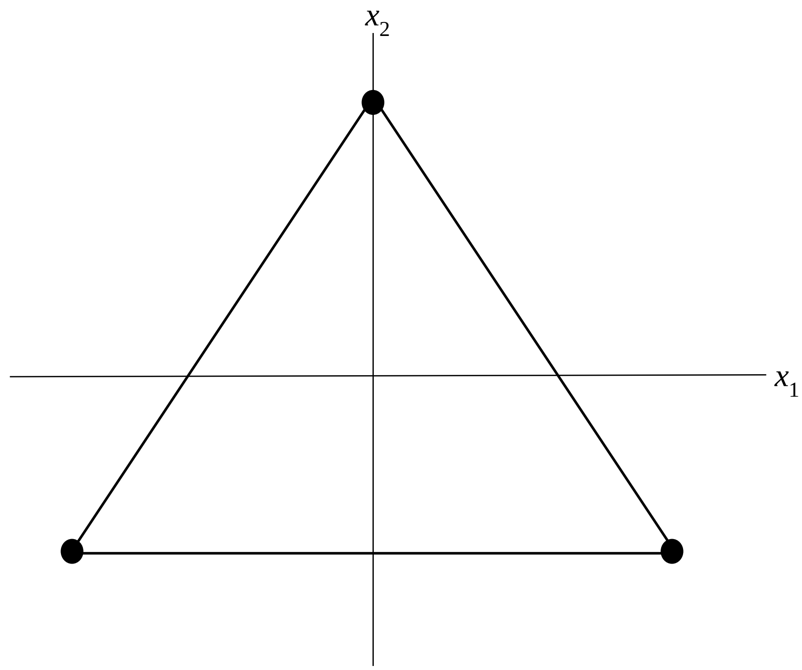

Figure 2.17 Simplex design for fitting first-order models for two factors

2.4.3. Designs fitting second-order models

2.4.3.1. 3^k factorial designs

The 3^k factorial design is a factorial arrangement with k factors, each at three levels. The levels of factor refer to as low, intermediate, and high, represented by the digit 0 (low), 1 (intermediate), and 2 (high). When the measurements on the response variable contain all possible combinations of the levels of the factors, this type of experimental design is called a complete factorial experiment.

In general, the 3^k design require many runs, therefore it is unlikely that all 3^k runs can be carried out under homogeneous conditions. As a result, the confounding in blocks is unavoidable.

A fractional factorial design is a revision of a factorial design without having to run the full factorial design. The fractional factorial design partitions full 3^k runs into blocks, but running only one of the blocks. This design allows an experimenter to get information on the main effects and the low-order interactions. A fractional factorial model can be conducted to study the response surface.

2.4.3.2. Central composite designs

Central composite design (CCD) was originally developed by Box and Wilson (1951) and improved by Box and Hunter (1957). The search for more efficient designs fitting the second-order models led to the development of these designs. CCD are the most widely used designs for fitting the second-order response surfaces. They can give as much information as a three-level factorial, but require less tests than the full factorial and has been proven to be enough to describe the majority of steady-state process responses (Crozier, 1992).

The number of test required for CCD includes standard 2^k factorial with its origin at the centre, 2k points fixed axially at a distance β from the centre to generate the quadratic terms, and replicate tests at the centre; where k is the number of variables. The axial points are chosen such that they allow rotatability (Box and Hunter, 1957) which ensures that the variance of the model prediction is constant at all points equidistant from the design centre. Replicates of the test at the centre point are very important as they provide an independent estimate of the experimental error. For three variables, the recommended number of tests at the centre is six (Box and Hunter, 1957). Therefore, the total number of tests required for the three independent variables is $2^3 + (2\times3) + 6 = 20$. Figure 2.18 shows the CCD for k=3 factors.

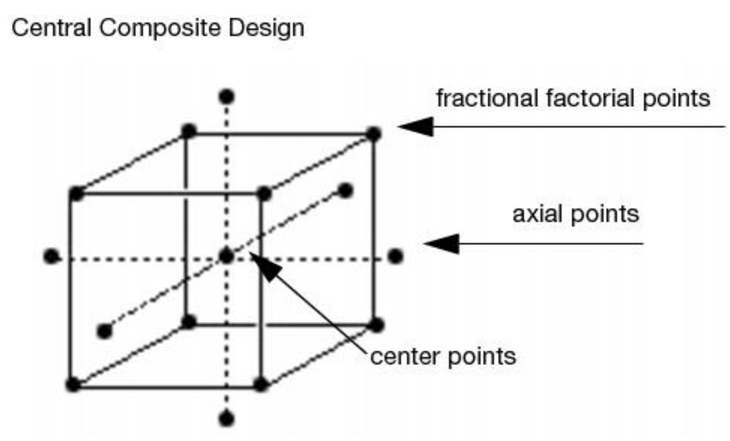

Figure 2.18 Central composite design for three factors

Once the desired ranges of values of the variables are defined, they are coded to lie at ±1 for the factorial points, 0 for the centre points and ±β for the axial points.

CHAPTER 3: EXPERIMENTAL MATERIALS AND METHODOLOGY

3.1. Materials

Synthetic ore was used to represent the composition of a gold ore, as it has been shown previously that synthetic ore can accurately simulate gold ore under gravity test conditions (Laplante *et al*., 1995a,b, Laplante and Nickoletopoulos, 1997). The synthetic ore was prepared by mixing tungsten (1%) and quartz (99%). Tungsten was used as it has a density similar to that of gold (19.25 g cm^{-3} and 19.30 g cm^{-3} respectively) and therefore will behave the same way in a centrifugal separator. Grey polyhedral tungsten particles (Zhuzhou Cemented Carbide Work of China) were used in this study. The particles have a tungsten content of 99.9% and a density of 17.98 g cm^{-3}. Quartz (Unimin Canada Ltd.) was used as the low−density gangue (2.65 g cm^{-3}). Figure 3.1 shows the size distributions of the quartz and tungsten used in the experimental studies, determined by Ling (1998) to be ideal for wet processing and by Greenwood et al. (2013) to be a good starting point for dry processing using a 3" Knelson Concentrator. The tungsten and quartz were pulverized using a LM2−P pulverizing mill (Labtechnics, Australia) and screened to achieve the required size fractions (-425+300 µm, -300+212 µm, -212+150 µm, -150+106 µm, -106+75 µm, -75+53 µm and -53 µm).

3.2. Knelson Concentrator

A modified 3" laboratory Knelson Concentrator was used in this investigation (Figure 3.2). The unit was adapted for pneumatic fluidization by the fitting of a specialized rotating union and regulator to control air pressure into the inner bowl. The feed cone at the top of the Knelson Concentrator was replaced with a clear Plexiglas lid to prevent loss of material as dust during tests. A foam plate was used for sealing. A gate valve connected the bottom of the hopper to a straight feed tube which fed into the Knelson Concentrator, controlling the solids feed rate. The tailing fraction was discharged into a sealed pail. In order to increase the flow of solids into the tailings container, air lances were set up in the launder of the Knelson Concentrator to remove the solids. This ensured that the launder did not become clogged with solids.

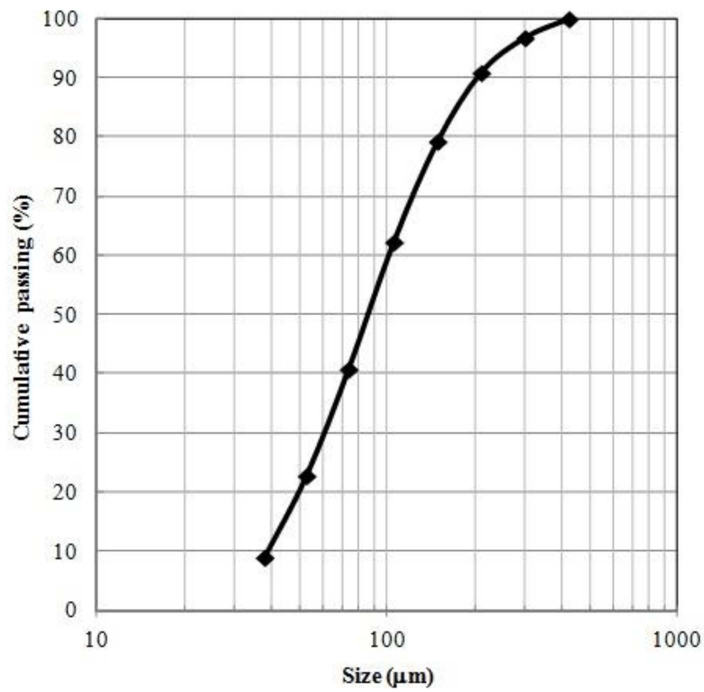

Figure 3.1 Particle size distribution of quartz and tungsten

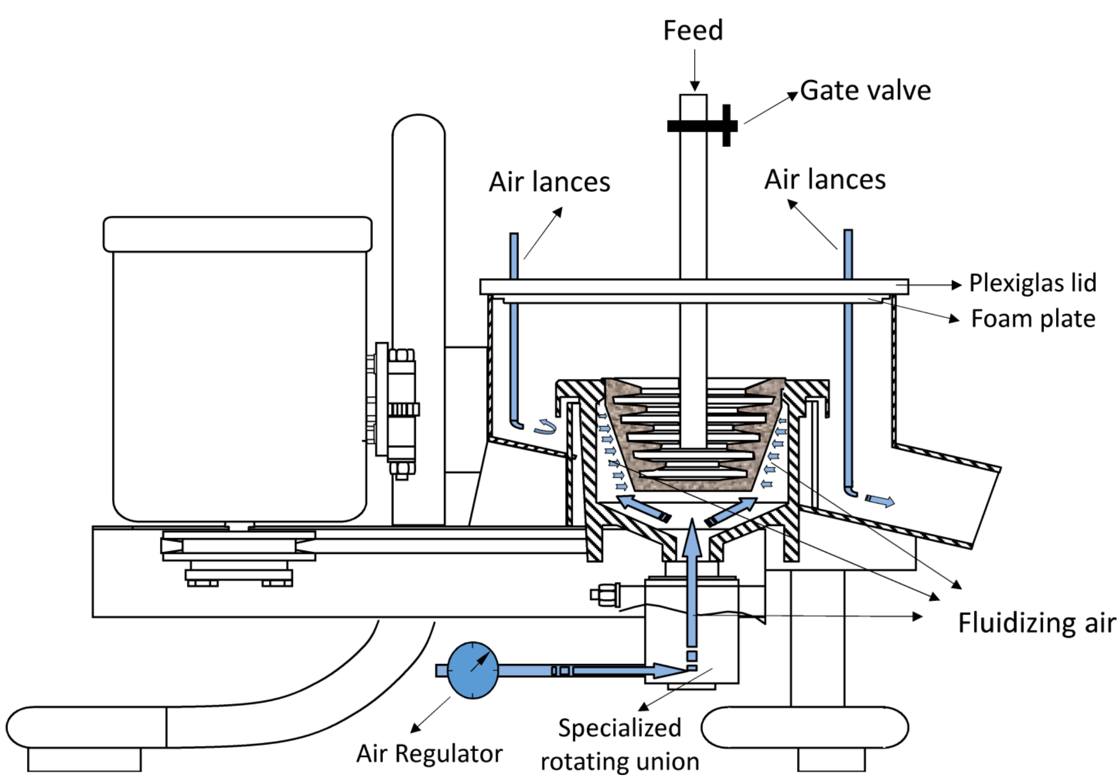

Figure 3.2 Modified Knelson Concentrator

3.3. Sample analysis

The concentrate of each test was analysed using an elutriator (mini hydrosizer) as shown Figure 3.3 to separate the tungsten from the quartz. As in a full scale hydrosizer the feed enters the top of the unit *via* a central feed funnel. Fluidising water is injected the bottom of the unit to generate an upward rising current. A zone of suspended or “teetered” solids is established. Low density particles (quartz) flow over a weir at the top of the unit. After removing all light materials heavy materials (tungsten) are collected as the underflow product. Tungsten was dried and weighed, and the concentrate grade and tungsten recovery was calculated.

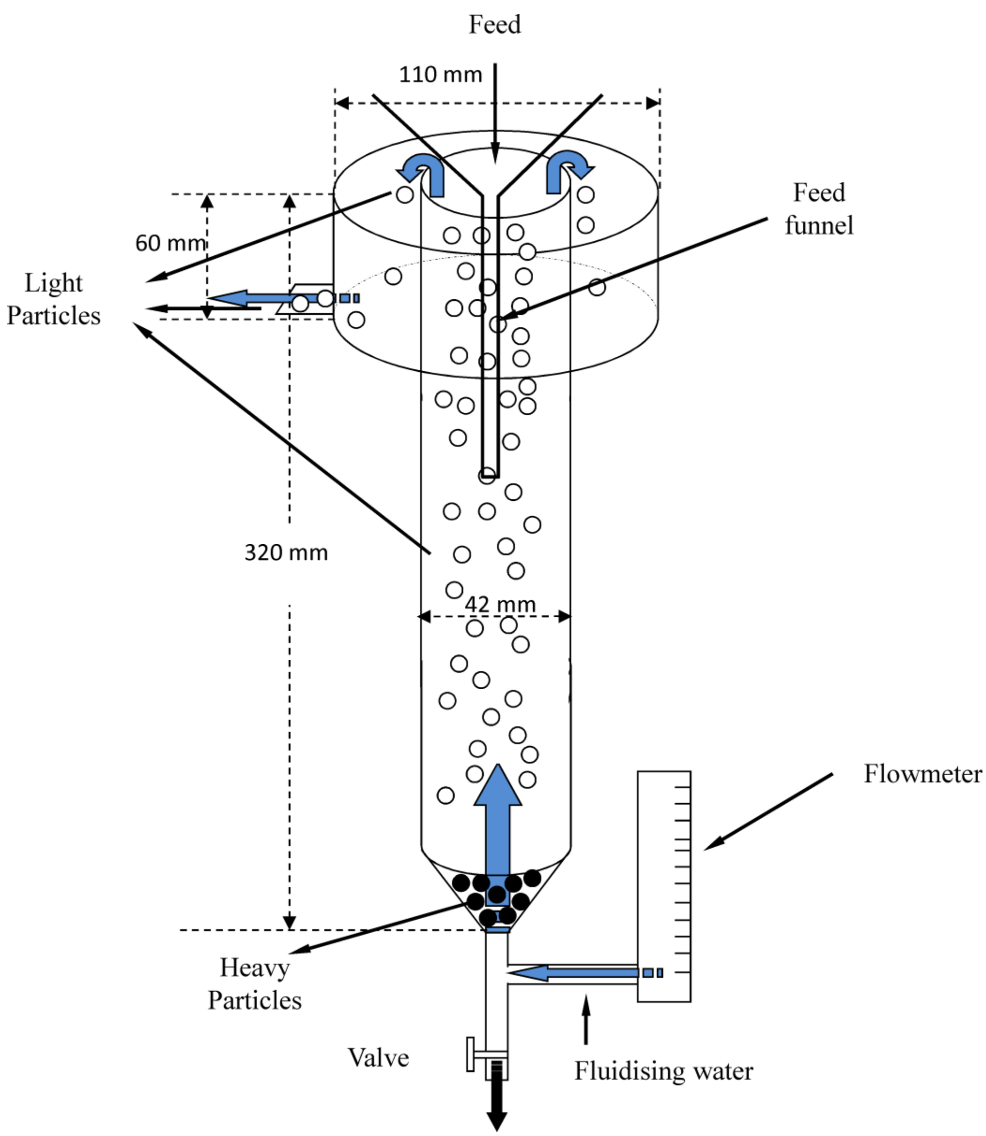

Figure 3.3 A schematic diagram of elutriator

3.4. Experimental design

In this study, central composite experimental design (CCD), which is the most popular and well suited RSM designs for fitting second-order response surface (Box and Wilson, 1951, Box and Hunter, 1957, Montgomery, 2009, Yi *et al*., 2010, Chen and Parlar, 2013), was used with three independent variables (motor power (G), solid feed rate (g/min) and air fluidizing pressure (psi)) and their five levels ($\pm\beta$, ±1, 0) (where $\beta=2^{3/4}$ = 1.682) to investigate the relationship between the responses (concentrate grade and tungsten recovery) on the separation performance of the dry Knelson process. Because of the controller of the Knelson Concentrator indicates the motor power only in decimal scale, except the specific 40 G and 60 G which were already set up on the scale, it is quite difficult to adjust the exact rotating speed needed by using the G forces. In this work, the motor power was chosen as the variable rather than the traditional G forces or the measurement of RPM. To make better understanding, the correlation between the motor power (%), bowl speed (rpm) and G's was shown in Table 3.1.

Table 3.1 Correlation between motor power, bowl's speed and G forces

MP (%)	Bowl Speed (rpm)	G's
20	225	1.5
30	520	7.5
40	800	18.0
50	1100	34.0
60	1380	53.0
70	1620	73.0
80	1870	97.5

The required tests number for the CCD includes the standard 2^k factorial with its origin at the centre, $2k$ points fixed axially at a distance, supposing β, from the centre to generate the quadratic terms, and replicate tests at the centre; where k is the number of variables and is given at Equation (3.1) (Box and Hunter, 1957, Montgomery, 2009, Kökkılıç *et al*., 2015).

$$N = 2^k + 2k + n_0 \qquad \textbf{(3.1)}$$

The number of tests was calculated for the three independent variables to be 20 (2^3 + (2 x 3) + 6) by choosing replicates of the test at the centre point (n_0), which are very important as they provide an independent estimate of the experimental error, as six are recommended in the literature (Obeng *et al*., 2005, Box and Hunter, 1957, Montgomery, 2009, Kökkılıç *et al*., 2015). The variables chosen for the study are designated as x_1, x_2 and x_3 and the predicted responses, namely Grade and Recovery are designated as y_1 and y_2 respectively.

The coded and corresponding actual values were calculated as shown in Table 3.2. These were then used to determine the actual levels of the independent variables for each of the 20 experiments as given in Table 3.3.

Table 3.2 Independent variables and their levels

Factors	Symbol	Coded variable level				
		Lowest	Low	Centre	High	Highest
		$-\beta^*$	-1	0	+1	$+\beta^*$
Motor Power (MP), %	x_1	20	32	50	68	80
Solid Feed Rate (SFR), g/min	x_2	100	140	200	260	300
Air Fluidizing Pressure (AFP), psi	x_3	4	6	8	10	12

* $\beta = 1.648$

For each test, 1 kg synthetic ore was used and the motor power (%), solid feed rate (g/min) and air fluidizing pressure (psi) were changed successively during the tests with respect to the central composite experimental design.

The mathematical relationship between the three independent variables and responses can be approximated by the second order model based Equation (3.2):

$$\begin{aligned} y = {} & \beta_0 + \beta_1 x_1 + \beta_2 x_2 + \beta_3 x_3 + \beta_{11} x_1^2 + \beta_{22} x_2^2 + \beta_{33} x_3^2 \\ & + \beta_{12} x_1 x_2 + \beta_{13} x_1 x_3 + \beta_{23} x_2 x_3 + \varepsilon \end{aligned} \tag{3.2}$$

Where y is the predicted response, β_0 is the model constant; x_1, x_2 and x_3 are the variables; β_1, β_2 and β_3 are linear coefficients; β_{12}, β_{13} and β_{23} are cross-product coefficients and β_{11}, β_{22} and β_{33} are the quadratic coefficients (Gunaraj and Murugan, 1999, Montgomery, 2009, Kwak, 2005, Kökkılıç *et al*., 2015).

The coefficients, i.e. the main effect (β_i), the quadratic effect (β_{ii}) and two-factor interactions (β_{ij}) have been estimated from the experimental results by using the statistical software package "Minitab® Statistical Software".

Table 3.3 Coded and actual levels of three variables of Knelson experiments

Run	Coded levels of variables			Actual levels of variables		
	x_1	x_2	x_3	MP (%)	SFR (g/min)	AFP (psi)
1	-1	+1	-1	50	200	8
2	+1.682	0	0	50	300	8
3	-1	-1	-1	32	140	6
4	0	0	0	50	200	12
5	+1	-1	-1	32	260	6
6	0	0	0	50	200	8
7	0	+1.682	0	68	140	10
8	-1	+1	+1	32	260	10
9	+1	+1	-1	68	260	10
10	0	0	0	68	140	6
11	-1.682	0	0	50	100	8
12	0	0	-1.682	68	260	6
13	0	0	0	80	200	8
14	0	0	0	50	200	4
15	+1	+1	+1	20	200	8
16	+1	-1	+1	50	200	8
17	-1	-1	+1	50	200	8
18	0	-1.682	0	50	200	8
19	0	0	0	32	140	10
20	0	0	+1.682	50	200	8

3.5. Statistical analysis

At the end of the experiments, using experimental data based on grade and recovery, two second-order regression models which describe concentration are produced. Analysis of Variance (ANOVA) was used to determine the regression coefficients and to detect the harmony of the second-order regression models. By using the Fischer (F) test and p-values, statistical momentousness of each factor on responses can be found choosing 95% confidence level. The F-test for the model indicates the level of significance of the model prediction. If the calculated F value from the ANOVA table is higher than the F value found from the related F-statistics Table (in this case the related F-statistics Table is with 0.05 P-values) the regression model is considered acceptable. Using the 5% significance level, a model is considered significant if the *p*-value (significance probability value) is less than 0.05. R^2 and correlation factors were examined by comparing model values and real values. These models were analysed with response surface methods and optimization was realized by response surface and contour plots for different interactions of any two independent variables, while holding the value of the third variable constant at the central (0) level. All statistical analysis was produced by using the statistical software package "Minitab® Statistical Software".

The motor power (%), solid feed rate (g/min) and air fluidizing pressure (psi) were chosen as independent variables while response variables are the concentrate grade and the tungsten recovery for each size fraction.

CHAPTER 4: SIZE-BY-SIZE ANALYSIS OF DRY GRAVITY SEPARATION USING A KNELSON CONCENTRATOR

For +106 µm size fractions, the particles fed inside the cone directly from the feed tube. However, for the -106 µm size fractions, the fine particles migrated through the air cavity in the bowl due to the geometry limitation of the concentrate bowl. Fine particles that clogged the concentrate cone will damage the bowl at high speed, and prevent the air from entering the inner bowl. To solve this operating problem, certain amount of -425+300 µm silica was mixed with 50 g silica from each size fraction and fed before the synthetic ore. This created an artificial fluidised bed, thus preventing the fine particles from migrating through the holes in the concentrate bowl.

4.1. -425+300 µm size fraction

After running 20 experiments, the response variables (grade and recovery) were calculated and are detailed in Table 4.1.

From the experimental results, the second order response functions, based on the polynomial function in Equation (3) representing the grade of the concentrate and recovery of the tungsten fraction, were expressed as a function of motor power, solid feed rate and air fluidizing pressure. The model equations produced from coded values of factor levels for the grade (y_1) of the concentrate and recovery (y_2) of the tungsten fraction are presented in Equations (4.1) and (4.2) respectively.

$$y_1 = 3.24 - 1.43x_1 - 0.29x_2 + 0.96x_3 + 0.65x_1^2 - 0.12x_2^2 + 0.06x_3^2 - 0.01x_1x_2 - 0.60x_1x_3 + 0.19x_2x_3 \tag{4.1}$$

$$y_2 = 47.90 - 19.49x_1 - 4.02x_2 + 14.28x_3 + 7.90x_1^2 - 1.77x_2^2 + 1.55x_3^2 - 0.10x_1x_2 - 9.09x_1x_3 + 2.94x_2x_3 \tag{4.2}$$

In order to estimate the significance of the developed models, ANOVA was applied as shown in Table 4.2.

Table 4.1 Result of concentrate grade and tungsten recovery. MP = Motor power, SFR = Solid feed rate, AFP = Air fluidizing pressure

Run	Variables			Response	
	MP (%)	SFR (g/min)	AFP (psi)	Grade (%W)	Recovery (%)
1	50	143.3	8	2.52	33.60
2	50	283.0	8	2.29	33.00
3	32	130.2	6	4.53	66.50
4	50	150.4	12	4.76	70.80
5	32	229.9	6	3.75	55.10
6	50	200.7	8	2.89	41.80
7	68	128.5	10	3.09	45.60
8	32	238.1	10	6.66	98.10
9	68	244.9	10	2.86	42.20
10	68	131.9	6	2.70	40.10
11	50	100.2	8	3.47	51.50
12	68	229.0	6	2.33	34.70
13	80	197.4	8	2.16	32.30
14	50	142.9	4	2.13	32.00
15	20	183.5	8	7.62	99.60
16	50	147.1	8	3.84	57.20
17	50	193.5	8	3.33	49.10
18	50	185.2	8	3.20	47.70
19	32	157.5	10	6.72	99.70
20	50	209.1	8	3.78	56.50

From Table 4.2, the calculated F-values of grade and recovery are shown to be 23.04 and 14.70 respectively, both are higher than the F value founded from the F-statistics Table with P=0.05 ($F_{0.05(9,10)}$=3.14). Accordingly, it can be concluded that the regression models are considered acceptable and fit well. Moreover, the *p*-values (P) of the regression models which are 0.0001 for grade and 0.0001 for recovery are smaller than 0.05, thus these models are considered suitable for modelling the response behaviours.

Table 4.2 ANOVA table for grade and recovery

Source	DF	Grade (y_1)				Recovery (y_2)			
		Seq SS	Adj MS	F	P	Seq SS	Adj MS	F	P
Regression	9	46.10	5.12	23.04	0.000	8714.11	968.23	14.70	0.000
Linear	3	37.11	11.00	49.48	0.000	7147.75	2105.38	31.97	0.000
x_1 (MP)	1	28.86	25.73	115.74	0.000	5336.78	4753.07	72.17	0.000
x_2 (SFR)	1	0.12	0.81	3.64	0.086	28.41	155.36	2.36	0.156
x_3 (AFP)	1	8.13	6.09	27.40	0.000	1782.56	1342.16	20.38	0.001
Square	3	6.69	2.18	9.82	0.003	1035.34	334.32	5.08	0.022
x_1^2 (MP^2)	1	6.38	5.56	25.02	0.001	944.78	831.67	12.63	0.005
x_2^2 (SFR^2)	1	0.24	0.12	0.52	0.487	53.37	24.52	0.37	0.555
x_3^2 (AFP^2)	1	0.07	0.05	0.22	0.650	37.19	30.27	0.46	0.513
Interaction	3	2.30	0.77	3.45	0.059	531.02	177.01	2.69	0.103
x_1x_2 (MP*SFR)	1	0.02	0.00	0.00	0.980	4.70	0.05	0.00	0.978
x_1x_3 (MP*AFP)	1	2.10	1.98	8.92	0.014	483.44	455.87	6.92	0.025
x_2x_3 (SFR*AFP)	1	0.18	0.18	0.81	0.388	42.88	42.88	0.65	0.439
Residual Error	10	2.22	0.22			658.56	65.86		
Total	19	48.32				9372.67			

DF = degrees of freedom, Seq SS = sequential sums of squares, Adj MS = Adjusted mean squares

The qualities of the fit of the polynomial model was expressed by R^2 values and can be calculated using experimental results and the predicted values which were produced using the models (Equations (4.1) and (4.2)) and are tabulated in Table 4.3. As can be seen from these results, good agreements between experimental and predicted values are obtained. Also, the R^2 value for the concentrate grade and the tungsten recovery are 0.95 and 0.93 respectively. From these values, it can be assumed that a good correlation was obtained, indicating a good fit by the model, for which an $R^2 \geq 0.80$ is suggested (Montgomery, 2009). The standard deviations of both the predicted models are 0.47 and 8.12 for grade and recovery respectively which are acceptable values.

Table 4.3 Observed and predicted values of grade and recovery

Run	Grade (%W)			Recovery (%)		
	Observed	Predicted	Residual	Observed	Predicted	Residual
1	2.52	3.41	-0.89	33.60	50.13	-16.53
2	2.29	2.60	-0.30	33.00	38.84	-5.84
3	4.53	4.43	0.11	66.50	62.06	4.44
4	4.76	4.92	-0.16	70.80	74.30	-3.50
5	3.75	3.82	-0.06	55.10	53.33	1.77
6	2.89	3.24	-0.35	41.80	47.85	-6.05
7	3.09	2.78	0.31	45.60	41.10	4.50
8	6.66	6.58	0.08	98.10	94.77	3.33
9	2.86	2.62	0.24	42.20	39.41	2.79
10	2.70	2.56	0.14	40.10	38.31	1.79
11	3.47	3.38	0.09	51.50	49.67	1.83
12	2.33	1.94	0.39	34.70	29.45	5.25
13	2.16	2.67	-0.51	32.30	37.66	-5.36
14	2.13	2.27	-0.14	32.00	35.25	-3.25
15	7.62	7.55	0.08	99.60	103.97	-4.37
16	3.84	3.40	0.44	57.20	50.08	7.12
17	3.33	3.27	0.06	49.10	48.32	0.78
18	3.20	3.30	-0.10	47.70	48.79	-1.09
19	6.72	6.73	-0.02	99.70	96.57	3.13
20	3.78	3.19	0.58	56.50	47.25	9.25

The normal probability plot of the residuals and the plot of the residuals versus the predicted response for both the concentrate grade and tungsten recovery are presented in Figure 4.1 and Figure 4.2, respectively. Figure 4.1 shows that the residuals generally lie on a straight line, which indicates that errors are distributed normally. From Figure 4.2 it can be seen that the residuals scatter randomly, suggesting that the predictions of the models are adequate.

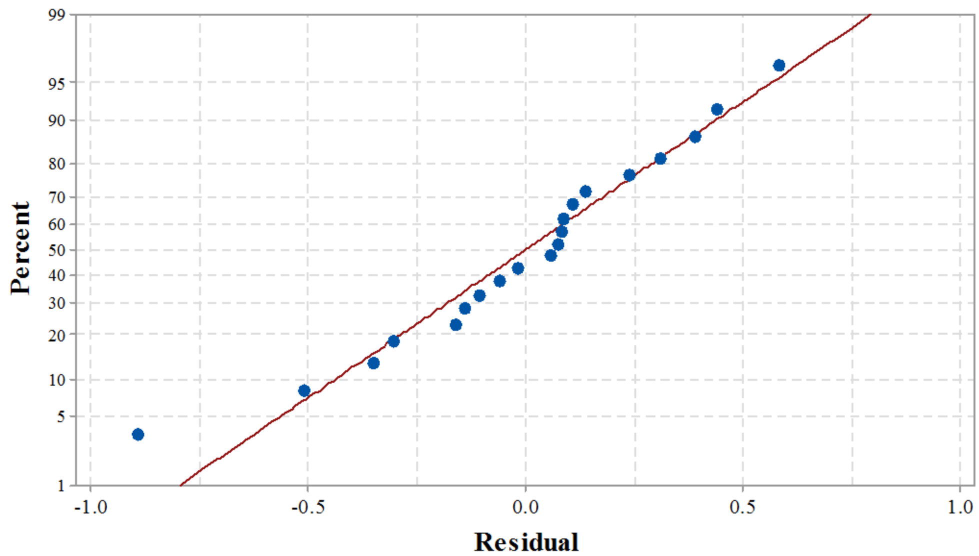

(a) Normal probability plot of residuals for grade

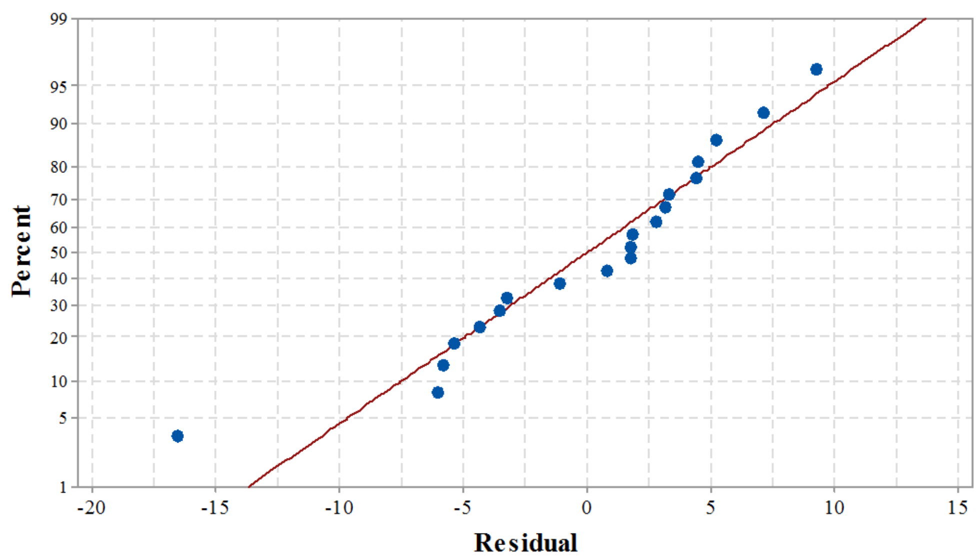

(b) Normal probability plot of residuals for recovery

Figure 4.1 Normal probability plot of residuals for grade (a) and recovery (b) (-425+300 µm)

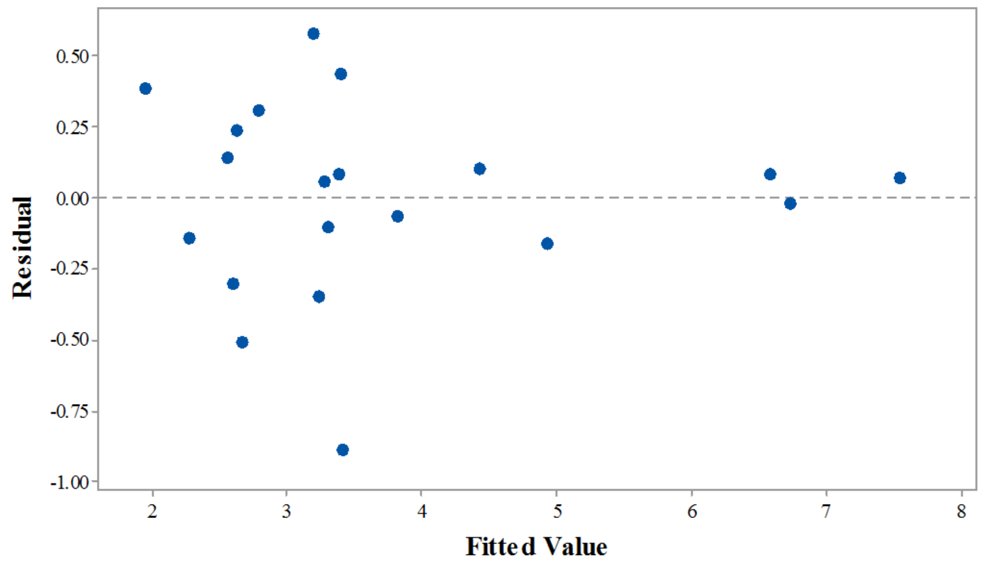

(a) Plot of residuals versus fitted response for grade

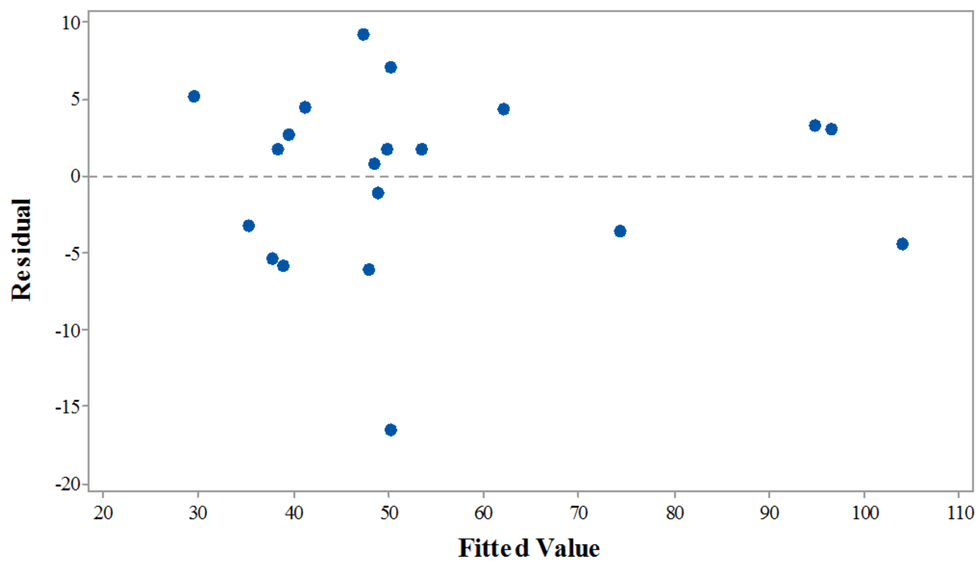

(b) Plot of residuals versus fitted response for recovery

Figure 4.2 Plot of residuals versus predicted response for grade (a) and recovery (b) (-425+300 µm)

In Table 4.4, estimated regression coefficients, factor effects (T) of the models and associated *p*-values (P) for responses are presented.

Table 4.4 Coefficients, factor effects and associated *p*-values for responses

Term	Grade (y1)			Recovery (y2)		
	Coef	T	P	Coef	T	P
x_1	-1.434	-10.76	**0.000**	-19.49	-8.50	**0.000**
x_2	-0.290	-1.91	0.086	-4.02	-1.54	0.156
x_3	0.962	5.23	**0.000**	14.28	4.51	**0.001**
x_1^2	0.646	5.00	**0.001**	7.90	3.55	**0.005**
x_2^2	-0.122	-0.72	0.487	-1.77	-0.61	0.555
x_3^2	0.062	0.47	0.650	1.55	0.68	0.513
x_1x_2	-0.005	-0.03	0.980	-0.10	-0.03	0.978
x_1x_3	-0.600	-2.99	**0.014**	-9.09	-2.63	**0.025**
x_2x_3	0.191	0.90	0.388	2.94	0.81	0.439

From Table 4.4, it can be seen that the factor effects (T) of motor power (x_1) for grade and recovery are 10.76 and 8.50, respectively and the sign of these coefficients are negative. This means that the response y_1 (concentrate grade) and y_2 (tungsten recovery) were significantly affected by a negative linear effect of motor power (x_1), with a *p*-value of 0.000 for both y_1 and y_2, as seen from Table 4.2 and Table 4.3. The responses (y_1 and y_2) were also affected by a positive linear effect of air fluidizing pressure (x_3) due to their positive coefficients, 5.23 and 4.51, with a *p*-value of 0.000 and 0.001, respectively. The linear negative effect of motor power causes an decrease in grade and recovery while an increasing motor power and the positive linear effect of air fluidizing pressure causes an increase of the grade and recovery while the air fluidizing pressure increases.

Additionally, the T value of the quadratic term of motor power (x_1^2) for grade and recovery are 5.00 and 3.55, respectively and the sign of these values are positive. This means that it has a positive quadratic effect on the grade and recovery. Positive quadratic effects means that with a decreasing of the factors there will be a faster decrease in the response values.

The T value of the interaction term of motor power and fluidizing air pressure (x_1x_3) for grade and recovery are 2.99 and 2.63 respectively and the sign of these coefficients are negative. Negative interaction effects means that up to a certain point with an increasing of the factors there will be an increase in the response values. However, after that certain point if the factor levels still increase the value of responses will decrease.

In order to obtain a better understanding of the results and for optimization, the predicted models are presented in Figure 4.3 and Figure 4.4 as contour plots. The Figures show the relationship between two variables and responses while the other variable is at centre (0) level.

Figure 4.3 (a) shows the effect of motor power and solid feed rate on concentrate grade at the centre of air fluidizing pressure. As can be seen, the concentrate grade is significantly affected by decreasing the motor power. However, the solid feed rate has very little effect on the grade. It can also be seen that a high grade can be achieved by maintaining the motor power under 32 %, no matter what the solid feed rate is. Figure 4.3 (b) shows the effect of motor power and air fluidizing pressure on concentrate grade at the centre of solid feed rate. From Figure 4.3 (b) it is observed that the concentrate grade depends more on the motor power than the air fluidizing pressure; however both variables are important. When the motor power decreased under 32%, the concentrate grade increased significantly over 7% at > 7.5 psi air fluidizing pressure. Also, the limited effect of solid feed rate can be seen in Figure 4.3 (c) which shows both the effect of solid feed rate and air fluidizing pressure on concentrate grade at the centre of the motor power.

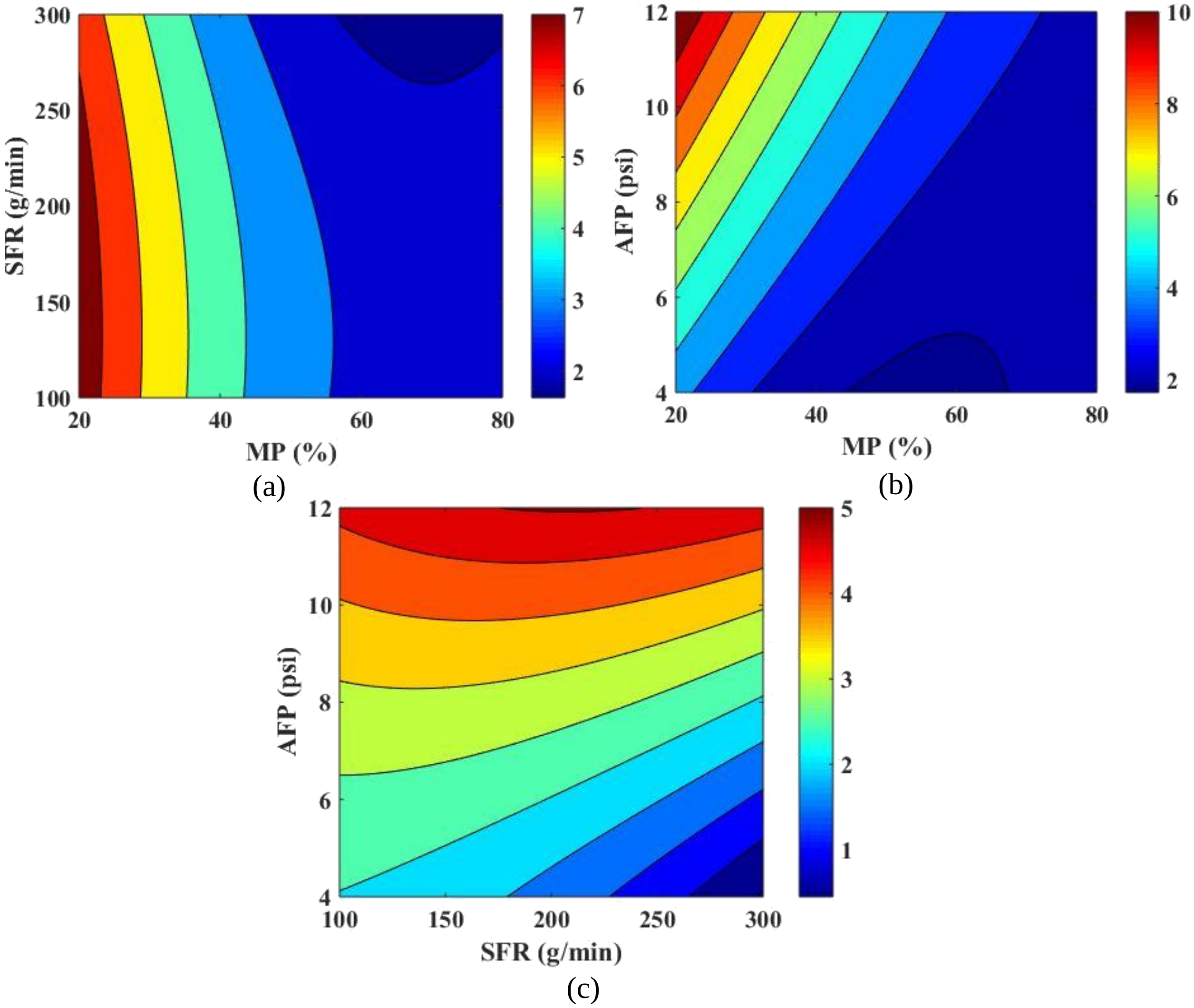

Figure 4.3 Response surface plots for concentrate grade. (a) Motor power and solid feed rate (b) motor power and air fluidizing pressure (c) solid feed rate and air fluidizing pressure (-425+300 μm)

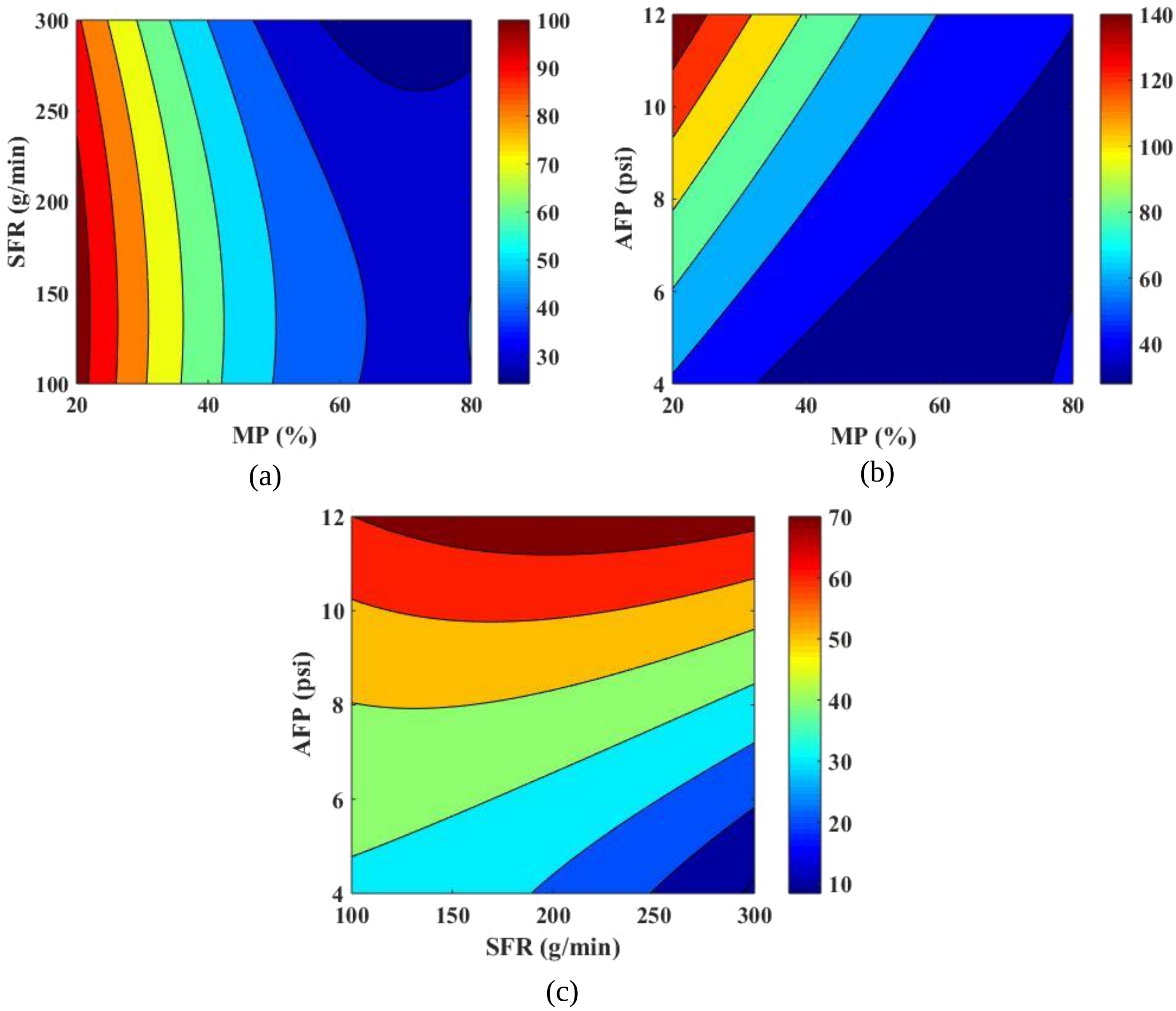

Figure 4.4 Response surface plots for tungsten recovery. (a) Motor power and solid feed rate (b) motor power and air fluidizing pressure (c) solid feed rate and air fluidizing pressure (-425+300 µm)

Figure 4.4 (a) shows the effect of motor power and solid feed rate on recovery of the tungsten at the centre of air fluidizing pressure. Tungsten recovery is shown to be affected by motor power. However, the solid feed rate has very little effect on the tungsten recovery. For a high recovery the motor power should be set below 24 % and the solid feed rate between 100 and 240 g/min. Figure 4.4 (b) shows the effect of motor power and air fluidizing pressure on tungsten recovery at the centre of solid feed rate. The general form of the relationship is similar to Figure 4.4 (b), however the effect of motor power is less pronounced. It can be seen that a high (> 99%) recovery of tungsten can be achieved with the motor power under 36 % and the air fluidizing pressure above 8 psi. Figure 4.4 (c) shows the effect of solid feed rate and air fluidizing pressure on recovery of the tungsten at the centre of the motor power. The insignificant effect of solid feed rate can be seen, the solid feed rate does not affect the recovery of the tungsten.

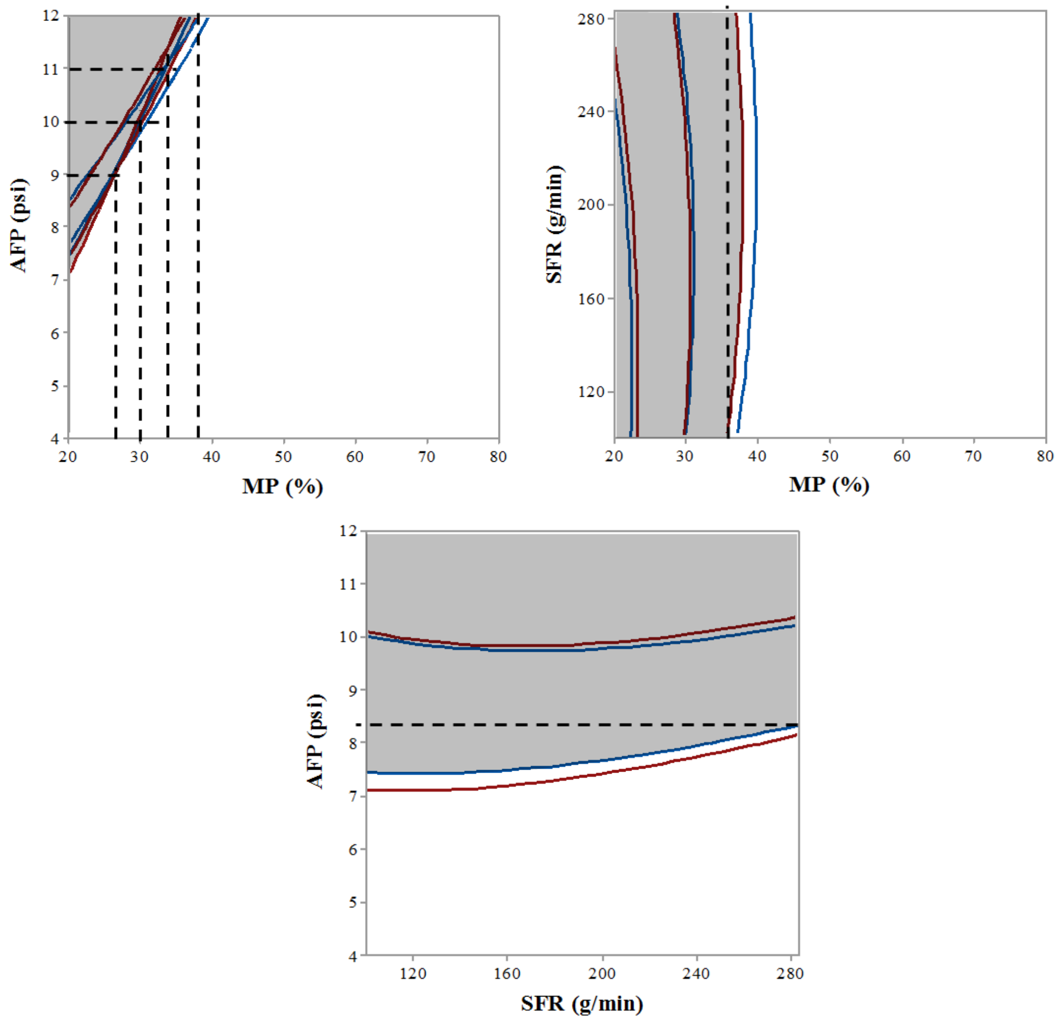

Figure 4.5 Optimum process conditions from overlaid contours (-425+300 μm)

Figure 4.5 shows the overlaid contours plotted using the values of independent variables and responses. The grey areas from overlaid contours indicate the optimum operating conditions to yield high concentrate grade and tungsten recovery. From the overlaid contour plots of MP/AFP, it can be seen that the values of MP and AFP should increase at the same time to assure the high responses. For 20% MP, AFP should be over 7 psi; for 27% MP, AFP should be above 9 psi; for 30% MP, AFP should be at least 10 psi and for 35% MP, AFP should be higher than 11 psi. The overlaid plots of MP/SFR shows that under 36% MP, SFR does not have any effect on responses. As for the plots of SFR/AFP, SFR does not affect the responses when AFP is over 8.5 psi.

The optimum condition ranges are 20-36 % for motor power, over 7.5 psi for air fluidizing pressure and 100-280 g/min for solid feed rate. The results of overlaid contours correspond well with the previous optimum operating ranges from contour and surface plots.

To determine the optimum condition, a response optimizer function was used. For the scenarios, target recoveries were set as 99.9% and 99.99%. The scenarios and the solutions are shown in Table 4.5 and Table 4.6.

Table 4.5 Response optimizer conditions

Condition	Response	Goal	Lower	Target	Upper
1	REC %	Target	90	99.9	100
2			95	99.99	100

Table 4.6 Response optimizer solutions

Solution		MP	SFR	AFP	REC % Fit	Composite Desirability
LS 1	1	20	100	12	99.90	1.00000
	2	33	283	11	99.90	1.00000
	3	30	270	10	99.90	1.00000
	4	36	197	11	99.90	1.00000
	5	30	183	10	99.90	1.00000
	6	33	100	11	99.90	1.00000
LS 2	1	36	190	11	99.99	1.00000
	2	30	270	10	99.99	1.00000
	3	33	100	11	99.99	1.00000
	4	33	283	11	99.99	1.00000
	5	30	172	10	99.99	0.99973
GLS		31.3	195.3	10.7		

LS: Local Solution, GLS: Global solution

The mean values of the parameters of the local solutions were calculated and shown in Table 4.6 as the global solution. Due to the precision control difficulty of the equipment, 30% rather than 31.3% was chosen as the optimum condition for motor power. 200 g/min for feed rate and 10 psi for the air fluidising pressure replaced 195.3 g/min and 10.7 psi respectively.

4.2. -300+212 µm size fraction

The response variables (grade and recovery) were calculated and are detailed in Table 4.7.

Table 4.7 Result of concentrate grade and tungsten recovery. MP = Motor power, SFR = Solid feed rate, AFP = Air fluidizing pressure

Run	Variables			Response	
	MP (%)	SFR (g/min)	AFP (psi)	Grade (%W)	Recovery (%)
1	50	201.3	8	4.67	66.20
2	50	271.5	8	4.65	65.80
3	32	136.4	6	6.00	84.90
4	50	183.5	12	5.94	84.50
5	32	247.9	6	6.39	89.70
6	50	180.2	8	4.75	67.90
7	68	139.2	10	3.83	54.20
8	32	229.9	10	7.24	98.50
9	68	303.0	10	3.00	42.20
10	68	137.0	6	2.91	41.70
11	50	80.5	8	4.50	63.80
12	68	265.5	6	2.79	39.80
13	80	192.9	8	3.09	44.50
14	50	185.8	4	3.23	46.20
15	20	193.5	8	8.29	99.30
16	50	177.0	8	4.55	65.30
17	50	203.4	8	4.30	61.20
18	50	190.5	8	4.27	60.80
19	32	135.1	10	7.17	99.40
20	50	208.3	8	4.50	64.30

The model equations produced from coded values of factor levels for the grade (y_1) of the concentrate and recovery (y_2) of the tungsten fraction are presented in Equations (4.3) and (4.4) respectively.

$$y_1 = 4.54 - 1.67x_1 - 0.02x_2 + 0.63x_3 + 0.41x_1^2 - 0.02x_2^2 + 0.02x_3^2 - 0.16x_1x_2 - 0.08x_1x_3 - 0.16x_2x_3 \quad \textbf{(4.3)}$$

$$y_2 = 65.01 - 20.68x_1 - 0.71x_2 + 8.35x_3 + 3.03x_1^2 - 0.34x_2^2 + 0.47x_3^2 - 1.81x_1x_2 - 0.40x_1x_3 - 2.72x_2x_3 \quad \textbf{(4.4)}$$

In order to estimate the significance of the developed models, ANOVA was applied as shown in Table 4.8.

Table 4.8 ANOVA table for grade and recovery

Source	DF	Grade (y_1)				Recovery (y_2)			
		Seq SS	Adj MS	F	P	Seq SS	Adj MS	F	P
Regression	9	46.53	5.17	94.24	0.000	7117.74	790.86	26.14	0.000
Linear	3	43.48	13.49	245.95	0.000	6873.97	2117.22	69.97	0.000
x_1 (MP)	1	38.86	34.86	635.51	0.000	6031.32	5345.69	176.66	0.000
x_2 (SFR)	1	0.02	0.01	0.11	0.751	14.93	6.24	0.21	0.659
x_3 (AFP)	1	4.60	4.24	77.37	0.000	827.72	748.65	24.74	0.001
Square	3	2.61	0.83	15.11	0.000	162.6	45.58	1.51	0.272
x_1^2 (MP^2)	1	2.43	2.42	44.18	0.000	126.73	131.59	4.35	0.064
x_2^2 (SFR^2)	1	0.18	0.01	0.10	0.764	34.54	1.86	0.06	0.809
x_3^2 (AFP^2)	1	0.00	0.00	0.07	0.802	1.33	2.87	0.09	0.764
Interaction	3	0.44	0.15	2.67	0.104	81.16	27.05	0.89	0.477
x_1x_2 (MP*SFR)	1	0.21	0.17	3.14	0.107	31.77	23.18	0.77	0.402
x_1x_3 (MP*AFP)	1	0.06	0.04	0.67	0.432	3.74	0.86	0.03	0.869
x_2x_3 (SFR*AFP)	1	0.17	0.17	3.03	0.112	45.65	45.65	1.51	0.247
Residual Error	10	0.55	0.05			302.6	30.26		
Total	19	47.08				7420.34			

DF = degrees of freedom, Seq SS = sequential sums of squares, Adj MS = Adjusted mean squares

From Table 4.8, the calculated F-values of grade and recovery are seen to be 94.24 and 26.14 respectively, both are higher than the F value founded from the F-statistics Table with P=0.05 ($F_{0.05(9,10)}$=3.14). Accordingly, it can be concluded that the regression models are considered acceptable and fit well. Moreover, the *p*-values (P) of the regression models which are 0.000 for both grade and recovery are smaller than 0.05, thus these models are considered suitable for modelling the response behaviours.

The experimental results and the predicted values which were produced using the models (Equations (4.3) and (4.4)) are tabulated in Table 4.9. The R^2 value for the concentrate grade and the tungsten recovery are 0.99 and 0.96 respectively. From these values, it can be assumed that a good correlation was obtained, indicating a good fit by the model. The standard deviations of both the predicted models are 0.23 and 5.50 for grade and recovery respectively which are acceptable values.

Table 4.9 Observed and predicted values of grade and recovery

Run	Grade (%W)			Recovery (%)		
	Observed	Predicted	Residual	Observed	Predicted	Residual
1	4.67	4.54	0.14	66.20	64.99	1.21
2	4.65	4.48	0.16	65.80	63.67	2.13
3	6.01	5.74	0.26	84.90	77.91	6.99
4	5.94	5.72	0.22	84.50	81.81	2.69
5	6.39	6.26	0.13	89.70	84.45	5.25
6	4.75	4.54	0.21	67.90	65.21	2.69
7	3.83	4.05	-0.22	54.20	58.81	-4.61
8	7.24	7.25	0.00	98.50	95.98	2.52
9	3.00	3.14	-0.14	42.20	44.89	-2.69
10	2.91	2.85	0.06	41.70	40.76	0.94
11	4.50	4.51	-0.01	63.80	65.06	-1.26
12	2.80	2.76	0.04	39.80	40.20	-0.40
13	3.09	2.93	0.17	44.50	39.26	5.24
14	3.23	3.47	-0.24	46.20	51.35	-5.15
15	8.29	8.48	-0.19	99.30	108.10	-8.80
16	4.55	4.54	0.01	65.30	65.23	0.07
17	4.30	4.54	-0.23	61.20	64.97	-3.77
18	4.27	4.54	-0.27	60.80	65.11	-4.31
19	7.17	7.23	-0.06	99.40	97.52	1.88
20	4.50	4.53	-0.03	64.30	64.90	-0.60

The normal probability plot of the residuals and the plot of the residuals versus the predicted response for both the concentrate grade and tungsten recovery are presented in Figure 4.6 and Figure 4.7, respectively. Figure 4.6 shows that the residuals generally lie on a straight line, which indicates that errors are distributed normally. From Figure 4.7 it can be seen that the residuals exhibit a random scatter, suggesting that the predictions of the models are adequate.

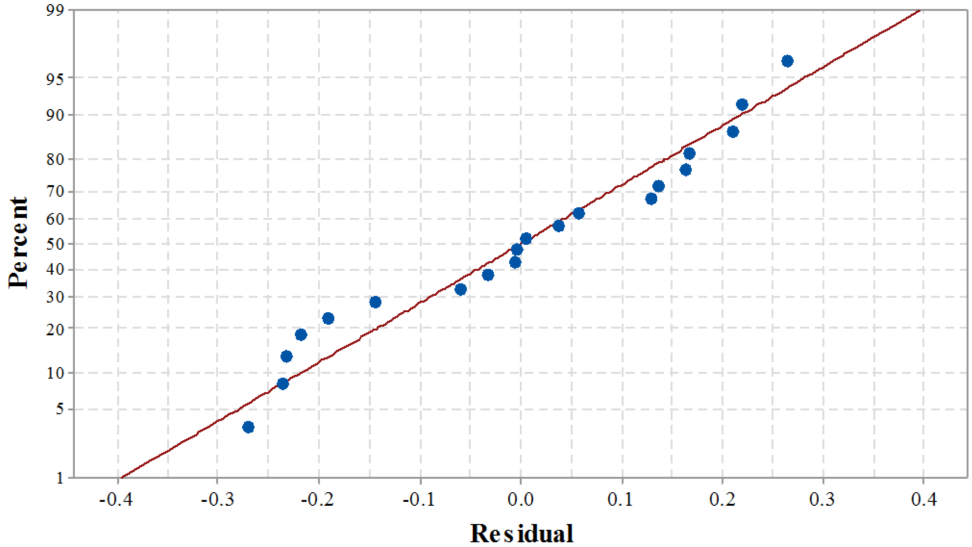

(a) Normal probability plot of residuals for grade

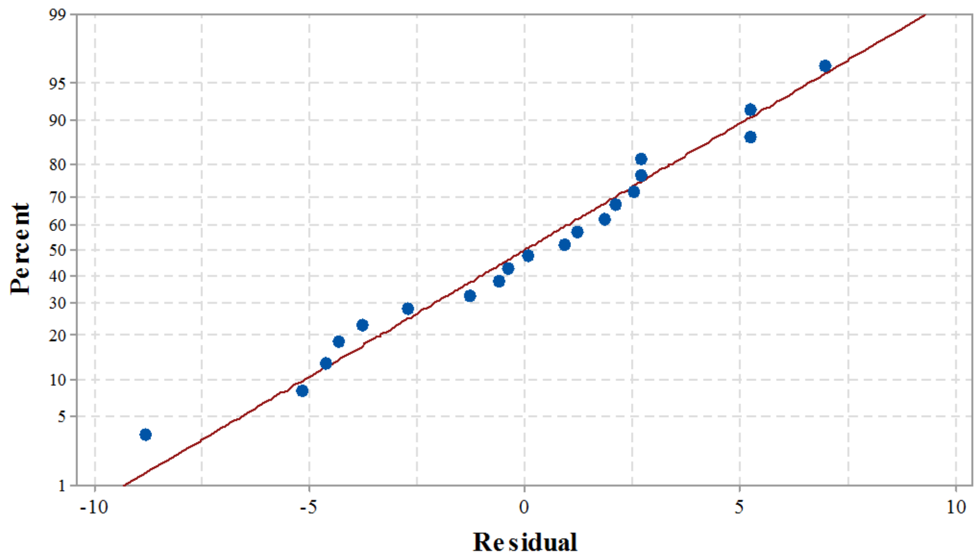

(b) Normal probability plot of residuals for recovery

Figure 4.6 Normal probability plot of residuals for grade (a) and recovery (b) (-300+212 μm)

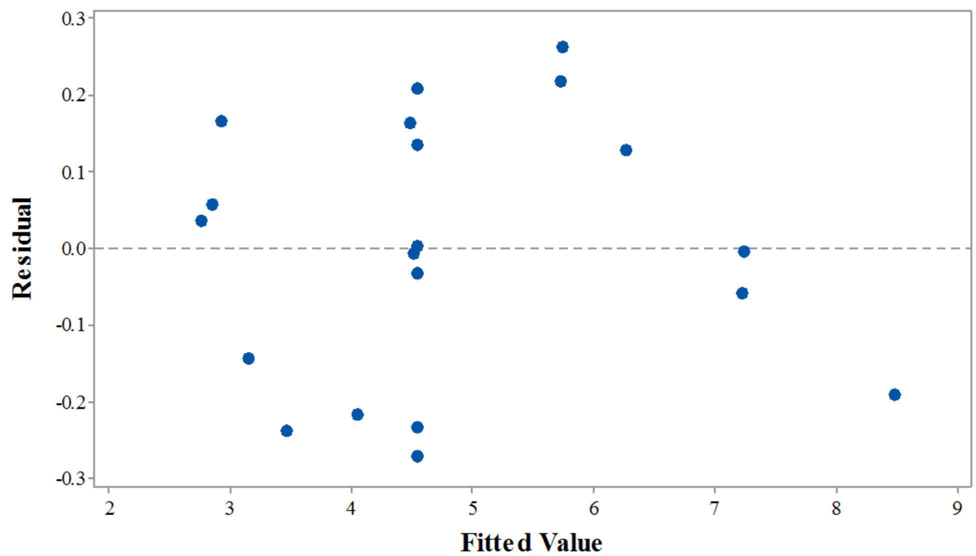

(a) Plot of residuals versus fitted response for grade

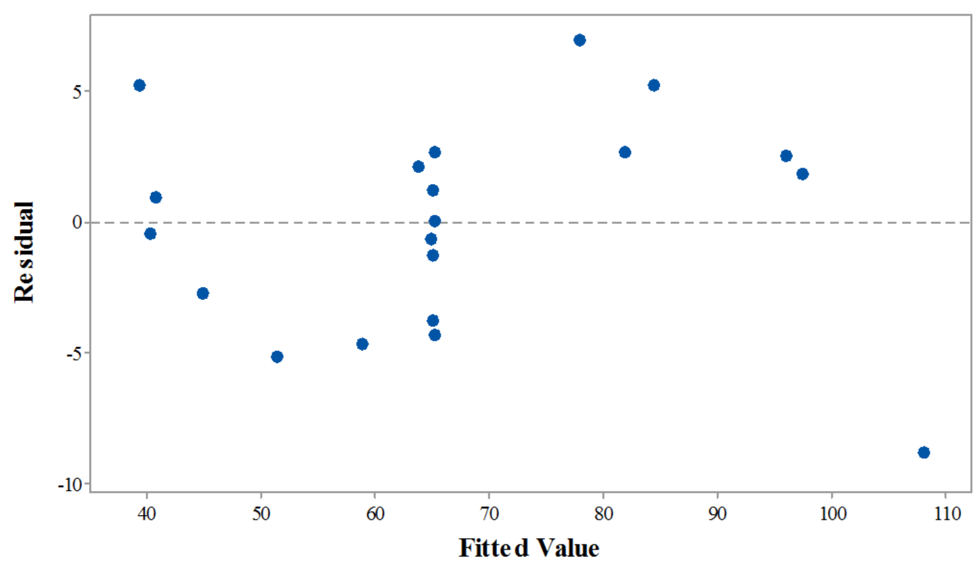

(b) Plot of residuals versus fitted response for recovery (-300+212 µm)

Figure 4.7 Plot of residuals versus predicted response for grade (a) and recovery (b)

In Table 4.10, estimated regression coefficients, factor effects (T) of the models and associated *p*-values (P) for responses are presented.

From Table 4.10 it can be seen that the factor effects (T) of motor power (x_1) for grade and recovery are 25.21 and 13.29, respectively, and the sign of each coefficient is negative. This means that the response y_1 (concentrate grade) and y_2 (tungsten recovery) were significantly affected by a negative linear effect of motor power (x_1), with a *p*-value of 0.000 for both y_1 and y_2, as seen from the Table 4.8 and Table 4.9. The responses (y_1 and y_2) were also affected by a positive linear effect of air fluidizing pressure (x_3) due to their positive coefficients, 8.80 and 4.97, with a *p*-value of 0.000 and 0.001, respectively.

Table 4.10 Coefficients, factor effects and associated *p*-values for responses

Term	Grade (y_1)			Recovery (y_2)		
	Coef	T	P	Coef	T	P
x_1	-1.670	-25.21	**0.000**	-20.68	-13.29	**0.000**
x_2	-0.022	-0.33	0.751	-0.71	-0.45	0.659
x_3	0.629	8.80	**0.000**	8.35	4.97	**0.001**
x_1^2	0.412	6.65	**0.000**	3.03	2.09	0.064
x_2^2	-0.018	-0.31	0.764	-0.34	-0.25	0.809
x_3^2	0.017	0.26	0.802	0.47	0.31	0.764
x_1x_2	-0.156	-1.77	0.107	-1.81	-0.88	0.402
x_1x_3	-0.083	-0.82	0.432	-0.40	-0.17	0.869
x_2x_3	-0.164	-1.74	0.112	-2.72	-1.23	0.247

T value of the quadratic term of motor power (x_1^2) for grade is 6.65. The sign of the value is positive, which means that it has a positive quadratic effect on the grade.

In order to obtain a better understanding of the results and for optimization, the predicted models are presented in Figure 4.8 and Figure 4.9 as contour plots.

As can be seen from Figure 4.8 (a), the concentrate grade is significantly affected by decreasing the motor power. However, the solid feed rate has very little effect on the grade. It can also be seen that a high grade can be achieved by maintaining the motor power under 30%, no matter what the solid feed rate is. From the Figure 4.8 (b), it is observed that the concentrate grade depends more on the motor power than the air fluidizing pressure; however both variables are important. When the motor power decreased under 38%, the air fluidizing pressure had very little effect on concentrate grade. Also, the limited effect of solid feed rate can be seen in Figure 4.8 (c). The concentrate grade increases by increasing the air fluidising pressure.

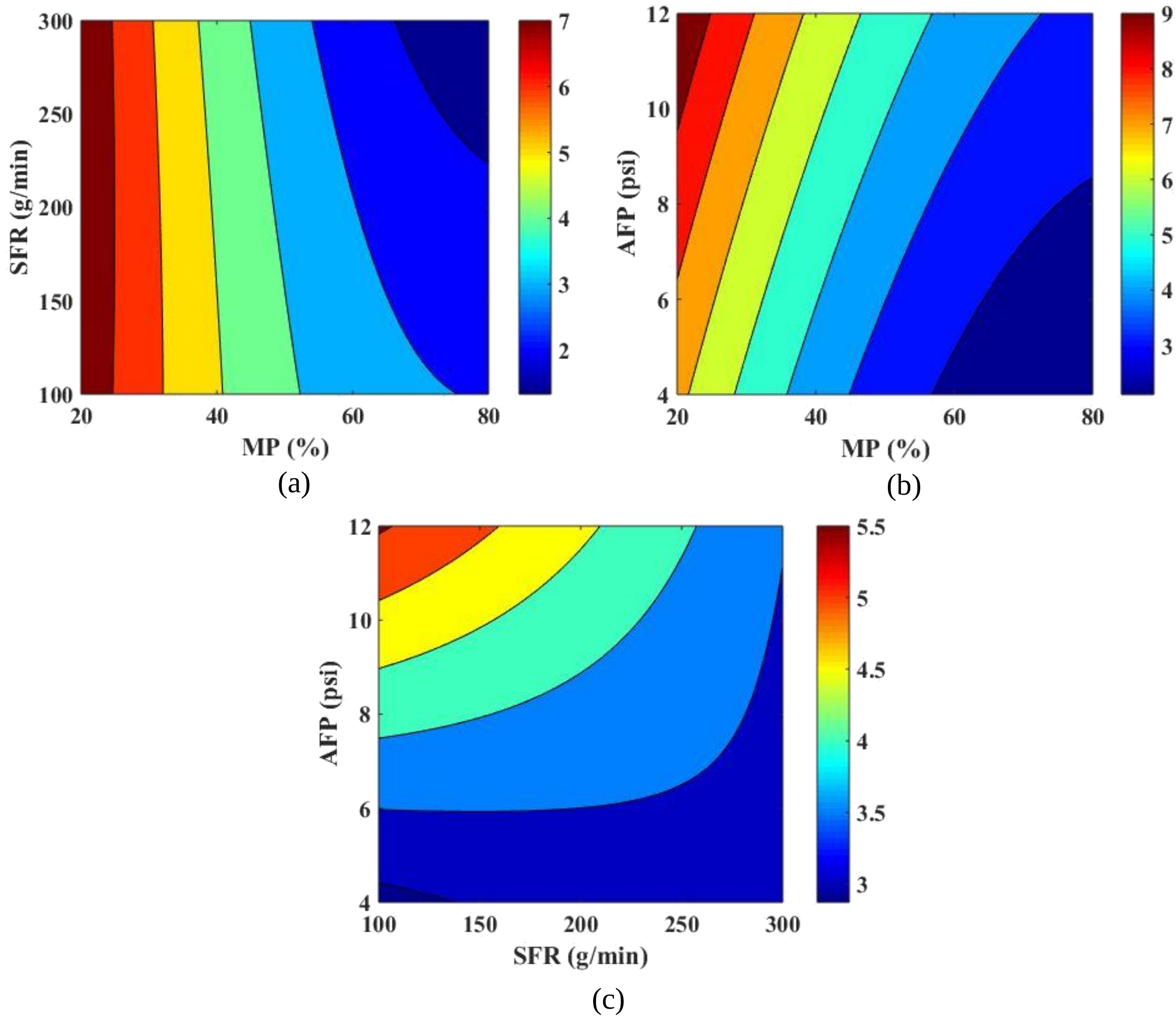

Figure 4.8 Response surface plots for concentrate grade. (a) Motor power and solid feed rate (b) motor power and air fluidizing pressure (c) solid feed rate and air fluidizing pressure (-300+212 μm)

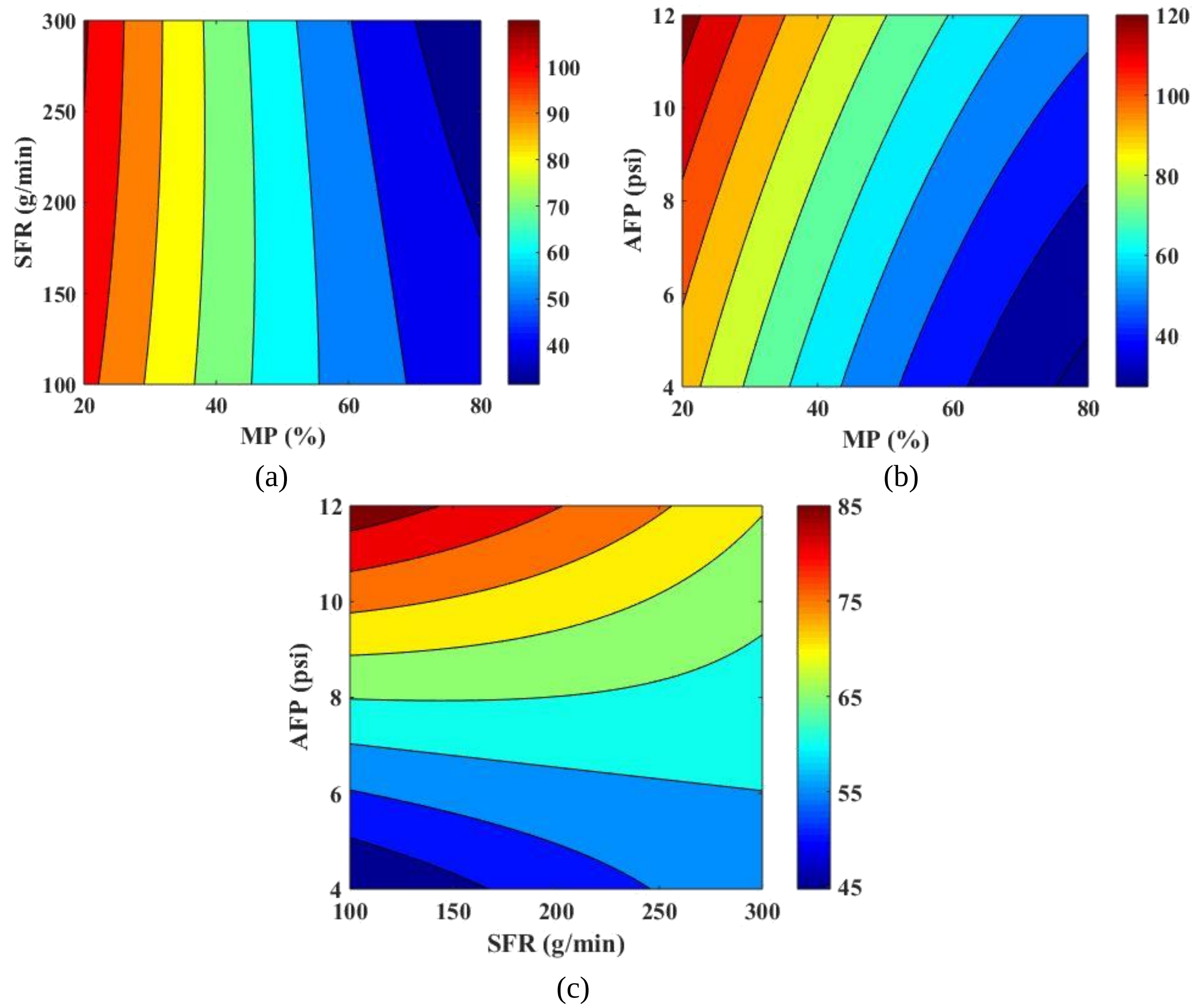

Figure 4.9 Response surface plots for tungsten recovery. (a) Motor power and solid feed rate (b) motor power and air fluidizing pressure (c) solid feed rate and air fluidizing pressure (-300+212 µm)

As can be seen in Figure 4.9 (a), for a high recovery the motor power should be set below 27 % and the solid feed rate does not affect the recovery. Figure 4.9 (b) shows that both motor power and air fluidizing pressure have large effect on recovery. It can be seen that a high recovery of tungsten can be achieved with the motor power under 31 % and the air fluidizing pressure above 5.5 psi. The insignificant effect of solid feed rate can be seen from Figure 4.9 (c). The recovery of the tungsten increased by increasing the air fluidizing pressure.

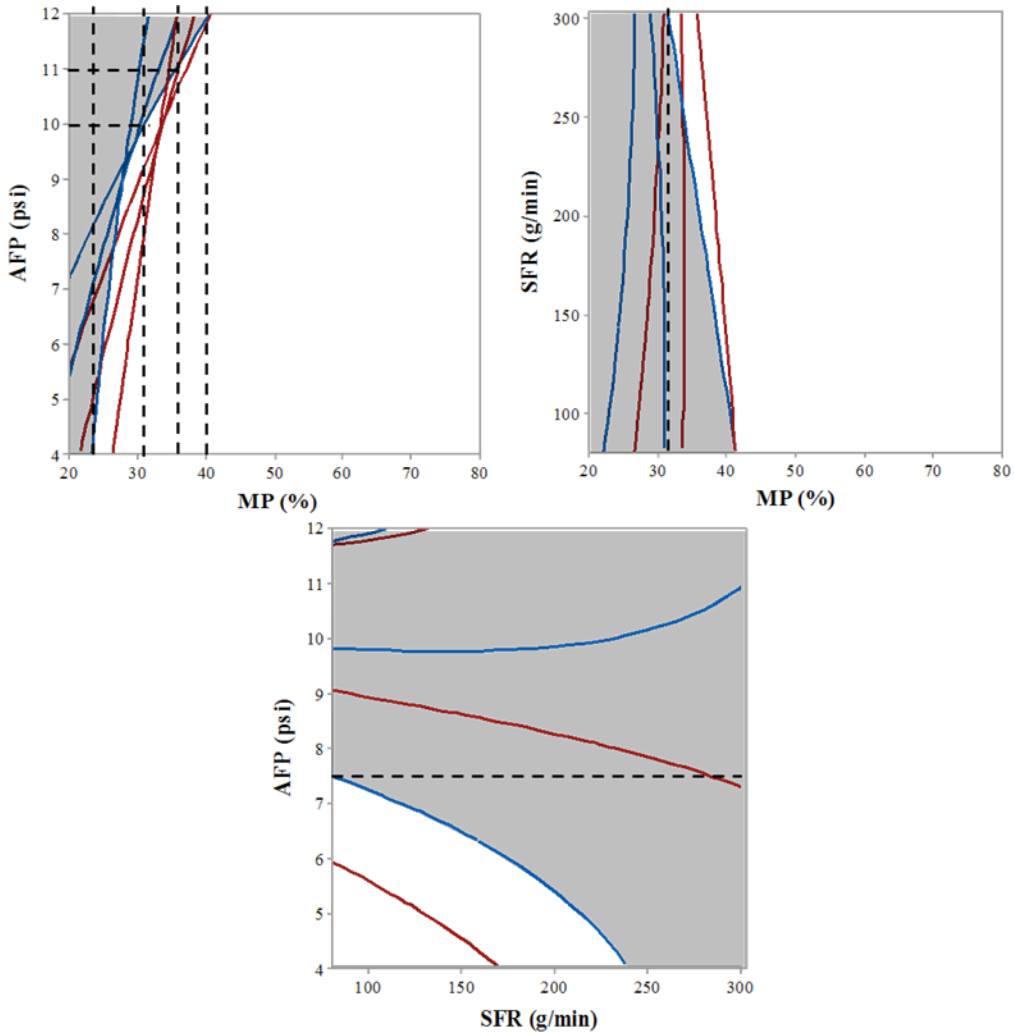

Figure 4.10 Optimum process conditions from overlaid contours (-300+212 µm)

From the overlaid contour plots of MP/AFP in Figure 4.10, it can be seen that under 24% MP, AFP does not affect the responses; however, over 24% MP, the values of MP and AFP should increase at the same time to assure the high responses. For 30% MP, AFP should be over 10 psi and for 35% MP, AFP should be above 11 psi. The overlaid plots of MP/SFR shows that under 31% MP, SFR does not have any effect on responses. Considering the plots of SFR/AFP, SFR does not affect the responses when AFP is over 7.5 psi.

The optimum condition are 20-40% for motor power, over 7.5 psi for air fluidizing pressure and 100-300 g/min for solid feed rate. The results of overlaid contours correspond well with the previous optimum operating ranges from contour and surface plots.

To determine the optimum condition, a response optimizer function was used. For the scenarios, target recoveries were set as 99.9% and 99.99%. The scenarios and the solutions are shown in Table 4.11 and Table 4.12.

Table 4.11 Response optimizer conditions

Condition	Response	Goal	Lower	Target	Upper
1	REC %	Target	90	99.9	100
2			95	99.99	100

Table 4.12 Response optimizer solutions

Solution		MP	SFR	AFP	REC % Fit	Composite Desirability
LS1	1	20	102	7	99.90	1.00000
	2	31	198	10	99.90	1.00000
	3	34	82	11	99.90	1.00000
	4	40	81	12	99.90	1.00000
	5	23	300	4	99.90	1.00000
	6	37	167	12	99.90	1.00000
	7	40	81	12	99.90	1.00000
	8	31	303	12	99.90	1.00000
	9	23	296	5	99.90	1.00000
LS2	1	40	81	12	99.99	1.00000
	2	31	303	12	99.99	1.00000
	3	34	82	11	99.99	1.00000
	4	35	200	12	99.99	1.00000
	5	28	197	9	99.99	1.00000
	6	23	296	5	99.99	1.00000
	7	40	81	12	99.99	1.00000
	8	23	301	4	99.99	0.99973
GLS		31.4	185.4	9.5		

LS: Local Solution, GLS: Global solution

The mean values of the parameters of the local solutions were calculated and shown in Table 4.12 as the global solution. Due to the precision control difficulty of the equipment, 30% rather than 31.4% was chosen as the optimum condition for motor power. 200 g/min for feed rate and 10 psi for the air fluidising pressure replaced 185.4 g/min and 9.5psi respectively.

4.3. -212+150 μm size fraction

The response variables (grade and recovery) were calculated and listed as shown in Table 4.13.

Table 4.13 Result of concentrate grade and tungsten recovery. MP = Motor power, SFR = Solid feed rate, AFP = Air fluidizing pressure

Run	Variables			Response	
	MP (%)	SFR (g/min)	AFP (psi)	Grade (%W)	Recovery (%)
1	50	201.3	8	4.67	66.20
2	50	271.5	8	4.65	65.80
3	32	136.4	6	6.00	84.90
4	50	183.5	12	5.94	84.50
5	32	247.9	6	6.39	89.70
6	50	180.2	8	4.75	67.90
7	68	139.2	10	3.83	54.20
8	32	229.9	10	7.24	98.50
9	68	303.0	10	3.00	42.20
10	68	137.0	6	2.91	41.70
11	50	80.5	8	4.50	63.80
12	68	265.5	6	2.79	39.80
13	80	192.9	8	3.09	44.50
14	50	185.8	4	3.23	46.20
15	20	193.5	8	8.29	99.30
16	50	177.0	8	4.55	65.30
17	50	203.4	8	4.30	61.20
18	50	190.5	8	4.27	60.80
19	32	135.1	10	7.17	99.40
20	50	208.3	8	4.50	64.30

The model equations produced from coded values of factor levels for the grade (y_1) of the concentrate and recovery (y_2) of the tungsten fraction are presented in Equations (4.5) and (4.6) respectively.

$$y_1 = 5.54 - 1.81x_1 - 0.20x_2 + 0.60x_3 + 0.44x_1^2 - 0.17x_2^2 - 0.14x_3^2 - 0.06x_1x_2 + 0.16x_1x_3 - 0.001x_2x_3 \quad \textbf{(4.5)}$$

$$y_2 = 78.49 - 17.86x_1 - 3.17x_2 + 7.01x_3 - 0.33x_1^2 - 1.99x_2^2 - 1.94x_3^2 + 0.37x_1x_2 + 4.17x_1x_3 - 0.67x_2x_3 \quad \textbf{(4.6)}$$

In order to estimate the significance of the developed models, ANOVA was applied as shown in Table 4.14.

Table 4.14 ANOVA table for grade and recovery

Source	DF	Grade (y_1)				Recovery (y_2)			
		Seq SS	Adj MS	F	P	Seq SS	Adj MS	F	P
Regression	9	53.04	5.89	22.12	0.000	5225.32	580.59	8.10	0.002
Linear	3	48.99	16.32	61.24	0.000	5043.43	1661.34	23.17	0.000
x_1 (MP)	1	44.66	44.72	167.84	0.000	4363.25	4342.75	60.57	0.000
x_2 (SFR)	1	0.16	0.46	1.74	0.216	89.15	119.63	1.67	0.226
x_3 (AFP)	1	4.16	3.93	14.74	0.003	591.04	539.73	7.53	0.021
Square	3	3.88	1.30	4.87	0.024	80.41	28.00	0.39	0.762
x_1^2 (MP^2)	1	3.36	2.63	9.86	0.011	0.77	1.53	0.02	0.887
x_2^2 (SFR^2)	1	0.27	0.38	1.42	0.261	31.10	53.16	0.74	0.409
x_3^2 (AFP^2)	1	0.25	0.25	0.94	0.354	48.54	47.58	0.66	0.434
Interaction	3	0.18	0.06	0.22	0.879	101.47	33.82	0.47	0.709
x_1x_2 (MP*SFR)	1	0.02	0.02	0.09	0.773	0.92	0.88	0.01	0.914
x_1x_3 (MP*AFP)	1	0.15	0.15	0.58	0.464	98.55	99.40	1.39	0.266
x_2x_3 (SFR*AFP)	1	0.00	0.00	0.00	0.998	2.00	2.00	0.03	0.871
Residual Error	10	2.66	0.27			716.95	71.69		
Total	19	55.71				5942.27			

DF = degrees of freedom, Seq SS = sequential sums of squares, Adj MS = Adjusted mean squares

From Table 4.14, the calculated F-values of grade and recovery are shown to be 22.12 and 8.10 respectively, both higher than the F value from the F-statistics Table with P=0.05 ($F_{0.05(9,10)}$=3.14). Accordingly, it can be concluded that the regression models are considered acceptable and fit well. Moreover, the *p*-values (P) of the regression models which are 0.000 for grade and 0.002 for recovery are smaller than 0.05, thus these models are considered suitable for modelling the response behaviours.

The experimental results and the predicted values which were produced using the models (Equations (4.5) and (4.6)) are tabulated in Table 4.15. As can be seen from these results, good agreements between experimental and predicted values are obtained. The R^2 value for the concentrate grade and the tungsten recovery are 0.95 and 0.88 respectively. From these values, it can be assumed that a good correlation was obtained, indicating a good fit by the model. The standard deviations of both the predicted models are 0.52 and 8.47 for grade and recovery respectively which are acceptable values.

Table 4.15 Observed and predicted values of grade and recovery

Run	Grade (%W)			Recovery (%)		
	Observed	Predicted	Residual	Observed	Predicted	Residual
1	5.40	5.60	-0.20	75.70	79.61	-3.91
2	4.25	4.75	-0.50	59.00	67.78	-8.78
3	7.23	7.29	-0.07	96.90	93.28	3.62
4	6.16	6.15	0.01	85.10	84.74	0.36
5	7.27	7.06	0.20	95.90	87.70	8.20
6	4.58	5.59	-1.01	63.70	79.33	-15.63
7	4.72	4.80	-0.08	66.30	69.60	-3.30
8	8.02	7.92	0.10	99.20	93.61	5.59
9	4.77	4.42	0.36	66.90	64.62	2.28
10	3.55	3.50	0.05	50.30	49.54	0.76
11	5.77	5.37	0.39	81.20	77.93	3.27
12	3.61	3.16	0.45	51.20	46.85	4.35
13	3.34	3.71	-0.37	47.50	47.36	0.14
14	3.95	4.16	-0.21	55.70	61.46	-5.76
15	9.88	9.81	0.21	99.40	107.32	-7.92
16	6.25	5.55	0.70	88.50	78.59	9.91
17	5.66	5.59	0.08	80.90	79.30	1.60
18	5.85	5.56	0.29	83.80	78.72	5.08
19	7.84	8.03	-0.19	99.40	99.29	0.11
20	5.52	5.58	-0.06	79.10	79.07	0.03

The normal probability plot of the residuals and the plot of the residuals versus the predicted response for both the concentrate grade and tungsten recovery are presented in Figure 4.11 and Figure 4.12, respectively. Figure 4.11 shows that the residuals generally lie on a straight line, which indicates that errors are distributed normally. From Figure 4.12 it can be seen that the residuals scatter randomly, suggesting that the predictions of the models are adequate.

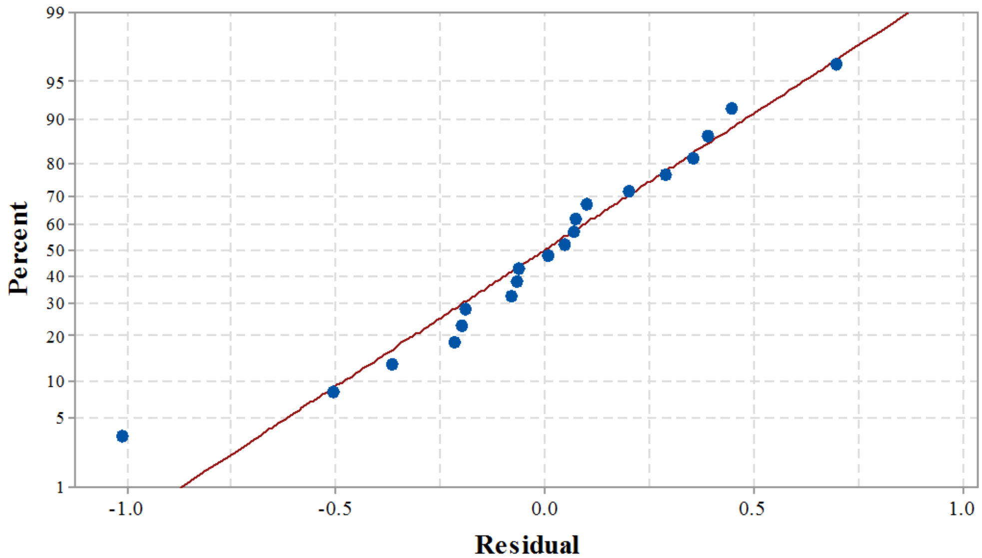

(a) Normal probability plot of residuals for grade

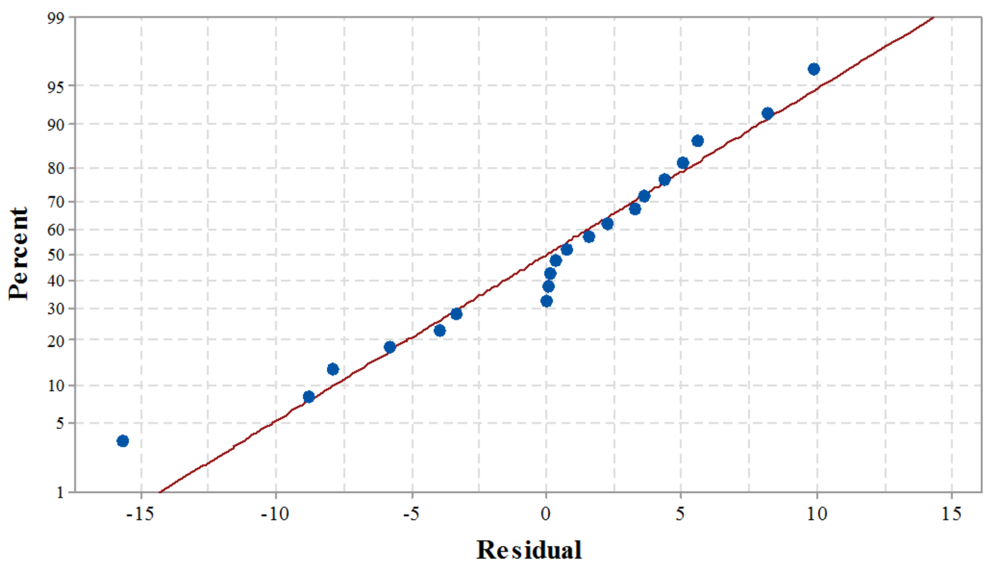

(b) Normal probability plot of residuals for recovery

Figure 4.11 Normal probability plot of residuals for grade (a) and recovery (b) (-212+150 μm)

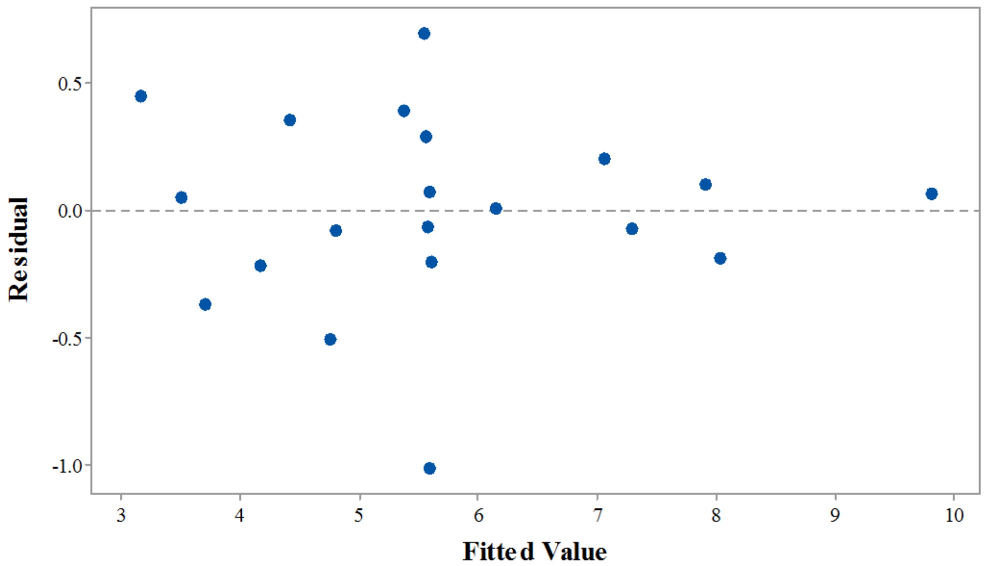

(a) Plot of residuals versus fitted response for grade

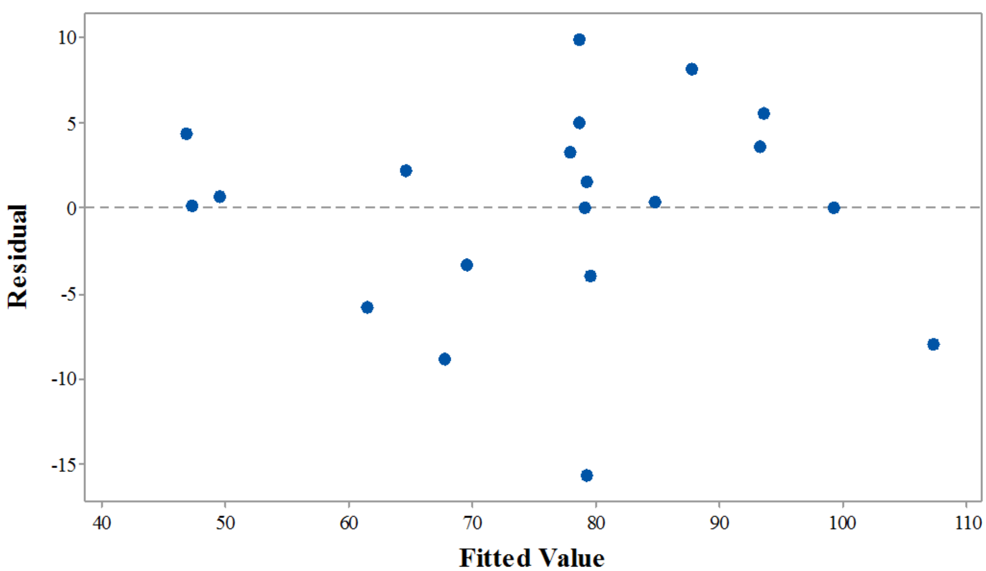

(b) Plot of residuals versus fitted response for recovery

Figure 4.12 Plot of residuals versus predicted response for grade (a) and recovery (b) (-212+150 µm)

In Table 4.16, estimated regression coefficients, factor effects (T) of the models and associated *p*-values (P) for responses are presented.

From Table 4.16 it can be seen that the factor effects (T) of motor power (x_1) for grade and recovery are 12.96 and 7.78, respectively and the sign of each coefficient is negative. This means that the response y_1 (concentrate grade) and y_2 (tungsten recovery) were significantly affected by a negative linear effect of motor powers (x_1), with a p-value of 0.000 for both y_1 and y_2, as seen from the Table 4.14 and Table 4.15. The responses (y_1 and y_2) were also affected by a positive linear effect of air fluidizing pressure (x_3) due to their positive coefficients, 3.84 and 2.74, with a p-value of 0.003 and 0.021, respectively.

Table 4.16 Coefficients, factor effects and associated p-values for responses

Term	Grade (y_1)			Recovery (y_2)		
	Coef	T	P	Coef	T	P
x_1	-1.813	-12.96	**0.000**	-17.86	-7.78	**0.000**
x_2	-0.198	-1.32	0.216	-3.17	-1.29	0.226
x_3	0.598	3.84	**0.003**	7.01	2.74	**0.021**
x_1^2	0.435	3.14	**0.011**	-0.33	-0.15	0.887
x_2^2	-0.168	-1.19	0.261	-1.99	-0.86	0.409
x_3^2	-0.141	-0.97	0.354	-1.94	-0.81	0.434
x_1x_2	-0.060	-0.30	0.773	0.37	0.11	0.914
x_1x_3	0.164	0.76	0.464	4.17	1.18	0.266
x_2x_3	-0.001	0.00	0.998	-0.67	-0.17	0.871

Additionally, T value of the quadratic term of motor power (x_1^2) for grade is 3.14, and the sign of the value is positive, which means that it has a positive quadratic effect on the grade and recovery.

In order to obtain a better understanding of the results and for optimization, the predicted models are presented in Figure 4.13 and Figure 4.14 as contour plots.

As can be seen, Figure 4.13 (a) shows the concentrate grade is significantly affected by decreasing the motor power. However, the solid feed rate has very little effect on the grade. It can also be seen that a high grade can be achieved by maintaining the motor power under 30%. Figure 4.13 (b) shows the effect of motor power and air fluidizing pressure on concentrate grade at the centre of solid feed rate. From the Figure 4.13 (b) it is observed that the concentrate grade depends mainly on the motor power. The air fluidizing pressure does not affect the concentrate grade. The limited effect of solid feed rate can be seen in Figure 4.13 (c).

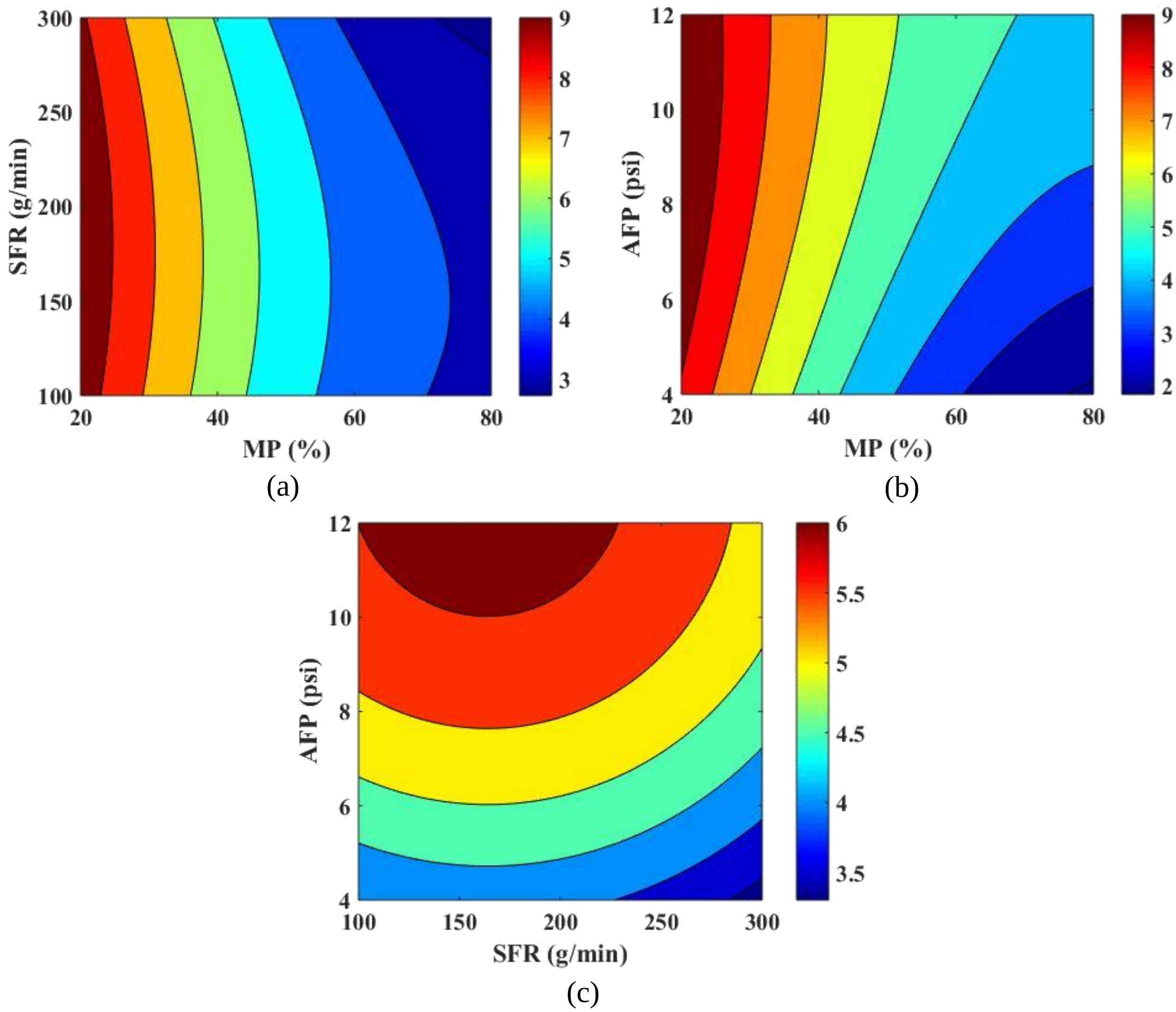

Figure 4.13 Response surface plots for concentrate grade. (a) Motor power and solid feed rate (b) motor power and air fluidizing pressure (c) solid feed rate and air fluidizing pressure (-212+150 μm)

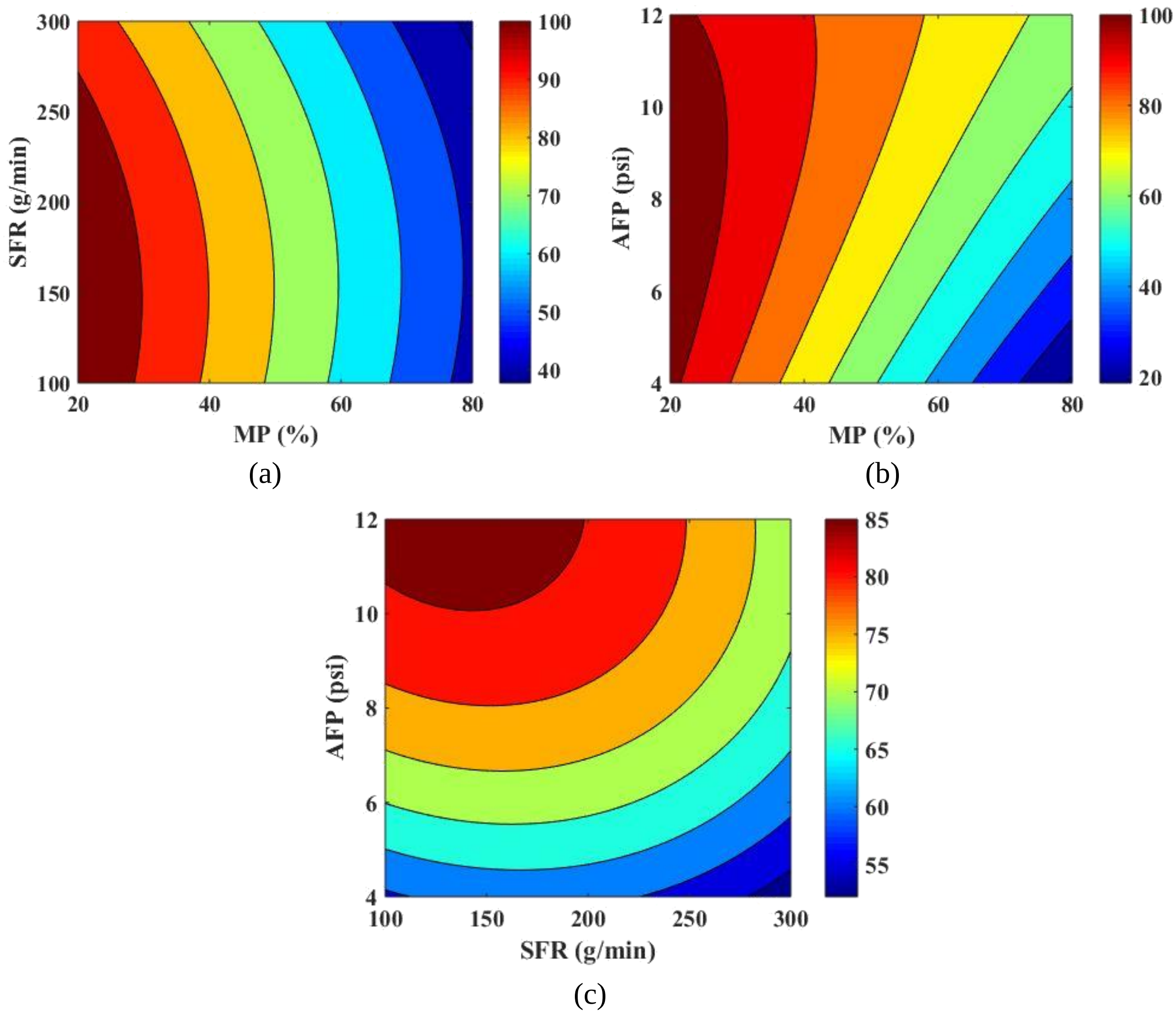

Figure 4.14 Response surface plots for tungsten recovery. (a) Motor power and solid feed rate (b) motor power and air fluidizing pressure (c) solid feed rate and air fluidizing pressure (-212+150 μm)

As seen from Figure 4.14 (a), tungsten recovery is affected mainly by motor power while the solid feed rate has very little effect on the tungsten recovery. For a high recovery the motor power should be set below 30% and the solid feed rate between 100 and 280 g/min. Figure 4.14 (b) shows that a high recovery can be achieved with the motor power under 27% no matter what the air fluidizing pressure is. The insignificant effect of solid feed rate can be seen from Figure 4.14 (c), the air fluidizing pressure should be higher to achieve a higher recovery.

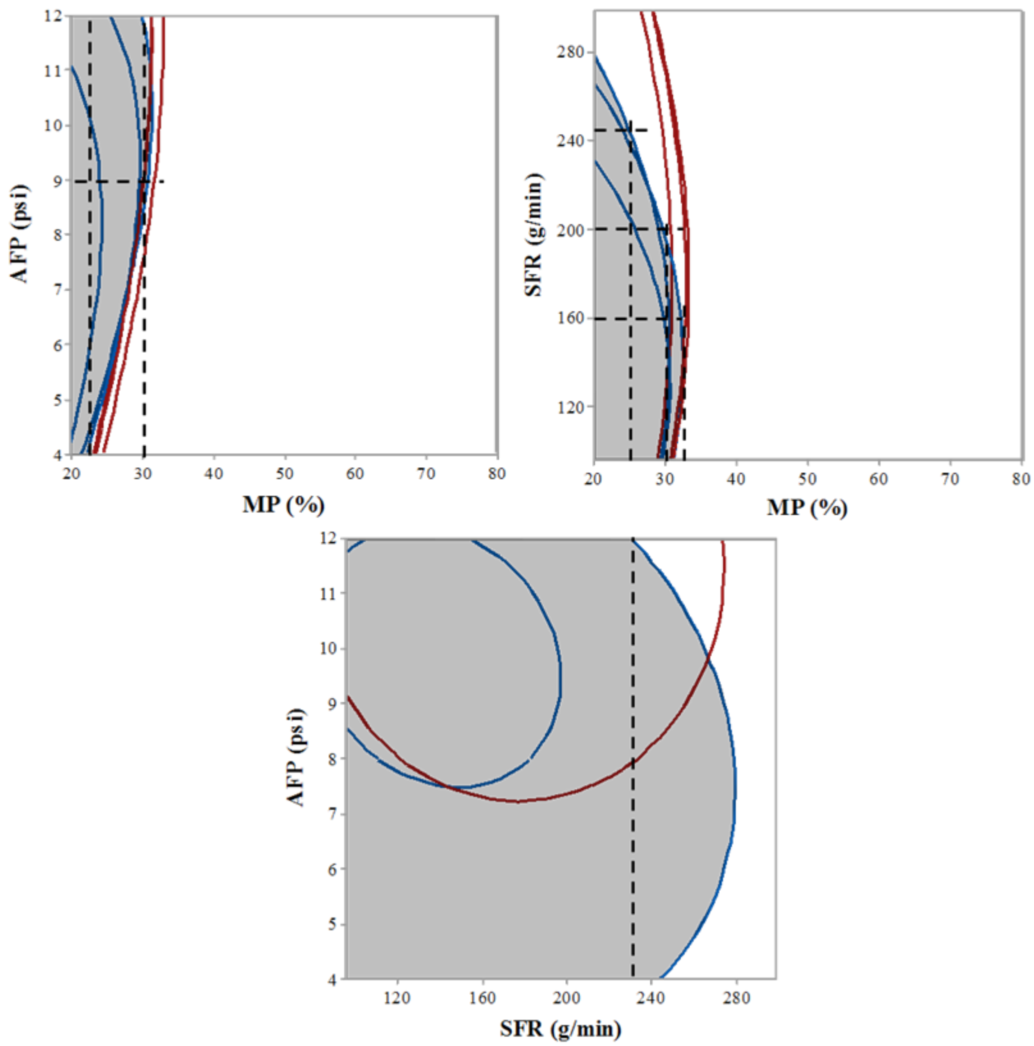

Figure 4.15 Optimum process conditions from overlaid contours (-212+150 μm)

From the overlaid contour plots of MP/AFP (Figure 4.15), it can be seen that under 23% MP, AFP does not affect the responses; however, when AFP is over 9 psi, high responses can be achieved. The overlaid plots of MP/SFR shows that under 25% MP, SFR does not have any effect on responses. When the MP becomes higher, the SFP should be low. For 30% MP, SFR under 200g/min is ideal. For 32% MP, SFR should be under 160 g/min. As for the plots of SFR/AFP, AFP does not affect the responses when SFR is under 230 g/min.

The optimum condition are 20%-30% for motor power, over 9 psi for air fluidizing pressure and 100-200 g/min for solid feed rate. The results of overlaid contours correspond well with the previous optimum operating ranges from contour and surface plots.

To determine the optimum condition, a response optimizer function was used. For the scenarios, target recoveries were set as 99.9% and 99.99%. The scenarios and the solutions are shown in Table 4.17 and Table 4.18.

Table 4.17 Response optimizer conditions

Condition	Response	Goal	Lower	Target	Upper
1	REC %	Target	90	99.9	100
2			95	99.99	100

Table 4.18 Response optimizer solutions

Solution		MP	SFR	AFP	REC % Fit	Composite Desirability
LS 1	1	20	96	4	99.90	1.00000
	2	28	96	12	99.90	1.00000
LS 2	1	20	96	4	99.99	1.00000
	2	28	96	12	99.99	1.00000
	3	20	273	8	99.99	1.00000
GLS		23.2	131.4	8		

The mean values of the parameters of the local solutions were calculated and shown in Table 4.18 as the global solution. Due to the precision control difficulty of the equipment, 30% rather than 23.2% was chosen as the optimum condition for motor power. 200 g/min for feed rate and 10 psi for the air fluidising pressure replaced 131.4 g/min and 8 psi respectively.

4.4. **-150+106 μm size fraction**

After running 20 experiments, the response variables (grade and recovery) were calculated and listed as shown in Table 4.19.

Table 4.19 Result of concentrate grade and tungsten recovery. MP = Motor power, SFR = Solid feed rate, AFP = Air fluidizing pressure

Run	Variables			Response	
	MP (%)	SFR (g/min)	AFP (psi)	Grade (%W)	Recovery (%)
1	50	184.6	8	6.53	98.0
2	50	300.0	8	6.33	96.1
3	32	130.4	6	7.76	93.8
4	50	230.8	12	7.04	99.5
5	32	241.9	6	7.93	96.4
6	50	195.4	8	7.28	97.8
7	68	137.3	10	6.58	91.2
8	32	277.8	10	8.55	91.8
9	68	240.0	10	6.19	82.5
10	68	151.5	6	5.15	75.8
11	50	83.7	8	7.03	96.2
12	68	253.2	6	3.67	53.6
13	80	155.0	8	3.81	59.0
14	50	198.0	4	5.96	84.8
15	20	185.8	8	11.37	97.6
16	50	210.5	8	6.70	93.1
17	50	185.2	8	6.59	92.2
18	50	184.1	8	6.52	92.1
19	32	138.9	10	8.57	97.0
20	50	187.5	8	6.52	93.3

The model equations produced from coded values of factor levels for the grade (y_1) of the concentrate and recovery (y_2) of the tungsten fraction are presented in Equations (4.7) and (4.8) respectively.

$$y_1 = 6.72 - 1.79x_1 - 0.20x_2 + 0.58x_3 + 0.24x_1^2 - 0.08x_2^2 - 0.07x_3^2 - 0.13x_1x_2 + 0.33x_1x_3 - 0.002x_2x_3 \quad \textbf{(4.7)}$$

$$y_2 = 94.48 - 11.20x_1 - 2.53x_2 + 5.40x_3 - 7.12x_1^2 - 0.46x_2^2 - 0.97x_3^2 - 3.11x_1x_2 + 6.36x_1x_3 + 0.12x_2x_3 \quad \textbf{(4.8)}$$

In order to estimate the significance of the developed models, ANOVA was applied as shown in Table 4.20.

Table 4.20 ANOVA table for grade and recovery

Source	DF	Grade (y_1)				Recovery (y_2)			
		Seq SS	Adj MS	F	P	Seq SS	Adj MS	F	P
Regression	9	48.31	5.37	12.28	0.000	2787.37	309.71	12.18	0.000
Linear	3	46.25	14.28	32.65	0.000	1835.24	621.61	24.45	0.000
x_1 (MP)	1	41.86	39.15	89.55	0.000	1450.73	1527.56	60.07	0.000
x_2 (SFR)	1	0.55	0.53	1.22	0.296	35.55	88.25	3.47	0.092
x_3 (AFP)	1	3.84	3.64	8.33	0.016	348.96	317.48	12.49	0.005
Square	3	1.28	0.36	0.83	0.506	647.61	231.54	9.11	0.003
x_1^2 (MP^2)	1	1.09	0.79	1.81	0.208	630.63	693.57	27.27	0.000
x_2^2 (SFR^2)	1	0.13	0.13	0.29	0.599	4.19	3.95	0.16	0.702
x_3^2 (AFP^2)	1	0.07	0.06	0.14	0.720	12.78	11.40	0.45	0.518
Interaction	3	0.77	0.26	0.58	0.639	304.53	101.51	3.99	0.042
x_1x_2 (MP*SFR)	1	0.14	0.15	0.34	0.571	75.83	78.76	3.10	0.109
x_1x_3 (MP*AFP)	1	0.62	0.62	1.43	0.259	228.62	228.58	8.99	0.013
x_2x_3 (SFR*AFP)	1	0.00	0.00	0.00	0.994	0.08	0.08	0.00	0.956
Residual Error	10	4.37	0.44			254.29	25.43		
Total	19	52.68				3041.66			

DF = degrees of freedom, Seq SS = sequential sums of squares, Adj MS = Adjusted mean squares

From Table 4.20, the calculated F-values of grade and recovery are shown to be 12.28 and 12.18 respectively, which means that the regression models are considered acceptable and fit well. Moreover, the *p*-values (P) of the regression models, which are 0.000 for both grade and recovery, are smaller than 0.05, thus these models are considered suitable for modelling the response behaviours.

The experimental results and the predicted values which were produced using the models (Equations (4.7) and (4.8)) are tabulated in Table 4.21. The R^2 values for the concentrate grade and the tungsten recovery are both 0.92. From these values, it can be assumed that a good correlation was obtained, indicating a good fit of the model. The standard deviations of both the predicted models are 0.66 and 5.04 for grade and recovery respectively which are acceptable values.

Table 4.21 Observed and predicted values of grade and recovery

Run	Grade (%W)			Recovery (%)		
	Observed	Predicted	Residual	Observed	Predicted	Residual
1	6.53	6.76	-0.23	98.00	95.11	2.89
2	6.33	6.15	0.18	96.10	88.91	7.19
3	7.76	8.47	-0.71	93.80	97.47	-3.67
4	7.04	7.37	-0.32	99.50	99.48	0.02
5	7.94	8.43	-0.50	96.40	98.83	-2.43
6	7.28	6.73	0.55	97.80	94.67	3.13
7	6.58	6.13	0.45	91.20	90.53	0.67
8	8.55	8.70	-0.15	91.80	97.11	-5.31
9	6.19	5.61	0.58	82.50	81.22	1.28
10	5.15	4.55	0.60	75.80	69.71	6.09
11	7.03	6.78	0.25	96.20	97.65	-1.45
12	3.67	3.97	-0.30	53.60	59.77	-6.17
13	3.81	4.66	-0.84	59.00	61.11	-2.11
14	5.96	5.55	0.41	84.80	82.75	2.05
15	11.37	10.40	0.97	97.60	92.50	5.10
16	6.71	6.68	0.03	93.10	94.02	-0.92
17	6.59	6.76	-0.17	92.20	95.08	-2.88
18	6.52	6.76	-0.24	92.10	95.12	-3.02
19	8.57	8.89	-0.32	97.00	95.76	1.24
20	6.52	6.75	-0.23	93.30	94.99	-1.69

The normal probability plot of the residuals and the plot of the residuals versus the predicted response for both the concentrate grade and tungsten recovery are presented in Figure 4.16 and Figure 4.17, respectively. Figure 4.16 shows that the residuals generally lie on a straight line, which indicates that errors are distributed normally. From Figure 4.17 it can be seen that the residuals scatter randomly, suggesting that the predictions of the models are adequate.

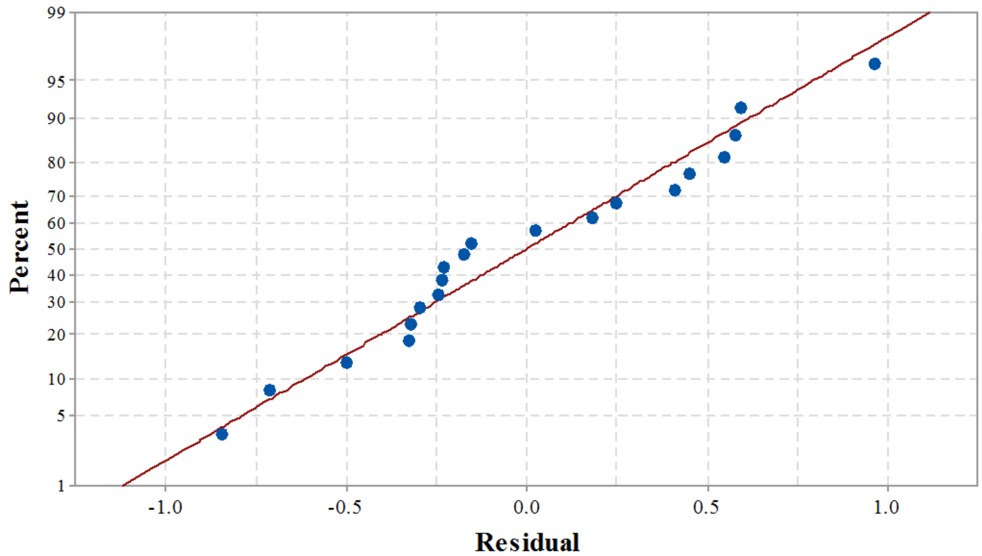

(a) Normal probability plot of residuals for grade

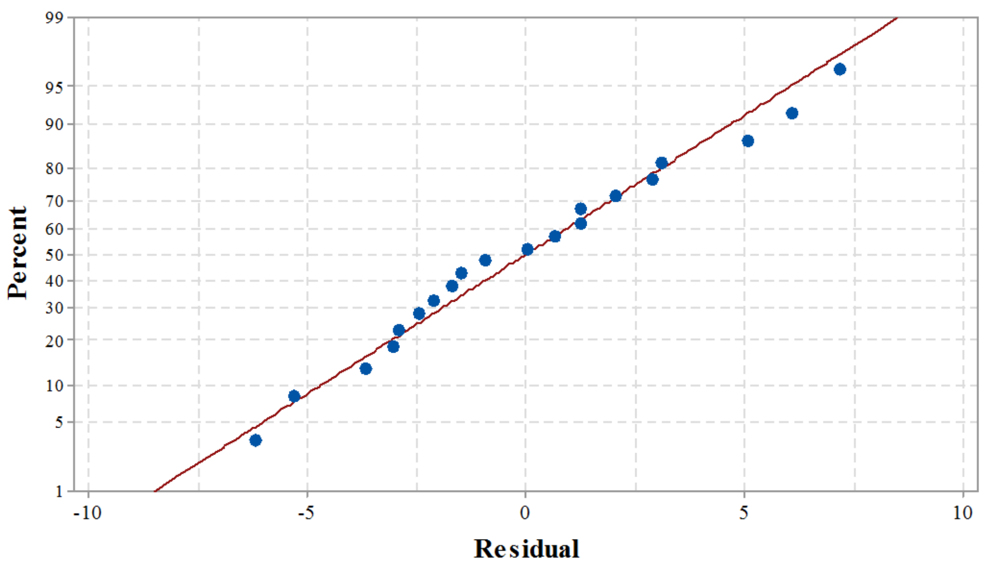

(b) Normal probability plot of residuals for recovery

Figure 4.16 Normal probability plot of residuals for grade (a) and recovery (b)

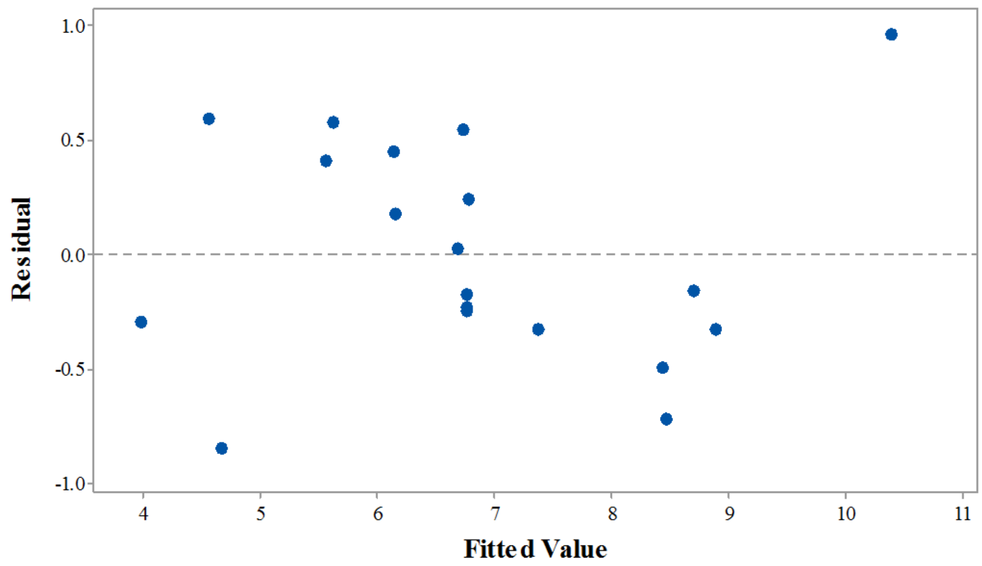

(a) Plot of residuals versus fitted response for grade

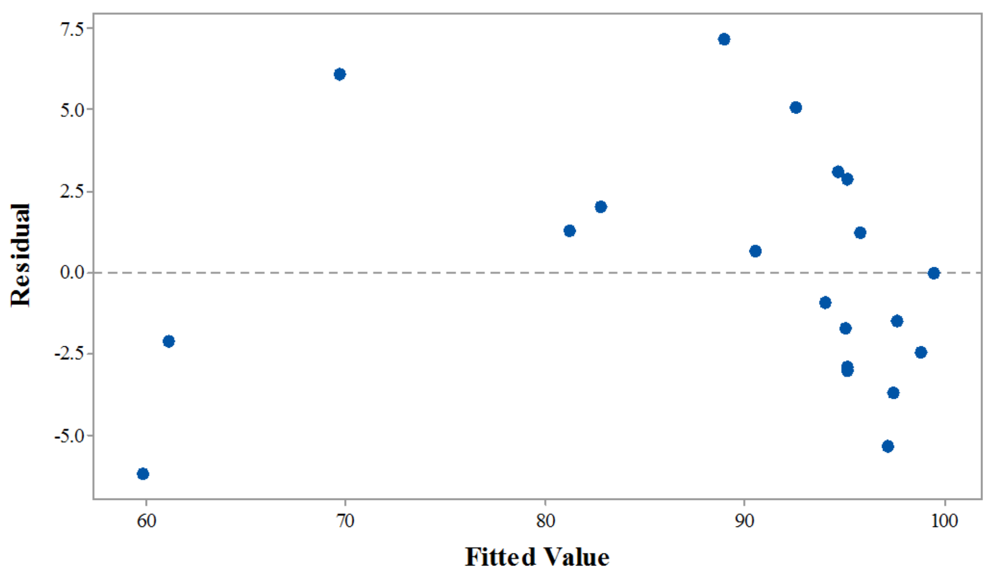

(b) Plot of residuals versus fitted response for recovery

Figure 4.17 Plot of residuals versus predicted response for grade (a) and recovery (b)

In Table 4.22, estimated regression coefficients, factor effects (T) of the models and associated *p*-values (P) for responses are presented.

Table 4.22 Coefficients, factor effects and associated *p*-values for responses

Term	Grade (y_1)			Recovery (y_2)		
	Coef	T	P	Coef	T	P
x_1	-1.792	-9.46	**0.000**	-11.20	-7.75	**0.000**
x_2	-0.196	-1.10	0.296	-2.53	-1.86	0.092
x_3	0.578	2.89	**0.016**	5.40	3.53	**0.005**
x_1^2	0.241	1.35	0.208	-7.12	-5.22	**0.000**
x_2^2	-0.084	-0.54	0.599	-0.46	-0.39	0.702
x_3^2	-0.070	-0.37	0.720	-0.97	-0.67	0.518
x_1x_2	-0.136	-0.59	0.571	-3.11	-1.76	0.109
x_1x_3	0.333	1.20	0.259	6.36	3.00	**0.013**
x_2x_3	0.002	0.01	0.994	0.12	0.06	0.956

From Table 4.22, it can be seen that the factor effects (T) of motor power (x_1) for grade and recovery are 9.46 and 7.75, respectively and the sign of each coefficient is negative. This means that the response y_1 (concentrate grade) and y_2 (tungsten recovery) were significantly affected by a negative linear effect of motor powers (x_1), with a *p*-value of 0.000 for both y_1 and y_2, as seen from the Table 4.20and Table 4.21The responses (y_1 and y_2) were also affected by a positive linear effect of air fluidizing pressure (x_3) due to their positive coefficients, 2.89 and 3.53, with a *p*-value of 0.016 and 0.005, respectively.

Additionally, T value of the quadratic term of motor power (x_1^2) for recovery is 5.22, and the sign of the value is negative. This means that it has a negative quadratic effect on the grade and recovery.

The T value of the interaction term of motor power and fluidizing air pressure (x_1x_3) for recovery is 3.00 with the positive sign, which means it has a negative interactive effect on recovery.

In order to obtain a better understanding of the results and for optimization, the predicted models are presented in Figure 4.18 and Figure 4.19 as contour plots.

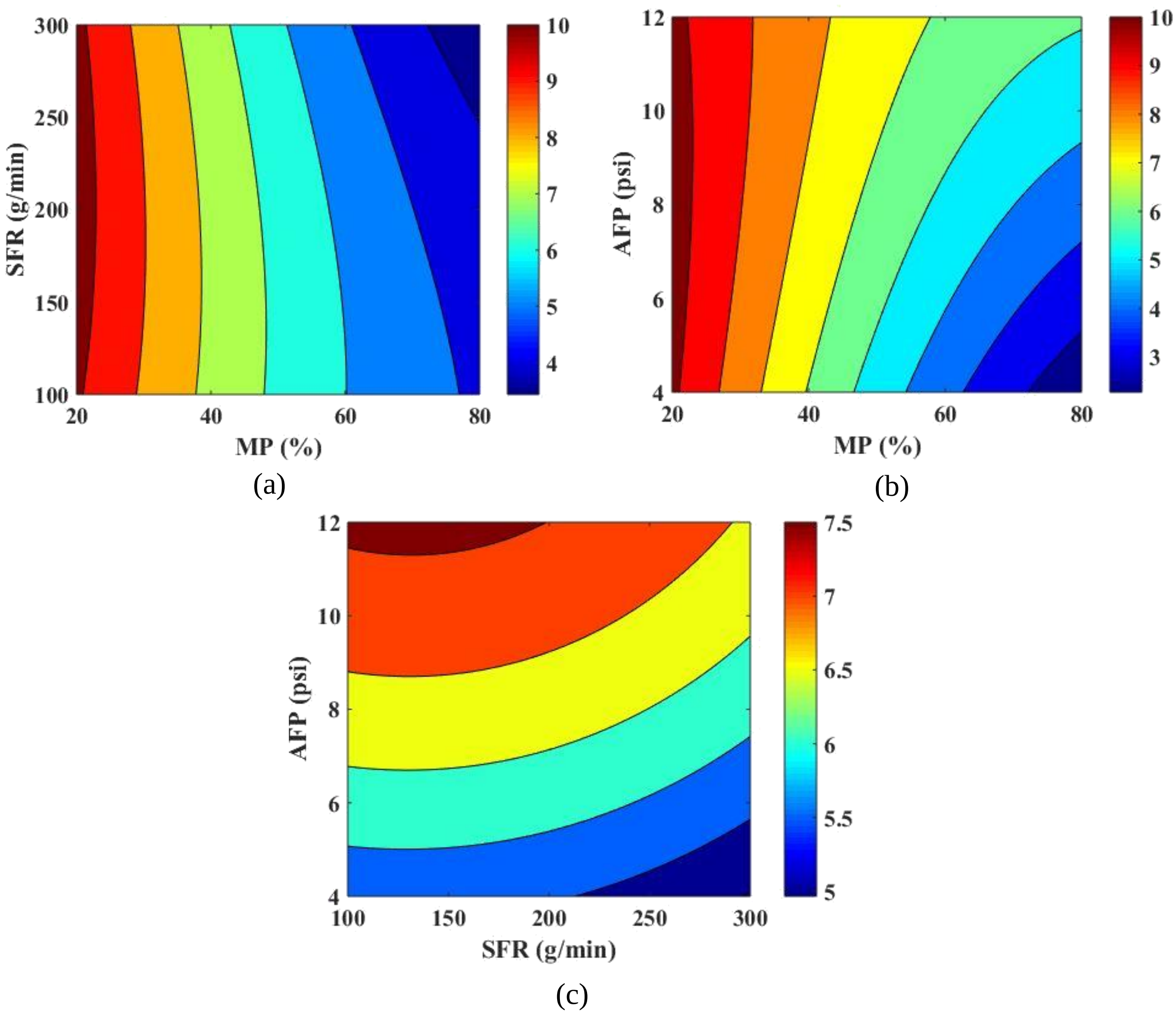

Figure 4.18 Response surface plots for concentrate grade. (a) Motor power and solid feed rate (b) motor power and air fluidizing pressure (c) solid feed rate and air fluidizing pressure (-150+106 μm)

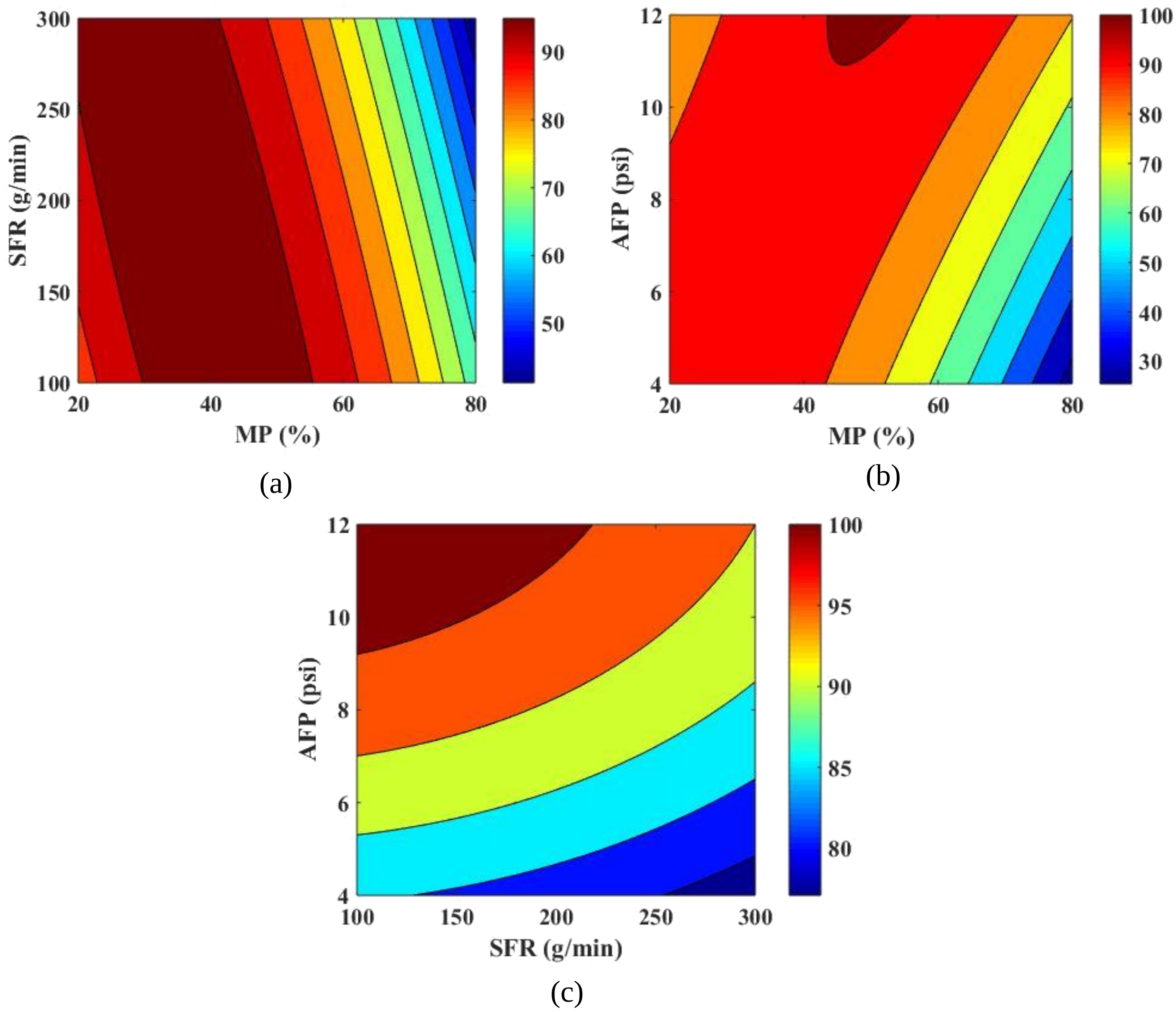

Figure 4.19 Response surface plots for tungsten recovery. (a) Motor power and solid feed rate (b) motor power and air fluidizing pressure (c) solid feed rate and air fluidizing pressure (-150+106 µm)

Figure 4.18 (a) shows that the concentrate grade significantly increased by decreasing the motor power. However, the solid feed rate does not affect the grade. It can also be seen that a high grade can be achieved by maintaining the motor power under 30%. From the Figure 4.18 (b), it is observed that the concentrate grade depends mainly on the motor power. The motor power decreased while concentrate grade increased. And the air fluidising pressure does not affect the concentrate grade. The limited effect of solid feed rate can be seen in Figure 4.18 (c) and the concentrate grade increases with the increasing air fluidising pressure.

As seen from Figure 4.19 (a), to achieve a high tungsten recovery the motor power should be set between 24% and 63%. The solid feed rate still does not affect the recovery. Figure 4.19 (b) shows both the motor power and the air fluidizing pressure are important It can be seen that a high recovery of tungsten can be achieved with the motor power under 27 and the air fluidizing pressure below 5.5 psi or the motor power between 35% and 55% and the air fluidizing pressure over 8.5 psi. The insignificant effect of solid feed rate can be seen from Figure 4.19 (c). The recovery increased by increasing the air pressure. For a high recovery, the air should over 8.5 psi and the solid feed rate should below 240 g/min.

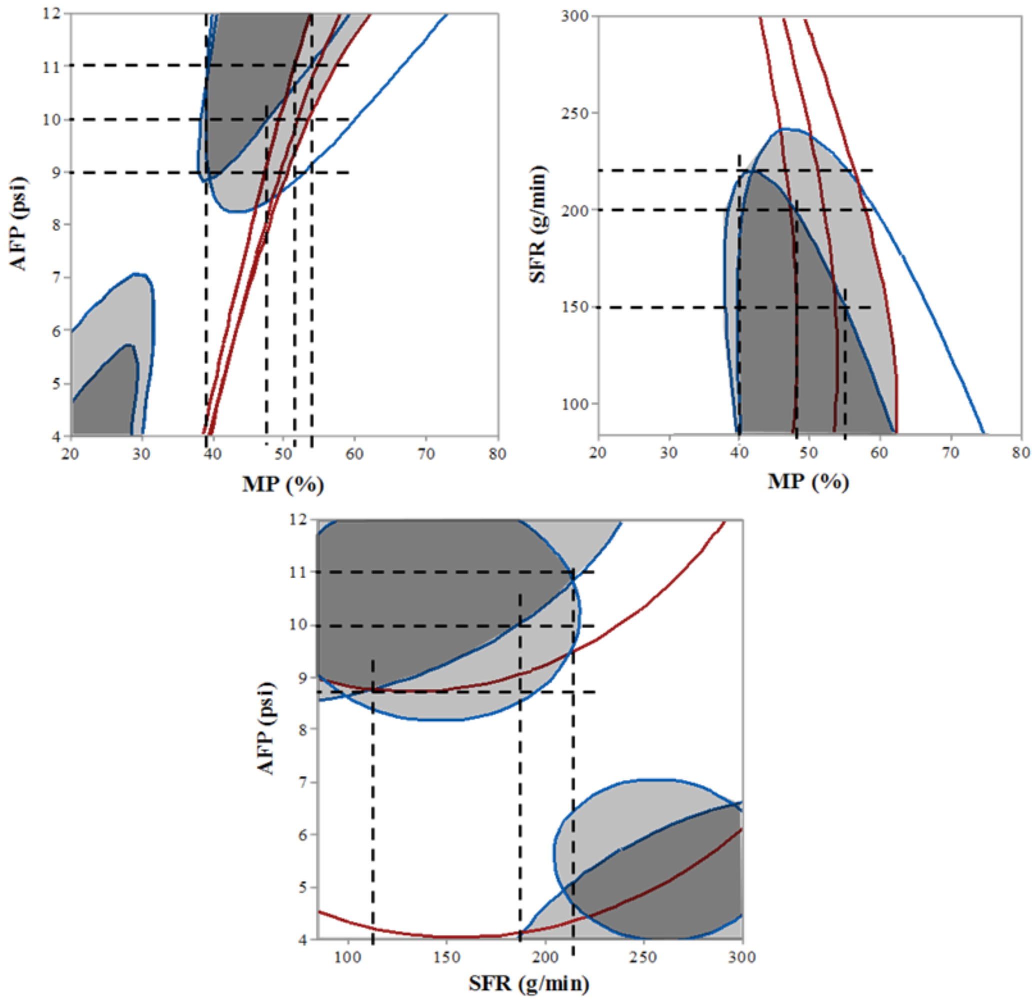

Figure 4.20 Optimum process conditions from overlaid contours (-150+106 µm)

In Figure 4.20, from the overlaid contour plots of MP/AFP, it can be seen that for higher MP between 40-52%, AFP should be over 9 psi, MP increases with the AFP at the same time. The overlaid plots of MP/SFR shows that MP should be 40-55%, while the SFP should below 220 g/min. The lower MP is, the higher SFP could reach. As for the plots of SFR/AFP, AFP could be low or high to achieve high responses. The optimum conditions are 40-55% for motor power, over 9 psi for air fluidizing pressure and 100-220 g/min for solid feed rate. The results of overlaid contours correspond well with the previous optimum operating ranges from contour and surface plots.

To determine the optimum condition, a response optimizer function was used. For the scenarios, target recoveries were set as 99.9% and 99.99%. The scenarios and the solutions are shown in Table 4.23 and Table 4.24.

Table 4.23 Response optimizer conditions

Condition	Response	Goal	Lower	Target	Upper
1	REC %	Target	90	99.9	100
2			95	99.99	100

Table 4.24 Response optimizer solutions

Solution		MP	SFR	AFP	REC % Fit	Composite Desirability
LS 1	1	52.04	83.70	9.15	99.90	1.00000
	2	43.94	209.58	12.00	99.90	1.00000
	3	61.74	171.75	12.00	99.90	1.00000
	4	50.00	200.00	11.06	99.90	1.00000
LS 2	1	55.35	204.37	12.00	99.99	1.00000
	2	73.22	83.70	12.00	99.99	1.00000
	3	45.90	83.70	8.94	99.99	1.00000
		48.73	199.01	10.96	99.99	1.00000
GLS		53.86	154.48	11.01		

The mean values of the parameters of the local solutions were calculated and shown in Table 4.24 as the global solution. Due to the precision control difficulty of the equipment, 50% rather than 53.86% was chosen as the optimum condition for motor power. 160 g/min for feed rate and 11 psi for the air fluidising pressure replaced 154.48 g/min and 11.01 psi respectively.

4.5. -106+75 μm size fraction

In this size fraction, 40 g -425+300 μm silica was mixed with 50 g -106+75 μm silica were fed before the synthetic ore.

After running 20 experiments, the response variables (grade and recovery) were calculated and listed as shown Table 4.25.

Table 4.25 Result of concentrate grade and tungsten recovery. MP = Motor power, SFR = Solid feed rate, AFP = Air fluidizing pressure

Run	Variables			Response	
	MP (%)	SFR (g/min)	AFP (psi)	Grade (%W)	Recovery (%)
1	50	181.4	8	7.79	98.80
2	50	297.1	8	7.87	98.70
3	32	135.7	6	8.27	98.50
4	50	169.1	12	7.79	98.20
5	32	227.7	6	8.41	98.10
6	50	169.6	8	7.81	98.60
7	68	124.8	10	7.14	94.00
8	32	260	10	9.80	98.60
9	68	232.8	10	6.86	90.70
10	68	181.4	6	6.13	85.30
11	50	99.5	8	7.76	98.40
12	68	207.3	6	6.19	85.10
13	80	212.9	8	5.83	80.40
14	50	201.3	4	7.22	95.60
15	20	214.4	8	9.89	98.10
16	50	202.6	8	7.89	99.10
17	50	186.3	8	7.90	99.10
18	50	171.4	8	7.77	99.00
19	32	137.1	10	9.64	98.90
20	50	172.9	8	7.95	98.90

The model equations produced from coded values of factor levels for the grade (y_1) of the concentrate and recovery (y_2) of the tungsten fraction are presented in Equations (4.9) and (4.10) respectively.

$$y_1 = 7.83 - 1.21x_1 + 0.03x_2 + 0.40x_3 + 0.01x_1^2 + 0.03x_2^2 - 0.11x_3^2 - 0.11x_1x_2 - 0.16x_1x_3 - 0.02x_2x_3 \quad \textbf{(4.9)}$$

$$y_2 = 98.57 - 5.07x_1 - 0.14x_2 + 1.32x_3 - 3.60x_1^2 - 0.03x_2^2 - 0.92x_3^2 - 0.59x_1x_2 + 1.94x_1x_3 - 0.64x_2x_3 \quad \textbf{(4.10)}$$

In order to estimate the significance of the developed models, ANOVA was applied as shown in Table 4.26.

Table 4.26 ANOVA table for grade and recovery

Source	DF	Grade (y_1)				Recovery (y_2)			
		Seq SS	Adj MS	F	P	Seq SS	Adj MS	F	P
Regression	9	22.62	2.51	37.71	0.000	590.13	590.13	43.66	0.000
Linear	3	22.22	7.12	106.81	0.000	383.20	364.10	80.81	0.000
x_1 (MP)	1	20.23	19.58	293.78	0.000	346.15	343.85	228.96	0.000
x_2 (SFR)	1	0.01	0.01	0.13	0.727	13.70	0.19	0.12	0.733
x_3 (AFP)	1	1.98	1.48	22.27	0.001	23.35	16.44	10.95	0.008
Square	3	0.19	0.06	0.93	0.460	181.53	183.89	40.82	0.000
x_1^2 (MP^2)	1	0.01	0.00	0.04	0.839	172.32	175.93	117.15	0.000
x_2^2 (SFR^2)	1	0.03	0.01	0.20	0.664	0.97	0.01	0.01	0.937
x_3^2 (AFP^2)	1	0.15	0.14	2.14	0.174	8.24	10.07	6.71	0.027
Interaction	3	0.22	0.07	1.08	0.401	25.41	25.41	5.64	0.016
x_1x_2 (MP*SFR)	1	0.07	0.07	1.04	0.331	2.93	1.85	1.23	0.293
x_1x_3 (MP*AFP)	1	0.14	0.14	2.12	0.176	21.20	21.22	14.13	0.004
x_2x_3 (SFR*AFP)	1	0.00	0.00	0.01	0.915	1.29	1.29	0.86	0.376
Residual Error	10	0.67	0.07			15.02	15.02		
Total	19	23.29				605.15			

DF = degrees of freedom, Seq SS = sequential sums of squares, Adj MS = Adjusted mean squares

From Table 4.26, the calculated F-values of grade and recovery are shown to be 37.71 and 43.66 respectively, both are higher than the F value founded from the F-statistics Table with P=0.05 ($F_{0.05(9,10)}$=3.14). Accordingly, it can be concluded that the regression models are considered acceptable and fit well. Moreover, the *p*-values (P) of the regression models which are 0.000 for both grade and recovery are smaller than 0.05, thus these models are considered suitable for modelling the response behaviours.

The experimental results and the predicted values which were produced using the models (Equations (4.9) and (4.10)) are tabulated in Table 4.27. As can be seen from these results, good agreements between experimental and predicted values are obtained. The R^2 value for the concentrate grade and the tungsten recovery are 0.97 and 0.98 respectively. From these values, it can be assumed that a good correlation was obtained, indicating a good fit by the model. The standard deviations of both the predicted models are 0.26 and 1.23 for grade and recovery respectively which are acceptable values.

Table 4.27 Observed and predicted values of grade and recovery

Run	Grade (%W)			Recovery (%)		
	Observed	Predicted	Residual	Observed	Predicted	Residual
1	7.79	7.82	-0.03	98.80	98.61	0.19
2	7.88	7.97	-0.09	98.70	98.26	0.44
3	8.27	8.39	-0.12	98.50	98.79	-0.29
4	7.80	8.20	-0.40	98.20	98.80	-0.60
5	8.41	8.60	-0.20	98.10	100.35	-2.25
6	7.81	7.82	-0.01	98.60	98.64	-0.04
7	7.14	6.92	0.22	94.00	93.46	0.54
8	9.80	9.62	0.18	98.60	98.71	-0.11
9	6.86	6.70	0.16	90.70	91.18	-0.48
10	6.13	6.37	-0.24	85.30	86.43	-1.13
11	7.76	7.87	-0.12	98.40	98.73	-0.33
12	6.19	6.34	-0.15	85.10	86.35	-1.25
13	5.83	5.80	0.03	80.40	79.61	0.80
14	7.22	6.85	0.37	95.60	93.76	1.85
15	9.89	9.96	-0.07	98.10	97.11	0.99
16	7.89	7.83	0.06	99.10	98.56	0.54
17	7.90	7.83	0.08	99.10	98.60	0.50
18	7.77	7.82	-0.05	99.00	98.63	0.37
19	9.64	9.35	0.28	98.90	98.89	0.01
20	7.95	7.82	0.12	98.90	98.63	0.27

The normal probability plot of the residuals and the plot of the residuals versus the predicted response for both the concentrate grade and tungsten recovery are presented in Figure 4.21 and Figure 4.22, respectively. Figure 4.21 shows that the residuals generally lie on a straight line, which indicates that errors are distributed normally. From Figure 4.22 it can be seen that the residuals scatter randomly, suggesting that the predictions of the models are adequate.

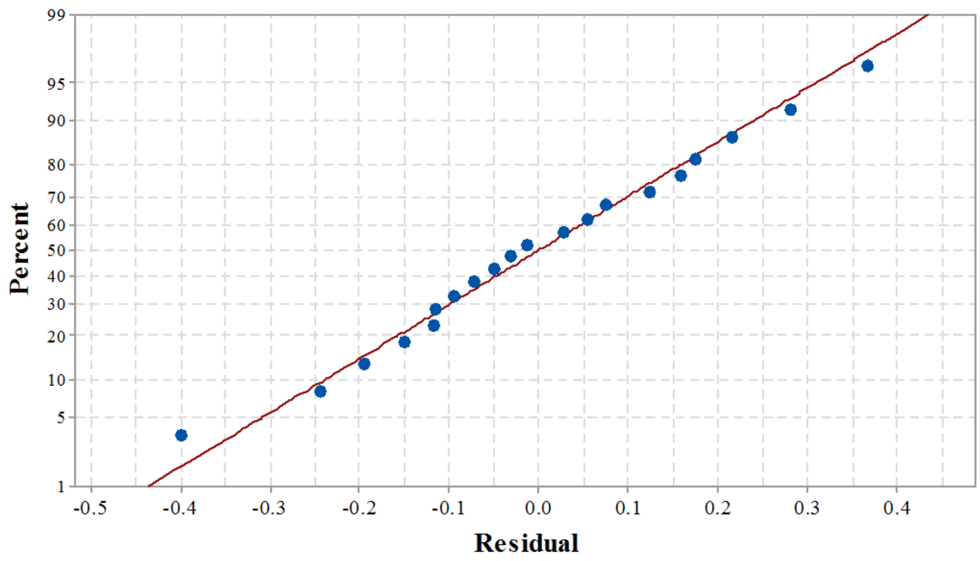

(a) Normal probability plot of residuals for grade

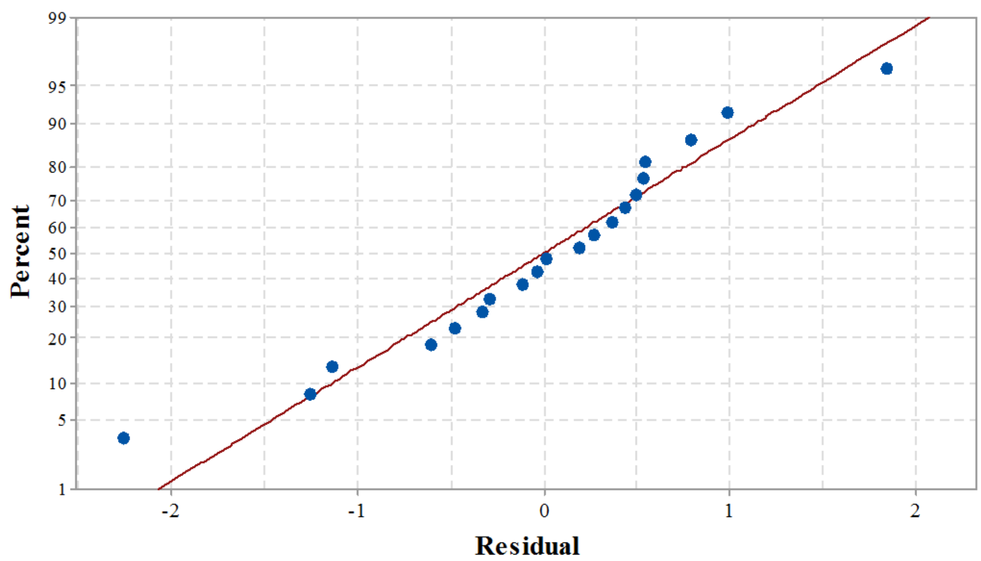

(b) Normal probability plot of residuals for recovery

Figure 4.21 Normal probability plot of residuals for grade (a) and recovery (b) (-106+75 µm)

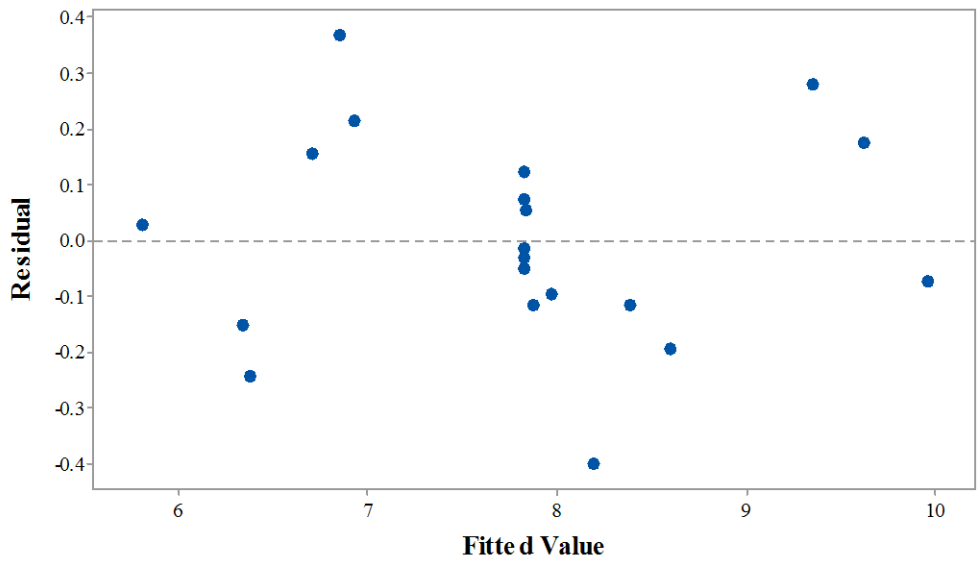

(a) Plot of residuals versus fitted response for grade

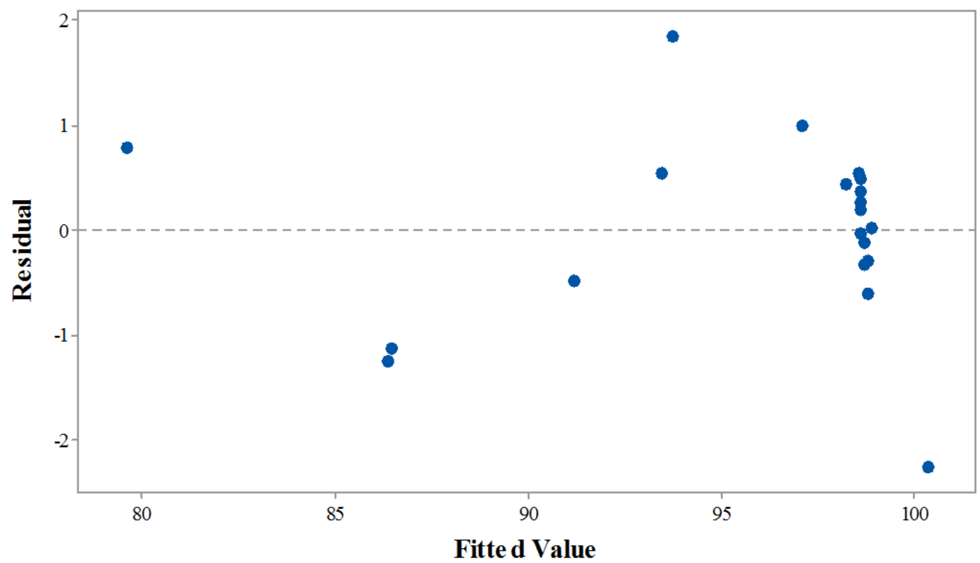

(b) Plot of residuals versus fitted response for recovery

Figure 4.22 Plot of residuals versus predicted response for grade (a) and recovery (b) (-106+75 µm)

In Table 4.28, estimated regression coefficients, factor effects (T) of the models and associated *p*-values (P) for responses are presented.

Table 4.28 Coefficients, factor effects and associated *p*-values for responses

Term	Grade (y_1)			Recovery (y_2)		
	Coef	T	P	Coef	T	P
x_1	-1.2098	-17.14	**0.000**	-5.069	-15.13	**0.000**
x_2	0.0307	0.36	0.727	-0.143	-0.35	0.733
x_3	0.3971	4.72	**0.001**	1.321	3.31	**0.008**
x_1^2	0.0147	0.21	0.839	-3.603	-10.82	0.000
x_2^2	0.033	0.45	0.664	-0.028	-0.08	0.937
x_3^2	-0.1099	-1.46	0.174	-0.924	-2.59	**0.027**
x_1x_2	-0.114	-1.02	0.331	-0.59	-1.11	0.293
x_1x_3	-0.158	-1.45	0.176	1.94	3.76	**0.004**
x_2x_3	-0.016	-0.11	0.915	-0.64	-0.93	0.376

From Table 4.28, it can be seen that the factor effects (T) of motor power (x_1) for grade and recovery are 17.14 and 15.13, respectively and the sign of each coefficient is negative. This means that the response y_1 (concentrate grade) and y_2 (tungsten recovery) were significantly affected by a negative linear effect of motor powers (x_1). The responses (y_1 and y_2) were also affected by a positive linear effect of air fluidizing pressure (x_3) due to their positive coefficients, 4.72 and 3.31 with a *p*-value of 0.001 and 0.008, respectively.

Additionally, the T value of the quadratic term of motor power (x_1^2) for recovery is 10.82 and the sign of the value is negative, which means that it has a negative quadratic effect on the recovery. Positive quadratic effects means that with a decreasing of the factors there will be a faster decrease in the response values. The quadratic term of air fluidizing pressure (x_3^2) also has a negative quadratic effect on the recovery as the T value is 2.59 with a negative sign.

The T value of the interaction term of motor power and fluidizing air pressure (x_1x_3) for recovery is 3.76 and the sign of the value is positive.

In order to obtain a better understanding of the results and for optimization, the predicted models are presented in Figure 4.23 and Figure 4.24 as contour plots.

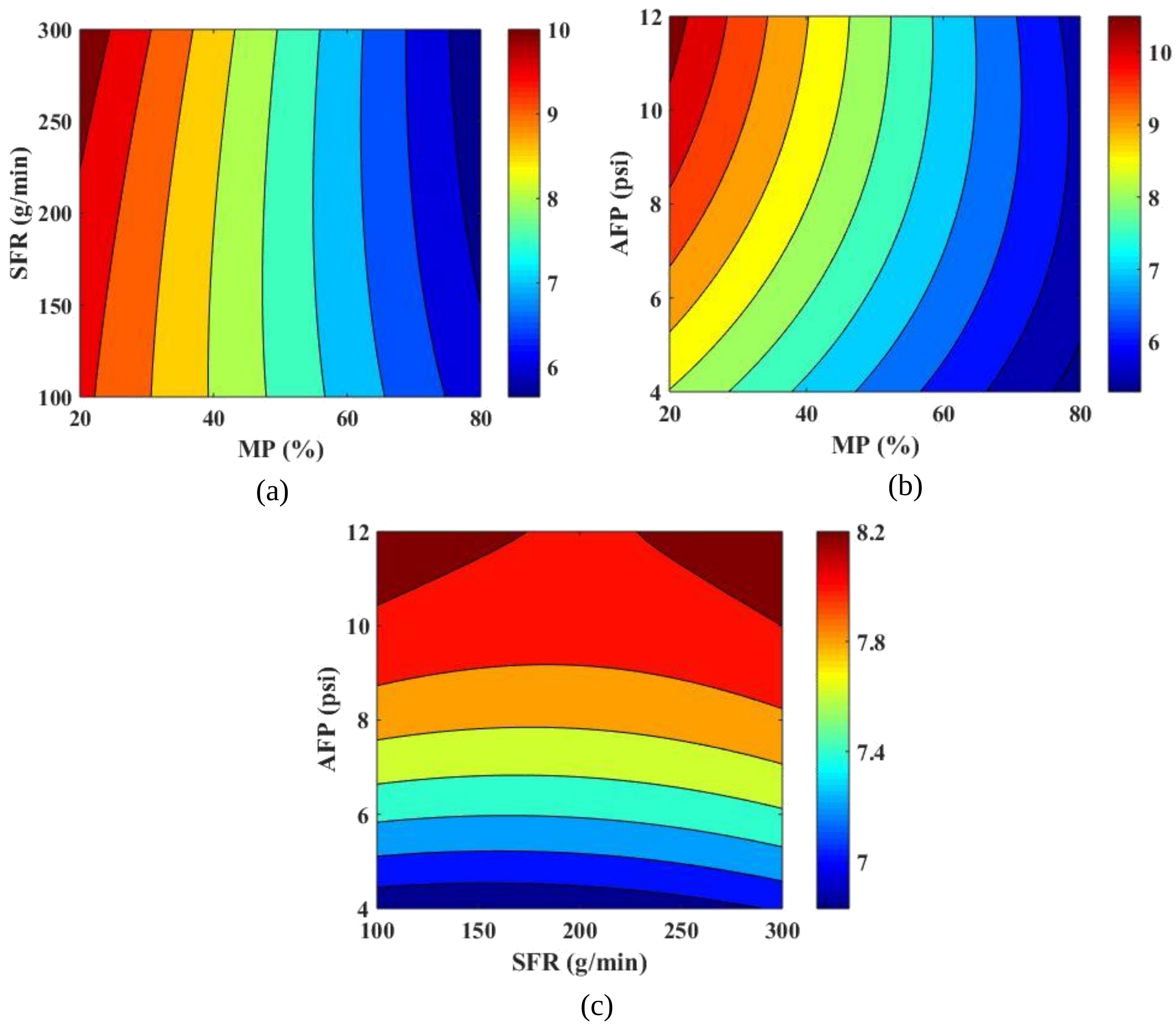

Figure 4.23 Response surface plots for concentrate grade. (a) Motor power and solid feed rate (b) motor power and air fluidizing pressure (c) solid feed rate and air fluidizing pressure (-106+75 µm)

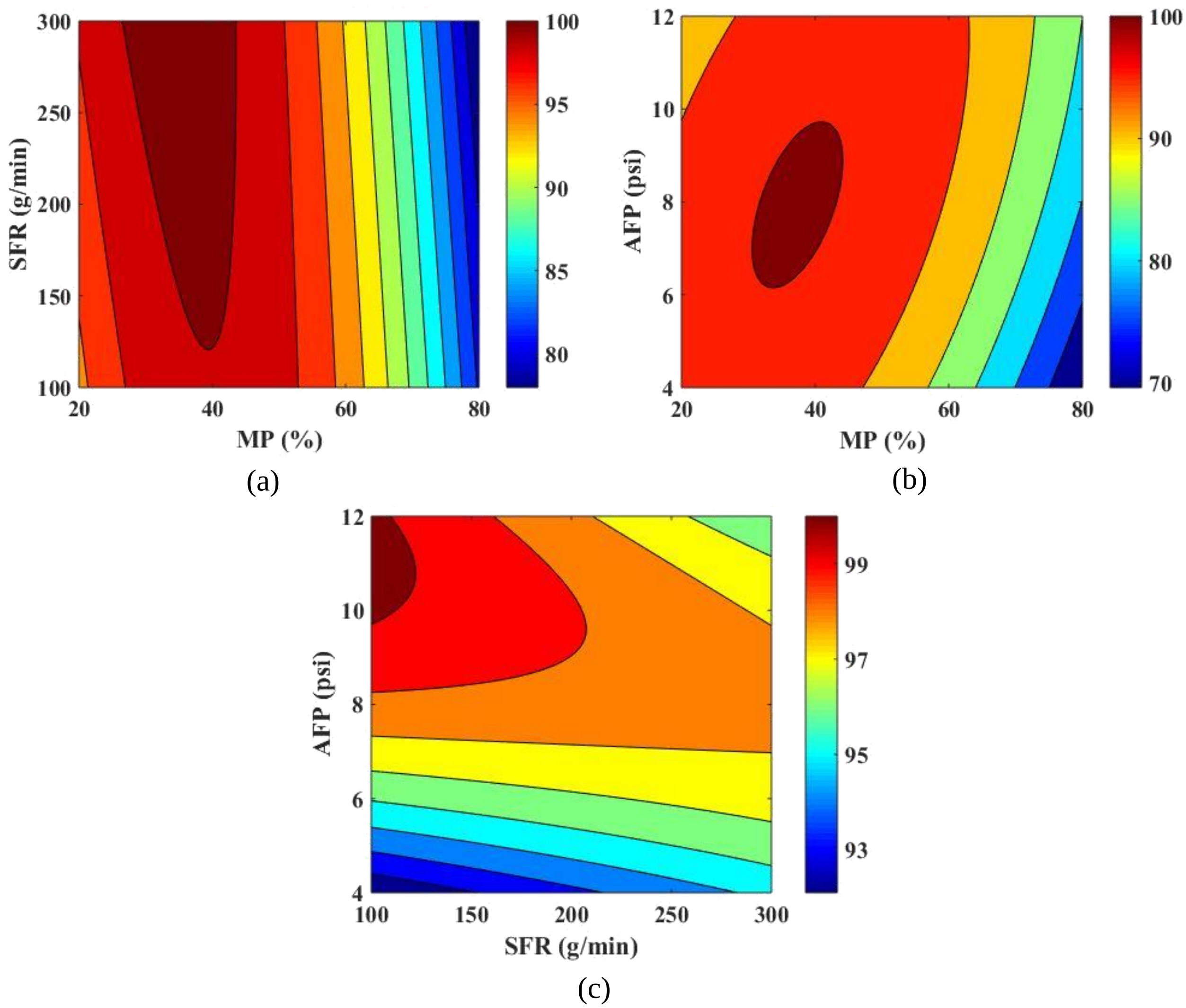

Figure 4.24 Response surface plots for tungsten recovery. (a) Motor power and solid feed rate (b) motor power and air fluidizing pressure (c) solid feed rate and air fluidizing pressure (-106+75 µm)

From Figure 4.23 (a), the concentrate grade is significantly affected by decreasing the motor power but the solid feed rate has little effect on the grade. It can also be seen that a high grade can be achieved by maintaining the motor power under 30% and no matter what the solid feed rate is. From Figure 4.23 (b) it is observed that when the motor power decreased and the air fluidizing pressure increased at the same time, the concentrate grade increased. Also, the limited effect of solid feed rate can be seen in Figure 4.23 (c); if one increases the air pressure, the concentrate grade will increase.

Figure 4.24 (a) shows that the tungsten recovery is affected by motor power. However, the solid feed rate has little effect on the tungsten recovery. To achieve high recovery, the motor power should be between 22-50%. From Figure 4.24 (b), both motor power and air fluidising pressure show their effect on recovery. For high recovery, motor power should between 24-50% while air fluidising pressure will be within 4.5-11 psi. The effect of solid feed rate can be seen from Figure 4.24 (c), the solid feed rate should be below 200 g/min. The range of the air fluidising pressure should be between 8.5 and 12 psi.

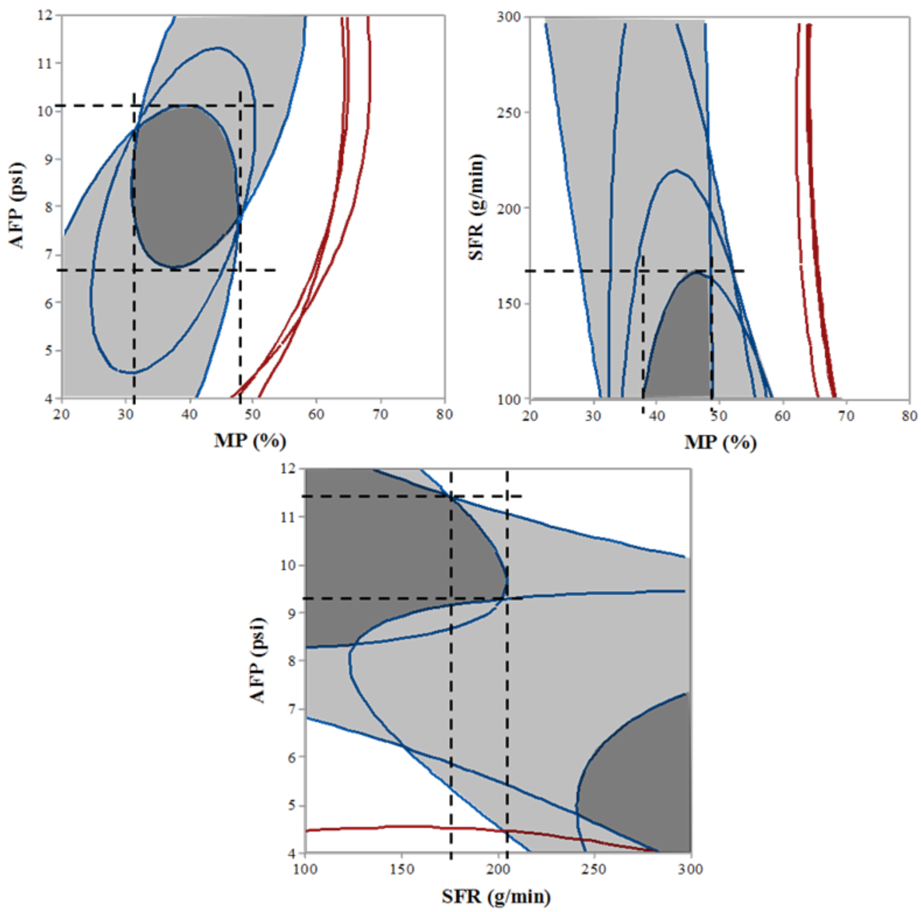

Figure 4.25 Optimum process conditions from overlaid contours (-106+75 µm)

From the overlaid contour plots of MP/AFP in Figure 4.25, high response area requires motor power to be within 32-48%, air fluidising pressure should be between 7 psi and 10 psi. The overlaid plots of MP/SFR shows that motor power should be within 37-48%, while the solid feed rate should be below 170 g/min. When the motor power decreases, the solid feed rate should decrease as well. As for the plots of SFR/AFP, air fluidising pressure should be high to achieve high recovery, from 9.5 to 11.5 psi. The range of solid feed rate will be very limited, from 175 to 200 g/min.

To determine the optimum condition, a response optimizer function was used. For the scenarios, target recoveries were set as 99.9% and 99.99%. The scenarios and the solutions are shown in Table 4.29 and Table 4.30.

Table 4.29 Response optimizer conditions

Condition	Response	Goal	Lower	Target	Upper
1	REC %	Target	90	99.9	100
2			95	99.99	100

Table 4.30 Response optimizer solutions

Solution		MP	SFR	AFP	REC % Fit	Composite Desirability
LS 1	1	50	113	12	99.90	1.00000
	2	53	100	12	99.90	1.00000
	3	53	100	12	99.90	1.00000
	4	53	100	12	99.90	1.00000
LS 2	1	50	108	12	99.99	1.00000
	2	51	101	10	99.99	1.00000
	3	52	100	12	99.99	0.99973
GLS		51.7	103.1	11.7		

The mean values of the parameters of the local solutions were calculated and shown in Table 4.30 as the global solution. Using the operating conditions ranges shown in overlaid contours and also response optimizer result, 50% was chosen as the optimum condition for motor power, 160 g/min for feed rate and 11 psi for the air fluidising pressure due to the precision control difficulty of the equipment.

4.6. **-75+53 µm size fraction**

In this size fraction, as for the -106+75 µm fraction, fine particles migrated through the air cavity in the bowl due to the geometry limitation of the concentrate bowl. Thus, 50 g -425+300 µm silica was mixed with 50 g -75+53 µm silica were fed before the synthetic ore.

After running 20 experiments, the response variables (grade and recovery) were calculated and listed as shown in Table 4.31.

Table 4.31 Result of concentrate grade and tungsten recovery. MP = Motor power, SFR = Solid feed rate, AFP = Air fluidizing pressure

Run	Variables			Response	
	MP (%)	SFR (g/min)	AFP (psi)	Grade (%W)	Recovery (%)
1	50	163.2	8	7.51	97.00
2	50	196.9	8	7.57	96.70
3	32	107.1	6	8.48	97.80
4	50	203.9	12	7.92	97.50
5	32	217.2	6	8.93	97.10
6	50	207.9	8	7.61	97.70
7	68	167.1	10	7.48	96.90
8	32	232.5	10	9.86	98.10
9	68	265.8	10	7.42	97.00
10	68	161.1	6	7.51	96.40
11	50	100.2	8	7.51	97.00
12	68	247.1	6	7.08	94.10
13	80	195.0	8	7.27	94.50
14	50	205.9	4	7.43	96.40
15	20	192.1	8	9.93	96.10
16	50	203.2	8	7.63	98.00
17	50	202.0	8	7.69	97.90
18	50	192.7	8	7.69	98.00
19	32	145.2	10	9.74	98.10
20	50	204.5	8	7.69	98.10

The model equations produced from coded values of factor levels for the grade (y_1) of the concentrate and recovery (y_2) of the tungsten fraction are presented in Equations (4.11) and (4.12) respectively.

$$y_1 = 7.66 - 0.90x_1 + 0.12x_2 + 0.25x_3 + 0.42x_1^2 + 0.11x_2^2 + 0.06x_3^2 - 0.16x_1x_2 - 0.27x_1x_3 - 0.001x_2x_3 \quad \textbf{(4.11)}$$

$$y_2 = 97.68 - 0.64x_1 - 0.31x_2 + 0.53x_3 - 0.74x_1^2 - 0.31x_2^2 - 0.16x_3^2 - 0.02x_1x_2 + 0.17x_1x_3 + 0.70x_2x_3 \quad \textbf{(4.12)}$$

In order to estimate the significance of the developed models, ANOVA was applied as shown in Table 4.32.

Table 4.32 ANOVA table for grade and recovery

Source	DF	Grade (y_1)				Recovery (y_2)			
		Seq SS	Adj MS	F	P	Seq SS	Adj MS	F	P
Regression	9	14.3314	1.59238	20.14	0.000	19.5562	19.5562	4.77	0.011
Linear	3	11.3877	3.77002	47.69	0.000	9.8405	9.8338	7.20	0.007
x_1 (MP)	1	10.5439	9.99730	126.46	0.000	6.4722	4.9523	10.87	0.008
x_2 (SFR)	1	0.1431	0.05764	0.73	0.413	0.1935	0.4171	0.92	0.361
x_3 (AFP)	1	0.7006	0.69648	8.81	0.014	3.1748	3.1609	6.94	0.025
Square	3	2.4174	0.83344	10.54	0.002	7.5156	7.8403	5.74	0.015
x_1^2 (MP^2)	1	2.3792	2.48387	31.42	0.000	7.1639	7.6124	16.71	0.002
x_2^2 (SFR^2)	1	0.0041	0.04792	0.61	0.454	0.0404	0.4046	0.89	0.368
x_3^2 (AFP^2)	1	0.0341	0.04143	0.52	0.486	0.3112	0.3320	0.73	0.413
Interaction	3	0.5263	0.17544	2.22	0.149	2.2002	2.2002	1.61	0.248
x_1x_2 (MP*SFR)	1	0.1360	0.09528	1.21	0.298	0.0004	0.0015	0.00	0.955
x_1x_3 (MP*AFP)	1	0.3903	0.35898	4.54	0.059	0.6011	0.1512	0.33	0.577
x_2x_3 (SFR*AFP)	1	0.0000	0.00000	0.00	0.995	1.5987	1.5987	3.51	0.091
Residual Error	10	0.7906	0.07906			4.5558	4.5558		
Total	19	15.1220				24.1120			

DF = degrees of freedom, Seq SS = sequential sums of squares, Adj MS = Adjusted mean squares

From Table 4.32, the calculated F-values of grade and recovery can be seen to be 20.14 and 4.77 respectively, both higher than the F value from the F-statistics Table, with P=0.05 ($F_{0.05(9,10)}$=3.14). Accordingly, it can be concluded that the regression models are considered acceptable and fit well. Moreover, the *p*-values (P) of the regression models which are 0.000 for grade and 0.011 for recovery are smaller than 0.05, thus these models are considered suitable for modelling the response behaviours.

The experimental results and the predicted values which were produced using the models (Equations (4.11) and (4.12)) are tabulated in Table 4.33. As can be seen from these results, good agreements between experimental and predicted values are obtained. The R^2 value for the concentrate grade and the tungsten recovery are 95% and 81% respectively. From these values, it can be assumed that a good correlation was obtained, indicating a good fit by the model. The standard deviations of both the predicted models are 0.28 and 0.67 for grade and recovery respectively which are acceptable values.

Table 4.33 Observed and predicted values of grade and recovery

Run	Grade (%W)			Recovery (%)		
	Observed	Predicted	Residual	Observed	Predicted	Residual
1	7.51	7.63	-0.12	97.00	97.76	-0.76
2	7.57	7.66	-0.09	96.70	97.70	-1.00
3	8.48	8.43	0.05	97.80	97.78	0.03
4	7.92	8.25	-0.33	97.50	98.18	-0.68
5	8.93	8.70	0.23	97.10	96.88	0.22
6	7.61	7.68	-0.07	97.70	97.64	0.06
7	7.48	7.26	0.21	96.90	96.54	0.37
8	9.86	9.67	0.20	98.10	97.84	0.26
9	7.42	7.28	0.15	97.00	96.68	0.32
10	7.51	7.31	0.20	96.40	96.05	0.35
11	7.51	7.77	-0.26	97.00	97.32	-0.32
12	7.08	7.26	-0.18	94.10	94.66	-0.56
13	7.27	7.34	-0.07	94.50	94.56	-0.06
14	7.43	7.42	0.01	96.40	96.18	0.22
15	9.93	10.32	-0.39	96.10	96.71	-0.61
16	7.63	7.67	-0.04	98.00	97.67	0.34
17	7.69	7.67	0.02	97.90	97.67	0.23
18	7.69	7.65	0.04	98.00	97.72	0.28
19	9.75	9.31	0.43	98.10	97.22	0.88
20	7.69	7.67	0.02	98.10	97.66	0.44

The normal probability plot of the residuals and the plot of the residuals versus the predicted response for both the concentrate grade and tungsten recovery are presented in Figure 4.26 and Figure 4.27, respectively. Figure 4.26 shows that the residuals generally lie on a straight line, which indicates that errors are distributed normally. From Figure 4.27 it can be seen that the residuals scatter randomly, suggesting that the predictions of the models are adequate.

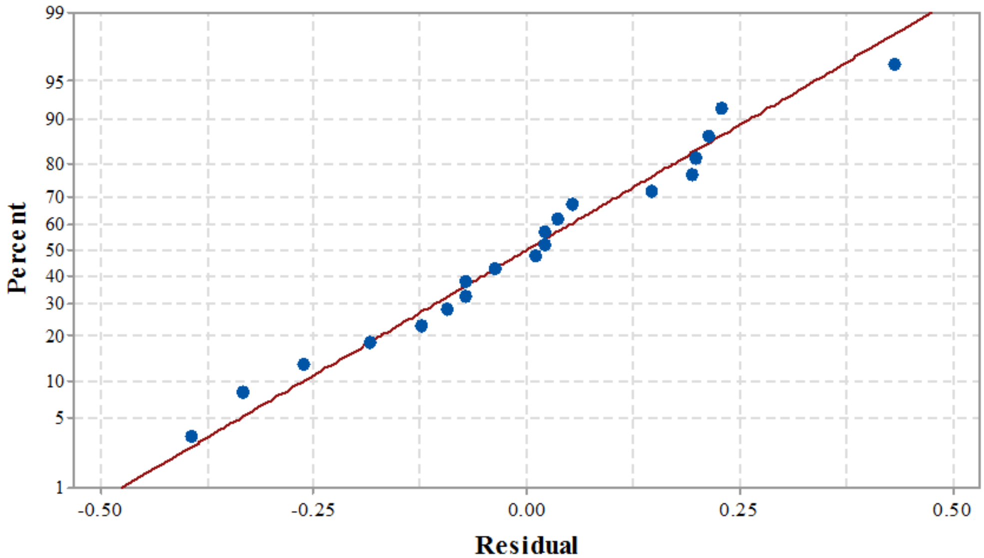

(a) Normal probability plot of residuals for grade

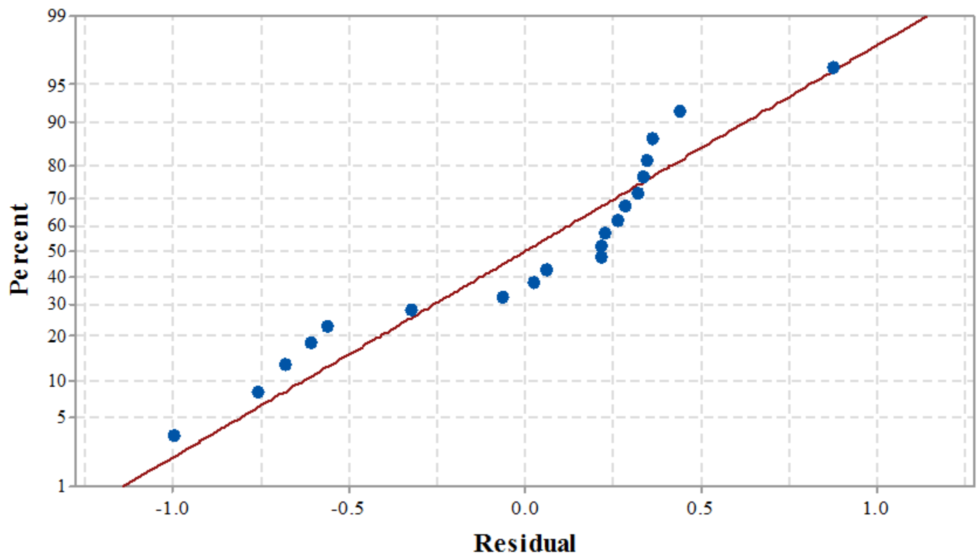

(b) Normal probability plot of residuals for recovery

Figure 4.26 Normal probability plot of residuals for grade (a) and recovery (b) (-75+53 µm)

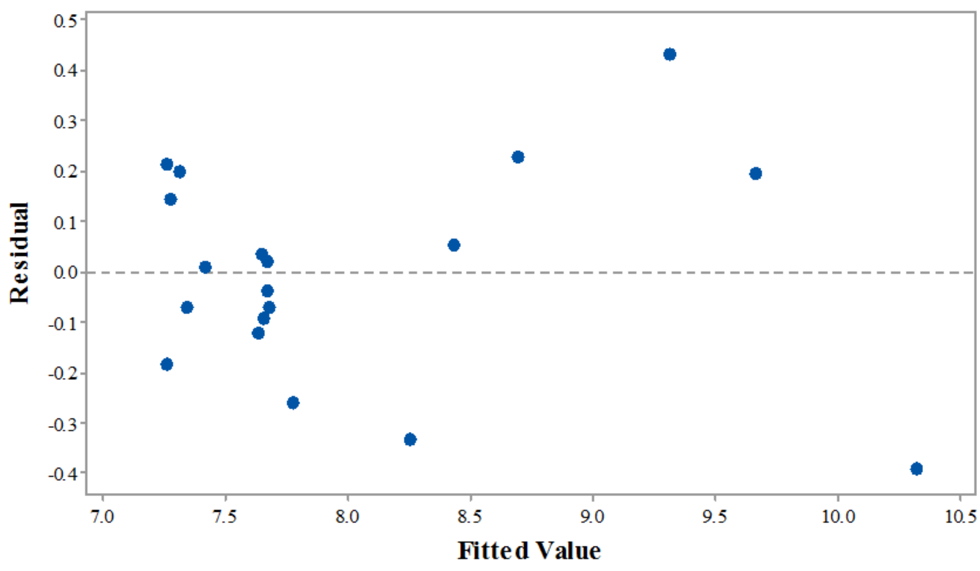

(a) Plot of residuals versus fitted response for grade

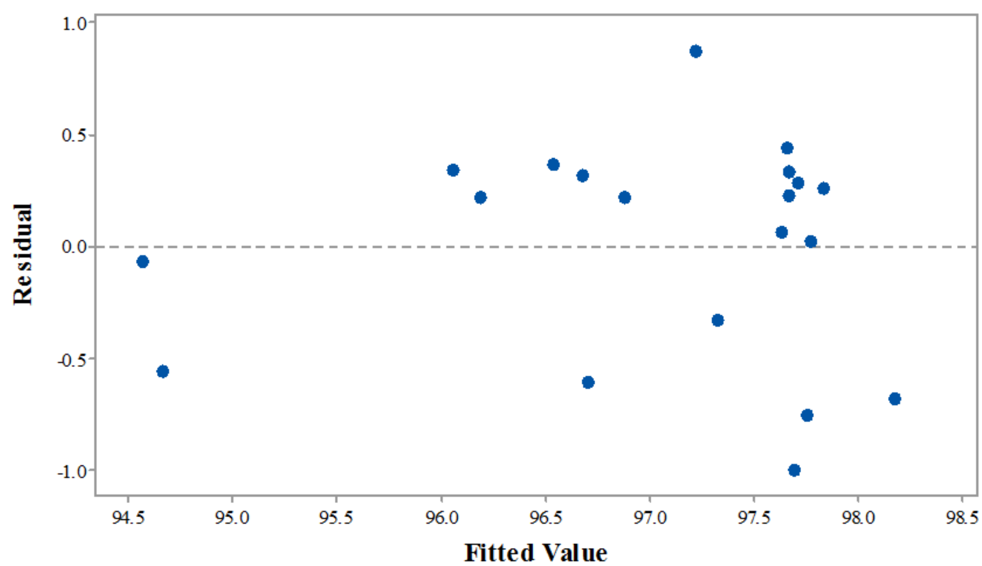

(b) Plot of residuals versus fitted response for recovery

Figure 4.27 Plot of residuals versus predicted response for grade (a) and recovery (b) (-75+53 µm)

In Table 4.34, estimated regression coefficients, factor effects (T) of the models and associated *p*-values (P) for responses are presented.

Table 4.34 Coefficients, factor effects and associated *p*-values for responses

Term	Grade (y_1)			Recovery (y_2)		
	Coef	T	P	Coef	T	P
x_1	-0.905	-11.250	**0.000**	-0.637	-3.300	**0.008**
x_2	0.115	0.850	0.413	-0.310	-0.960	0.361
x_3	0.250	2.970	**0.014**	0.533	2.630	**0.025**
x_1^2	0.420	5.610	**0.000**	-0.735	-4.090	**0.002**
x_2^2	0.107	0.780	0.454	-0.312	-0.940	0.368
x_3^2	0.057	0.720	0.486	-0.160	-0.850	0.413
x_1x_2	-0.164	-1.100	0.298	-0.021	-0.060	0.955
x_1x_3	-0.267	-2.130	0.059	0.173	0.580	0.577
x_2x_3	-0.001	-0.010	0.995	0.702	1.870	0.091

It can be seen that the factor effects (T) of motor power (x_1) for recovery is 3.30, and the sign of the coefficient is negative. This means that the response y (tungsten recovery) was significantly affected by a negative linear effect of motor powers (x_1), with a p-value of 0.008 like the previous size fractions. The response (y) was also affected by a positive linear effect of air fluidizing pressure (x_3) due to the positive coefficient, 2.63 with a p-value of 0.025 like the previous size fractions.

Additionally, T value of the quadratic term of motor power (x_1^2) for recovery is 4.09, and the sign of the values is negative. This means that it has a negative quadratic effect on recovery the same as last size fraction.

In order to obtain a better understanding of the results and for optimization, the predicted models are presented in Figure 4.28 and Figure 4.29 as contour plots.

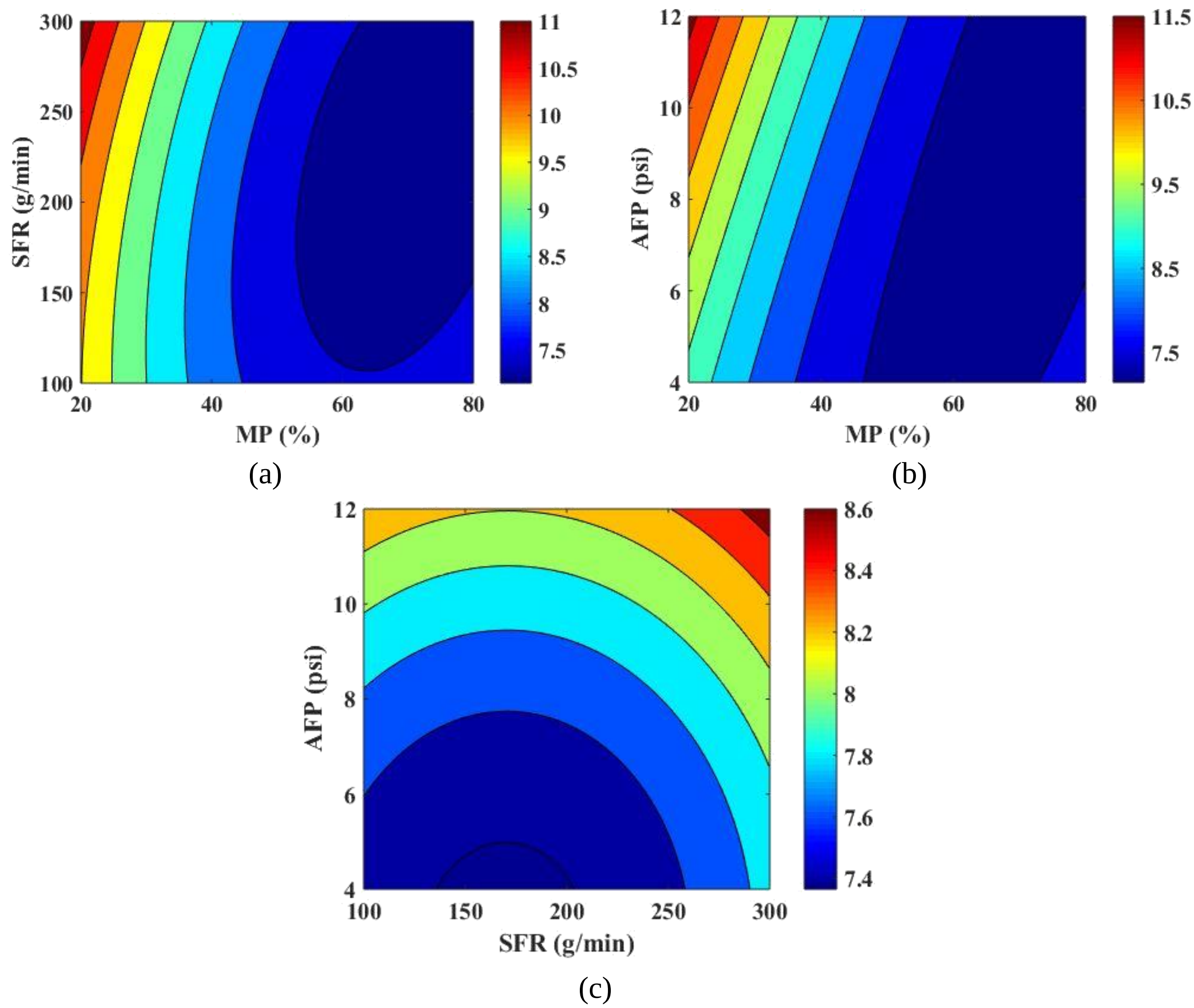

Figure 4.28 Response surface plots for concentrate grade. (a) Motor power and solid feed rate (b) motor power and air fluidizing pressure (c) solid feed rate and air fluidizing pressure (-75+53 µm)

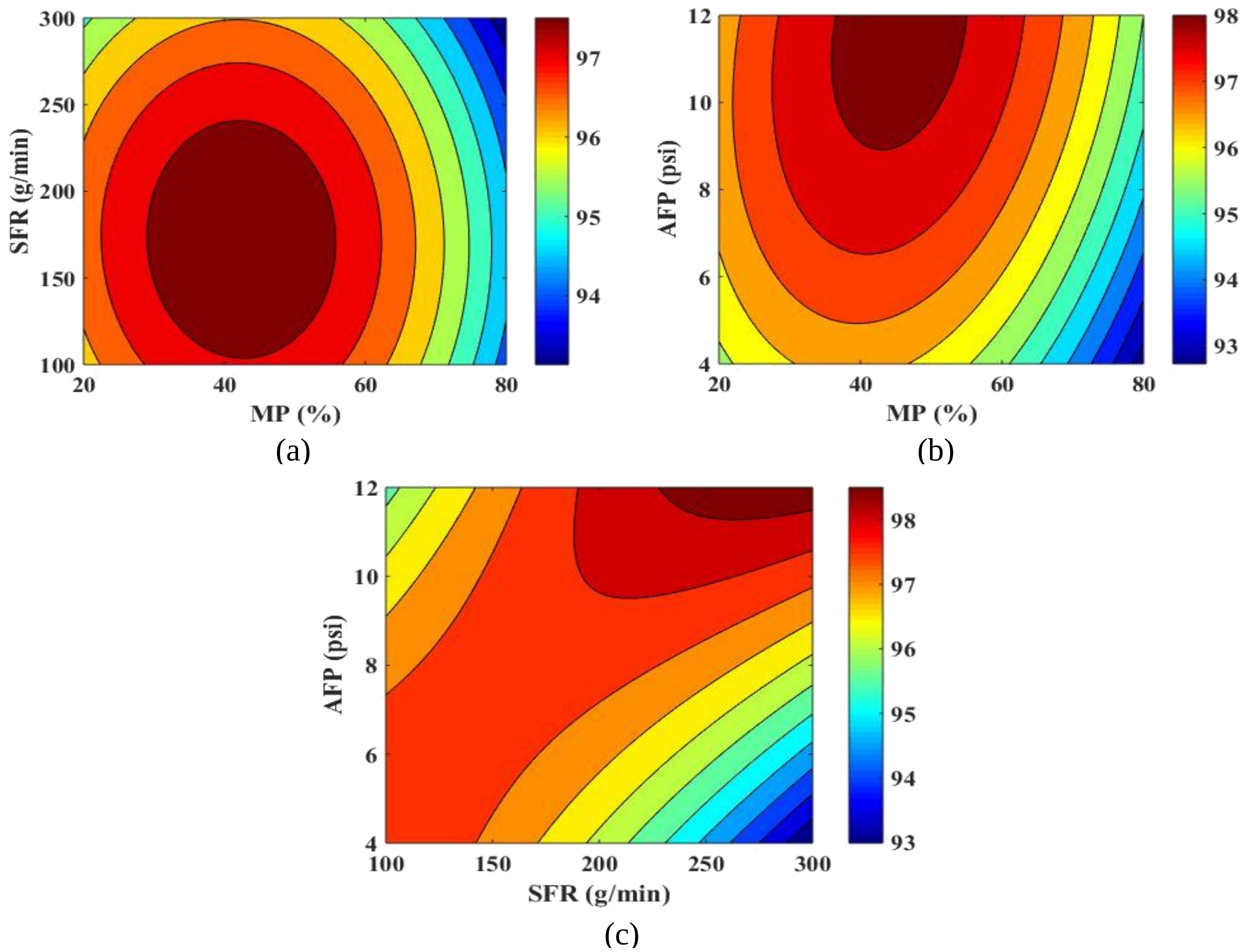

Figure 4.29 Response surface plots for tungsten recovery. (a) Motor power and solid feed rate (b) motor power and air fluidizing pressure (c) solid feed rate and air fluidizing pressure (-75+53 µm)

As seen from Figure 4.28 (a), the concentrate grade is significantly affected by decreasing the motor power. It can be seen that a high grade can be achieved by maintaining the motor power under 35%. The solid feed rate hardly affect the grade. From Figure 4.28 (b), it is observed that the concentrate grade depends more on the motor power than the air fluidizing pressure; to achieve high grade, motor power should be decreased and air pressure should be increased at the same time. In Figure 4.28 (c), high grade is seen to be achieved with high air pressure. The solid feed rate does not affect the grade.

Figure 4.29 (a) shows that the motor power should be between 24-60%, decreasing or increasing the motor, recovery will decrease. Solid feed rate has negligible effect on recovery. From Figure 4.29 (b), for high recovery, motor power should be within 36-53% and the air fluidising pressure should be greater than 9 psi. In Figure 4.29 (c), solid feed rate should be high (>180 g/min) and air fluidising pressure should be high (>9.5 psi) at the same time to achieve high recovery.

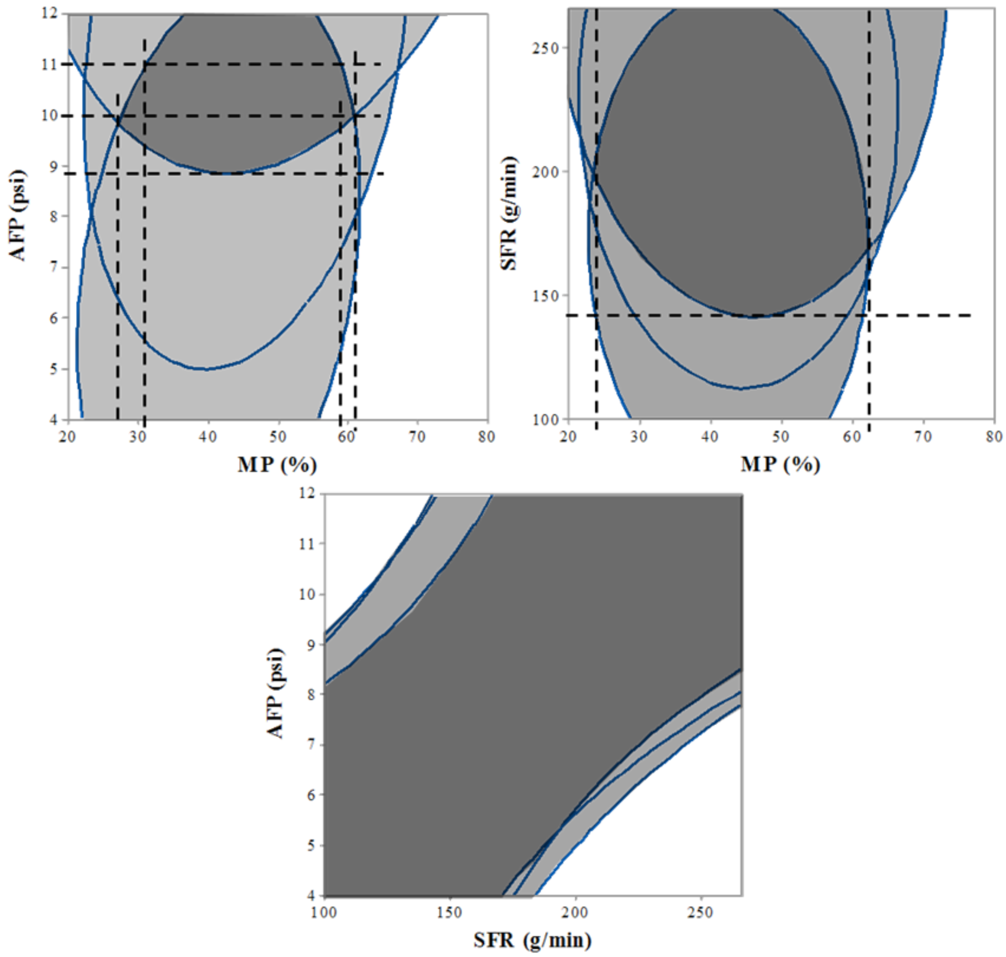

Figure 4.30 Optimum process conditions from overlaid contours (-75+53 µm)

From the overlaid contour plots of MP/AFP in Figure 4.30, high response area requires motor power to be within 27-61%, air fluidising pressure should be between 9 psi and 12 psi. The overlaid plots of MP/SFR shows that motor power should be within 24-62%, while the solid feed rate should above 145 g/min. As for the plots of SFR/AFP, air fluidising pressure has no limits, from 4 to 12 psi. When the motor power decreases, the solid feed rate should decrease as well to assure the high recovery.

For this size fraction, to determine the optimum conditions, the target recovery was set as 98%, which is the maximum value of the predicted model. The solution is 50% for motor power, 200 g/min for solid feed rate and 11 psi for air fluidising pressure. Using the operating conditions ranges shown in overlaid contours and also response optimizer result, 50% was chosen as the optimum condition for motor power, 160 g/min for feed rate and 11 psi for the air fluidising pressure.

4.7. -53 µm size fractions

As for the -53 µm size fraction, 60 g -425+300 µm silica was mixed with 50 g -53 µm silica were fed before the synthetic ore.

After running 20 experiments, the response variables (grade and recovery) were calculated and listed as shown in Table 4.35.

Table 4.35 Result of concentrate grade and tungsten recovery. MP = Motor power, SFR = Solid feed rate, AFP = Air fluidizing pressure

Run	Variables			Response	
	MP (%)	SFR (g/min)	AFP (psi)	Grade (%W)	Recovery (%)
1	50	144.5	8	7.37	92.6
2	50	248.4	8	7.06	87.3
3	32	133.1	6	8.31	88.5
4	50	181.7	12	7.44	89.2
5	32	191.0	6	7.64	85.3
6	50	215.6	8	7.16	90.4
7	68	148.3	10	7.05	95.5
8	32	200.0	10	8.82	86.7
9	68	245.6	10	6.91	93.0
10	68	132.2	6	7.39	91.0
11	50	75.9	8	7.21	91.2
12	68	205.2	6	6.89	90.0
13	80	192.1	8	6.94	89.9
14	50	191.2	4	7.15	90.1
15	20	175.7	8	8.10	78.8
16	50	191.6	8	7.30	90.7
17	50	184.9	8	7.21	90.3
18	50	166.1	8	7.47	91.9
19	32	145.5	10	8.65	82.5
20	50	181.7	8	7.10	87.1

The model equations produced from coded values of factor levels for the grade (y_1) of the concentrate and recovery (y_2) of the tungsten fraction are presented in Equations (4.13) and (4.14) respectively.

$$y_1 = 7.28 - 0.47x_1 - 0.29x_2 + 0.26x_3 + 0.13x_1^2 - 0.12x_2^2 + 0.06x_3^2 + 0.08x_1x_2 - 0.30x_1x_3 + 0.34x_2x_3 \qquad \textbf{(4.13)}$$

$$y_2 = 90.13 + 3.28x_1 - 1.65x_2 + 0.66x_3 - 1.93x_1^2 - 0.54x_2^2 - 0.07x_3^2 - 0.41x_1x_2 + 1.87x_1x_3 + 1.40x_2x_3 \qquad \textbf{(4.14)}$$

In order to estimate the significance of the developed models, ANOVA was applied as shown in Table 4.36

Table 4.36 ANOVA table for grade and recovery

Source	DF	Grade (y_1)				Recovery (y_2)			
		Seq SS	Adj MS	F	P	Seq SS	Adj MS	F	P
Regression	9	5.25	0.58	6.45	0.004	233.213	25.9126	7.07	0.003
Linear	3	4.11	0.96	10.61	0.002	158.537	28.5791	7.79	0.006
x_1 (MP)	1	3.74	1.63	18.05	0.002	149.385	79.3707	21.65	0.001
x_2 (SFR)	1	0.14	0.25	2.81	0.125	8.872	8.2677	2.25	0.164
x_3 (AFP)	1	0.23	0.46	5.12	0.047	0.280	3.0624	0.84	0.382
Square	3	0.51	0.16	1.82	0.208	49.158	16.0582	4.38	0.033
x_1^2 (MP^2)	1	0.40	0.22	2.47	0.147	48.980	46.4538	12.67	0.005
x_2^2 (SFR^2)	1	0.08	0.09	1.04	0.332	0.152	1.9099	0.52	0.487
x_3^2 (AFP^2)	1	0.04	0.04	0.43	0.527	0.025	0.0631	0.02	0.898
Interaction	3	0.63	0.21	2.31	0.138	25.518	8.5060	2.32	0.137
x_1x_2 (MP*SFR)	1	0.00	0.02	0.18	0.678	0.264	0.4625	0.13	0.730
x_1x_3 (MP*AFP)	1	0.38	0.46	5.09	0.048	21.121	18.3189	5.00	0.049
x_2x_3 (SFR*AFP)	1	0.24	0.24	2.69	0.132	4.134	4.1338	1.13	0.313
Residual Error	10	0.90	0.09			36.667	3.6667		
Total	19	6.15				269.880			

DF = degrees of freedom, Seq SS = sequential sums of squares, Adj MS = Adjusted mean squares

From Table 4.36, the calculated F-values of grade and recovery are shown to be 6.45 and 7.07 respectively, both are higher than the F value in the F-statistics Table with P=0.05

($F_{0.05(9,10)}$=3.14). Accordingly, it can be concluded that the regression models are considered acceptable and fit well. Moreover, the *p*-values (P) of the regression models which are 0.004 for grade and 0.003 for recovery are smaller than 0.05, thus these models are considered suitable for modelling the response behaviours.

The quality of the fit of the polynomial model is expressed by R^2 values, which can be calculated using experimental results and the predicted values produced using the models (Equations (4.13) and (4.14)) and are tabulated in Table 4.37. As can be seen from these results, good agreements between experimental and predicted values are obtained. The R^2 value for the concentrate grade and the tungsten recovery are 85% and 86% respectively. The standard deviations of both the predicted models are 0.30 and 1.91 for grade and recovery respectively which are acceptable values.

Table 4.37 Observed and predicted values of grade and recovery

Run	Grade (%W)			Recovery (%)		
	Observed	Predicted	Residual	Observed	Predicted	Residual
1	7.37	7.44	-0.07	92.60	91.20	1.40
2	7.06	6.96	0.10	87.30	88.43	-1.13
3	8.31	8.04	0.27	88.50	87.86	0.64
4	7.44	7.77	-0.33	89.20	90.78	-1.58
5	7.64	7.55	0.09	85.30	86.18	-0.88
6	7.16	7.19	-0.03	90.40	89.66	0.74
7	7.05	6.79	0.27	95.50	93.94	1.56
8	8.82	8.39	0.43	86.70	83.78	2.92
9	6.91	6.93	-0.02	93.00	92.56	0.44
10	7.39	7.42	-0.03	91.00	92.29	-1.29
11	7.21	7.36	-0.14	91.20	91.22	-0.02
12	6.89	6.97	-0.08	90.00	89.00	1.00
13	6.94	6.88	0.06	89.90	90.50	-0.60
14	7.15	7.13	0.03	90.10	89.40	0.70
15	8.10	8.60	-0.50	78.80	79.46	-0.66
16	7.30	7.31	-0.01	90.70	90.35	0.35
17	7.21	7.34	-0.13	90.30	90.52	-0.22
18	7.47	7.40	0.06	91.90	90.90	1.00
19	8.65	8.37	0.28	82.50	83.38	-0.88
20	7.10	7.35	-0.25	87.10	90.59	-3.49

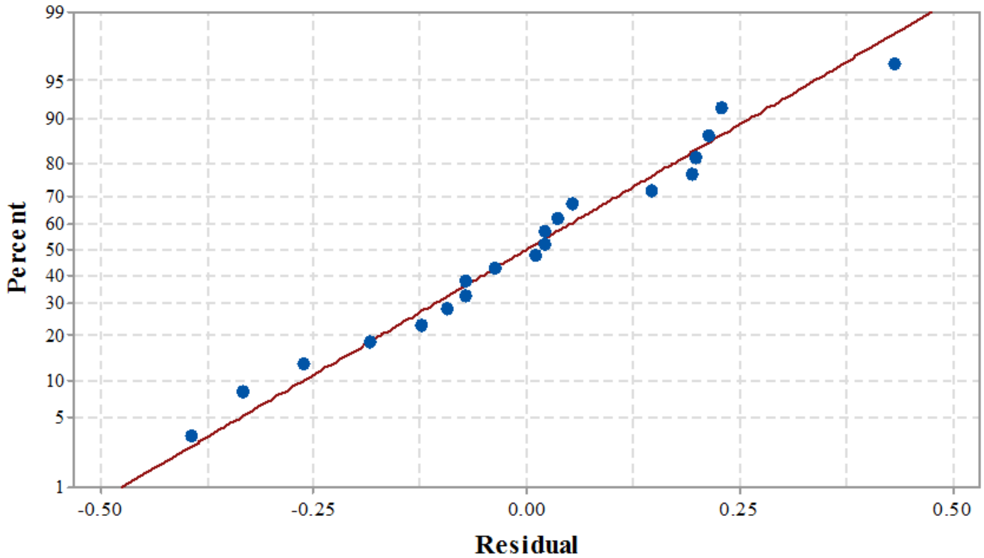

(a) Normal probability plot of residuals for grade

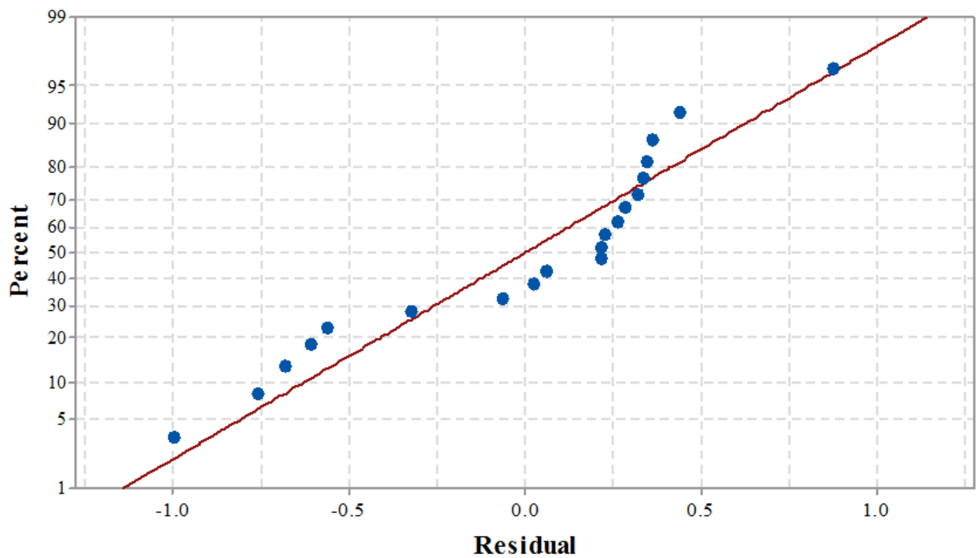

(b) Normal probability plot of residuals for grade

Figure 4.31 Normal probability plot of residuals for grade (a) and recovery (b) (-53 µm)

The normal probability plot of the residuals and the plot of the residuals versus the predicted response for both the concentrate grade and tungsten recovery are presented in Figure 4.31 and Figure 4.32, respectively. Figure 4.31 shows that the residuals generally lie on a straight line, which indicates that errors are distributed normally. From Figure 4.32 it can be seen that the residuals scatter randomly, suggesting that the predictions of the models are adequate.

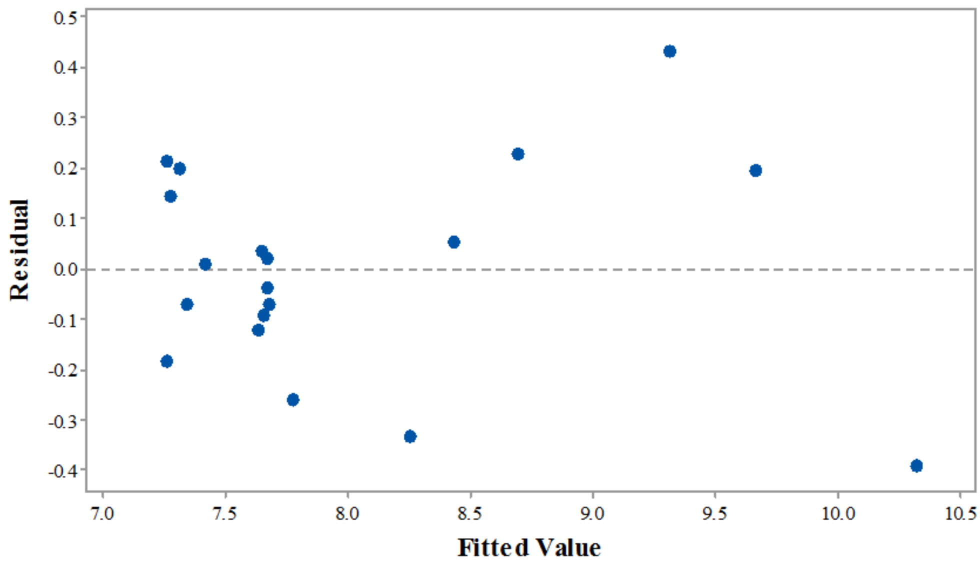

(a) Plot of residuals versus fitted response for grade

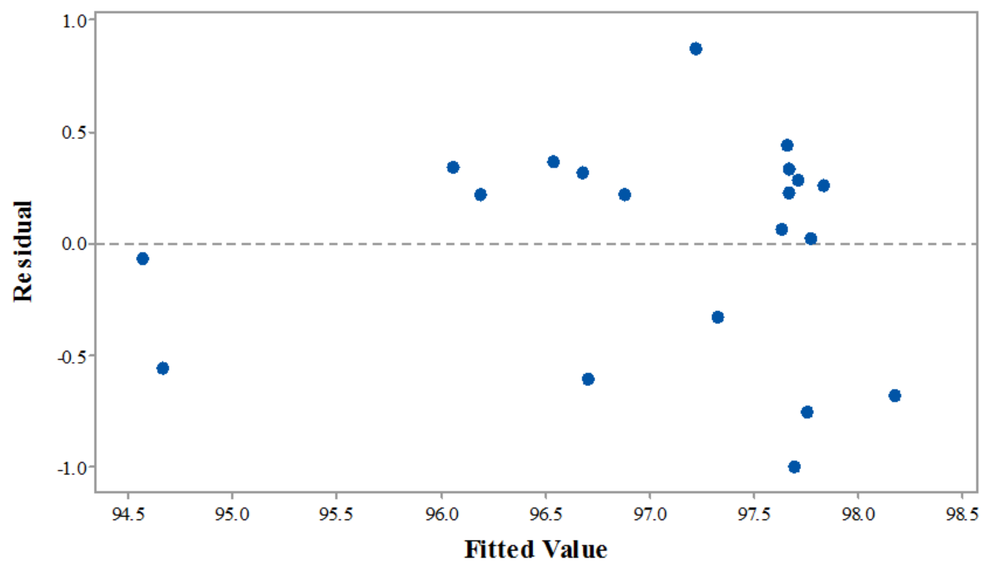

(b) Plot of residuals versus fitted response for grade

Figure 4.32 Plot of residuals versus predicted response for grade (a) and recovery (b) (-53 µm)

In Table 4.38, estimated regression coefficients, factor effects (T) of the models and associated *p*-values (P) for responses are presented.

Table 4.38 Coefficients, factor effects and associated *p*-values for responses

Term	Grade (y_1)			Recovery (y_2)		
	Coef	T	P	Coef	T	P
x_1	-0.471	-4.25	**0.002**	3.283	4.65	**0.001**
x_2	-0.290	-1.68	0.125	-1.65	-1.50	0.164
x_3	0.258	2.26	**0.047**	0.663	0.91	0.382
x_1^2	0.134	1.57	0.147	-1.928	-3.56	**0.005**
x_2^2	-0.12	-1.02	0.332	-0.543	-0.72	0.487
x_3^2	0.056	0.66	0.527	-0.071	-0.13	0.898
x_1x_2	0.078	0.43	0.678	-0.41	-0.36	0.730
x_1x_3	-0.296	-2.26	**0.048**	1.866	2.24	**0.049**
x_2x_3	0.339	1.64	0.132	1.40	1.06	0.313

It can be seen that the factor effects (*T*) of motor power (x_1) for recovery is 4.65, and the sign of the coefficient is positive. This means that the response *y* (tungsten recovery) was significantly affected by a positive linear effect of motor powers (x_1), with a *p*-value of 0.001.

Additionally, *T* value of the quadratic term of motor power (x_1^2) for recovery is 3.56 and the sign of the value is negative, which means that it has a negative quadratic effect on the recovery.

The *T* value of the interaction term of motor power and fluidizing air pressure (x_1x_3) for recovery is 2.24 and the sign of the value is positive. This means that it has a positive interactive effect on the recovery. Positive interaction effect means that an increasing of the factors there will be an increase in the response value.

In order to obtain a better understanding of the results and for optimization, the predicted models are presented in Figure 4.33 and Figure 4.34 as contour plots.

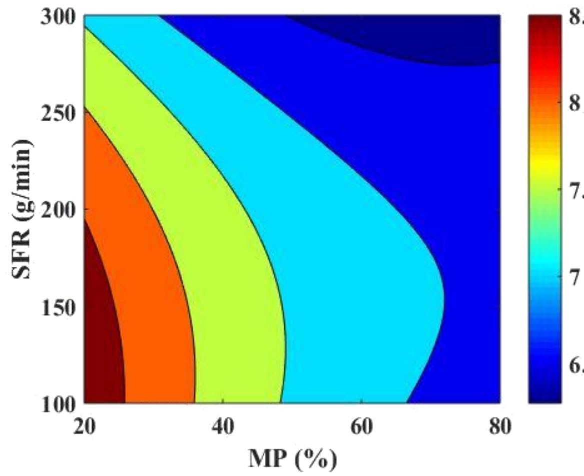

(a)

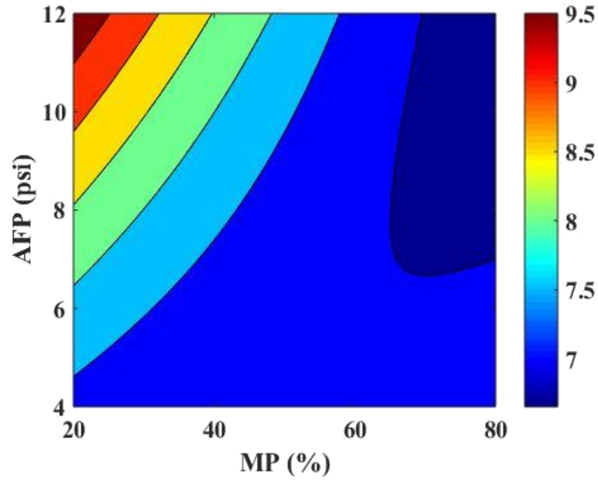

(b)

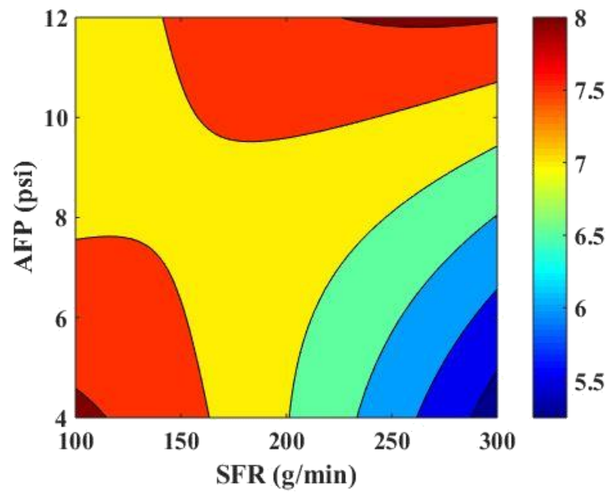

(c)

Figure 4.33 Response surface plots for concentrate grade. (a) Motor power and solid feed rate (b) motor power and air fluidizing pressure (c) solid feed rate and air fluidizing pressure (-53 µm)

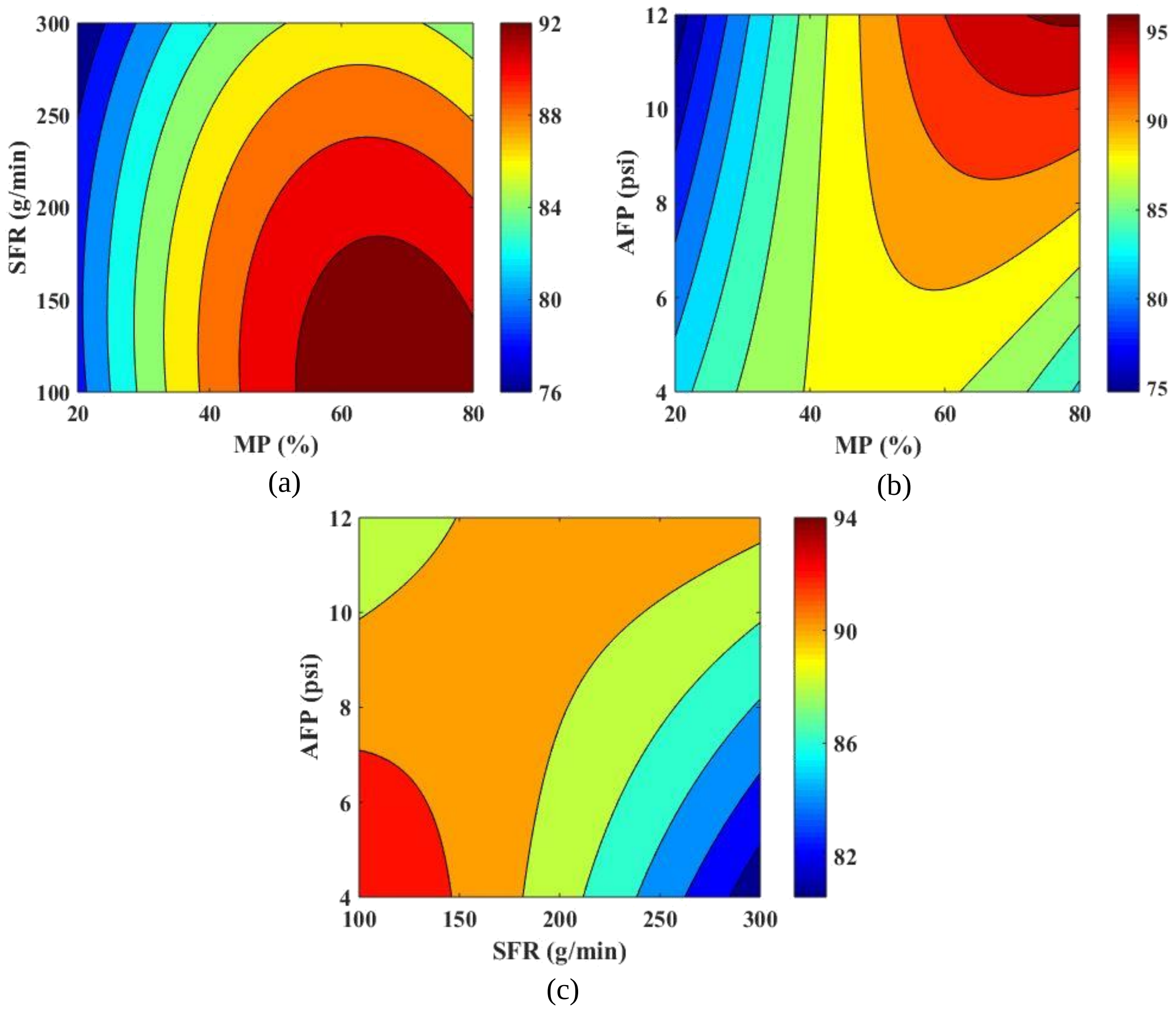

Figure 4.34 Response surface plots for tungsten recovery. (a) Motor power and solid feed rate (b) motor power and air fluidizing pressure (c) solid feed rate and air fluidizing pressure (-53 µm)

As seen from Figure 4.33 (a), the concentrate grade is significantly affected by the motor power. It can also be seen that a high grade can be achieved by decreasing the motor power. Figure 4.33 (b) shows that the concentrate grade increase when the motor power decrease and the air pressure increase at the same time. Figure 4.33 (c) shows that there are two high grade zones from the 3D plot as a result of saddle type surface. One is low pressure with low solid feed rate and the other is high pressure with high solid feed rate.

Figure 4.34 (a) shows that increasing the motor power leads to an increase in recovery increases. The solid feed rate should be under 180 g/min to reach high recovery. In Figure 4.34 (b), the recovery increases with the motor power. The air should be high (>10 psi). From Figure 4.34 (c), both the solid feed rate and the fluidising air pressure affect the recovery. It can be seen that there are two high recovery zones from the 3D plot as a result of saddle type surface. One is low pressure with low solid feed rate and the other is high pressure with high solid feed rate. To get high recovery, solid feed rate should be under 100 g/min and the fluidising air pressure should be smaller than 5 psi or solid feed rate should be greater than 200 g/min and the fluidising air pressure should be higher than 11 psi.

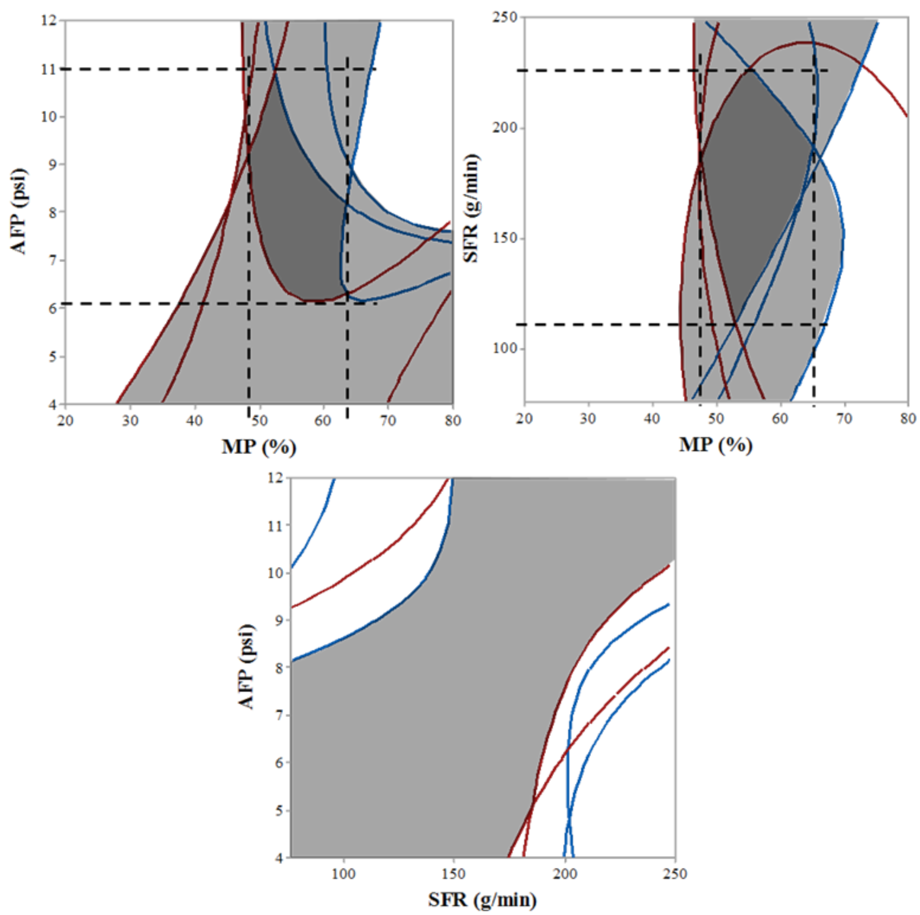

Figure 4.35 Optimum process conditions from overlaid contours (-53 µm)

As seen from the overlaid contour plots of MP/AFP in Figure 4.35, high recovery area requires motor power within 48-63%, air fluidising pressure should be between 6 and 11 psi. The overlaid plots of MP/SFR shows that motor power should be between 47% and 65%, while the solid feed rate should be within 115-225 g/min. As for the plots of SFR/AFP, air fluidising pressure could be high or low to achieve high recovery, when the air fluidising pressure increases, the solid feed rate should increase at the same time.

For this size fraction, target recovery was set as 95%. The solution from the response optimizer is 64.9% for motor power, 248.4 g/min for solid feed rate and 12 psi for air fluidising pressure. Using the operating conditions shown in overlaid contours and also response optimizer result, 65% was chosen as the optimum condition for motor power, 200 g/min for feed rate and 11 psi for the air fluidising pressure.

4.8. **Validation tests**

Due to the fixed volume of the concentrate bowl and the limitation of the fluidising medium, the concentrate grade of the dry Knelson process is not as high as the traditional wet process. To determine the optimum operating conditions for dry process, tungsten recovery will be the primary consideration.

Once the optimum operating conditions for each size fraction were obtained, to confirm the validity of the proposed equations, further experiments were carried out. The validation test for each size fraction was repeated five times. The comparisons between the actual and model predicted data for every size fraction are presented in Table 4.39. The actual values are the mean values of the repeated tests. It can be considered that the proposed equations adequately predict tungsten recovery (error<5%).

Table 4.39 Comparative data at optimum conditions for validation purpose

Size fractions (μm)	Optimum conditions			Validation tests		
	Motor Power (%)	Feed rate (g/min)	Air pressure (psi)	Fitted	Actual	%Error
-425+300				100.0	99.8	-0.2
-300+212	30	200	10	99.7	99.1	-0.6
-212+150				98.7	98.8	0.1
-150+106				100.0	97.0	-3.0
-106+75	50	160	11	99.4	99.1	-0.3
-75+53				97.6	97.5	-0.1
-53	65	200	11	94.2	93.4	-0.9

30% MP= 7.5 G, 50% MP= 34 G, 65% MP= 63 G

It can be seen that some of the mono size fractions have the same optimum operating conditions after the optimization studies, the validation test results show that all mono size fractions could be separated into three size fractions.

4.9. **Discussion**

The size-by-size analysis and the validation tests show very promising results. For most sizes, the recoveries can reach as high as 98%-100%. The recovery decreases when the size goes down to -53 μm, but still above 93%. This is a little bit lower than the traditional wet Knelson process which yields a recovery around 95% in that size fraction (Ling, 1998). Compared to the size-by-size results from the wet Knleson process, dry Knelson process achieves higher recoveries in the coarse sizes, such as -425+300 μm, -300+212 μm and -212+150 μm. The recoveries from wet and dry Knleson process are nearly the same for -150+106 μm, -106+75 μm and -75+53 μm size fractions.

The effects of three variables are discussed follows.

Motor power shows the dominated effect on recoveries regardless of the sizes. The order of importance of the variables can be shown as MP (%) > AFP (psi) > SFR (g/min) from the results above. It also shows that as the particle size decreased the motor power requirement increased which is corresponded well with the traditional wet Knleson process. When the particle size becomes very fine, the efficiency of gravity separation becomes very poor. Therefore, centrifugal forces and fluidization have been introduced to overcome this limitation (Ancia, *et al*., 1997). According to the optimum motor power conditions for different sizes, dry process shows difference from the wet one. For the coarse sizes and middle sizes, dry separating process needs much lower G force than the traditional wet separation with 60 G's. The G force is the same when the size becomes fine (-53 μm).

In this research, air fluidising pressure is higher compared to the previous researches (Greenwood, *et al*., 2013, Kökkılıç *et al*., 2015). It can be seen with lower air pressure, the recoveries are much lower than the optimised results found in this work. Kökkılıç *et al*. (2015) offers the optimised results which shows that the air fluidising pressure reached the upper limit of the pressure ranges. In this research, the range of air fluidising pressure was enlarged to make better investigation. The optimised air fluidising pressures for all size fractions are with the range which shows that the new range is more reasonable and acceptable; higher air fluidising pressure is necessary for higher recovery. There is not big change in air fluidising pressure for different sizes from 10 to 11 psi. However, the fluidising water changes a lot in wet process (Ling, 1998). High water velocity is required with coarse feeds while low water velocity is needed for fine sizes.

Solid feed rate does not show any effect until the particle size become fine. For the coarse sizes (-425+300 µm, -300+212 µm and -212+150 µm), the solid feed rate has no effect on recovery, the optimised solid feed rate was chosen as the middle of the range which is 200 g/min. Although solid feed rate shows its effect on fine size fractions, the influence is very limited. For the middle sizes (-150+106 µm, -106+75 µm and -75+53 µm), the solid feed rates are required within a lower range to ensure high recoveries (>98%). However, higher solid feed rate is also acceptable when the high recovery standard changes. According to the predications by using the models, 160 g/min is the highest solid feed rate within the range from overlaid contours which is ideal for all these size fractions to yield highest recovery. For the -53 µm, the solid feed rate still needs to be low compared to the coarse sizes. But with different trials of optimization study, there is not much difference between the recoveries within the feed rate range. Then the upper limit of the range was chosen as the optimized solid feed rate for this size fraction due to the economic consideration. Solid feed rate for dry process is much lower compared to the wet process. Especially when the feed size becomes fine, lower solid feed rate is needed to guarantee the high tungsten recovery.

Although the dry Knelson tests show great results, we still met some problems during the process.

The geometry limitation of the concentrate bowl cause a problem when feeding the fine particles. In this work, an artificial fluidised bed was created by feeding some coarse silica particles, thus preventing the fine particles from migrating through the holes in the concentrate bowl. But the coarse silica particles may replace the position of some fine tungsten particles, which will influence the actual recovery. There are two other possible solutions. First, making a concentrate bowl with smaller water cavity on the bowl. Second, wrapping a screen on the bowl to decrease the water cavity diameter.

Since the concentrating bowl has a fixed volume (62 cm^3) and according to the experimental studies, it will contain 100~150 g material (mostly silica) and the feed is only 1 kg with 10 grams tungsten (1% w/w) for each test, so the grades will be around 7-10% even with 100% recovery. Therefore, the grade is not taken into consideration for the optimization study. In gold processing, the main aim with gravity processing is to recover as much GRG as possible. To increase the concentrate grade, a simple way is to increase the mass of feed. 4 kg synthetic feed with 1% tungsten grade was used according to the wet Knleson process.

There is also a problem when feeding the very fine particles (-53 μm). The feed hardly flows, they tend to stay in the feeder. During the test, a long stick is required to stir the feed to avoid the stuck in the feed tube. It is difficult to adjust the feed rate with the fine size fraction. A lot of work need to be done to solve this problem.

The validation tests show the possibility to separate the mono size fractions into three ranges since they have same optimum conditions. Combining data for different sizes will only make sense for certain conditions since the recoveries differ a lot depending on conditions and sizes. Therefore, the validity of separating these size fractions into coarse, middle and fine sizes will be one of the future works.

CHAPTER 5: CONCLUSIONS

Response surface method of experimental design was used to examine the effect of motor power (%), solid feed rate (g/min) and air fluidizing pressure (psi) on the concentrate grade and tungsten recovery for a dry separation in a Knelson Concentrator size-by-size.

The main conclusions are as follows:

The empirical regression equations as a function of the independent process variables were derived by the RSM model for the concentrate grade and tungsten recovery.

The analysis of the variance showed that the calculated *F*-values of grade and recovery for each size fraction is higher than the *F* value founded from the *F*-statistics Table with P=0.05 ($F_{0.05(9,10)}$=3.14), and the regression models are considered acceptable and fit well.

The regression models for each size fraction have *p*-values less than 0.004 and 0.011 for concentrate grade and tungsten recovery respectively, thus the selected models are significant for the responses.

For -425+300 µm, -300+212 µm and -212+150 µm size fractions, motor power is the most important factor affected concentrate grade and recovery followed with the effect of air fluidising pressure. The solid feed rate affects the concentrate grade and tungsten recovery to a minimal extent for these size fractions. High concentrate grade and tungsten recovery could be achieved with low motor power and high air fluidising pressure.

For -150+106 µm, -106+75 µm and -75+53 µm size fractions, the solid feed rate starts to show an effect on the responses. Low solid feed rate will be required to get high concentrate grade and tungsten recovery. Motor power and air fluidising pressure still affect the responses significantly. Compared to the coarse size fractions, these finer sizes need higher motor power and higher air fluidising pressure to maximize the responses.

For the -53 µm size fraction, the solid feed rate behaves similar to the coarse sizes. High motor power and air fluidising pressure are required for maximum responses.

For all feed sizes studied, when the feed is fine, a higher motor power was needed to achieve a maximum recovery which corresponds well with the traditional wet process. It was observed that the maximum tungsten recovery drops significantly when the feed size becomes fine (<53 μm) compared to the coarse sizes.

Due to the fact that some of the mono size fractions have the same optimum operating conditions after the optimization studies, the validations test results show that all mono size fractions could be separated into three size fractions: -425+300 μm, -300+212 μm and -212+150 μm are considered to be one mono size coarse fraction; -150+106 μm, -106+75 μm and -75+53 μm are considered to be one mono size middle fraction; and -53 μm is considered to be the fine size fraction.

Surface plots confirmed that lower motor power (<30%) with high pressure (>10 psi) resulted in high recovery for coarse size fraction; for middle size fraction, higher motor power (>50%) with high pressure (>11 psi) is needed; and for fine size fraction, highest motor power (>60%) with high pressure (>11 psi) is necessary.

From the optimization studies, it can be found that the optimized values for the concentration with the highest recovery of motor power, solid feed rate and air fluidizing pressure are 30%, 200 g/min and 10 psi, respectively for coarse size fraction; for middle size fraction, the optimized values for the concentration with the highest recovery of motor power, solid feed rate and air fluidizing pressure are 50%, 160 g/min and 11 psi; for fine size fraction, the optimized values for the concentration with the highest recovery of motor power, solid feed rate and air fluidizing pressure are 65%, 200 g/min and 11 psi.

For the future work, dry Knelson process with lower grade synthetic ore feed will be investigated. It is also important to look forward to the behaviour of dry Knleson with lower density material, such as magnetite mixed with quartz.

In addition, the potential of dry Knleson with three mineral system feed comprised of tungsten, magnetite and quartz, will be investigated. Further on in this research, a standard GRG test will also be carried out under dry conditions, and compared to the standard GRG test.

REFERENCES

Agricola G., 1956. De Re Metallica. Dover Publications Inc, New York.

Appleyard, K.C., 1931. Dry cleaning of coal in England. Transactions of the American Institute of Mining and Metallurgical Engineers, 94, 235–266.

Arms, R.W., 1924. Dry cleaning of coal. Transactions of the American Institute of Mining and Metallurgical Engineers, 70, 758–774.

Aslan, N., 2007. Modelling and optimization of Multi Gravity Separator to produce celestite concentrate, Powder Technology, 174, 127-133.

Aslan, N., 2008. Application of response surface methodology and central composite rotatable design for modelling and optimization of a multi-gravity separator for chromite concentration, Powder Technology, 185, 80-86.

Axelsson, H., Madsen, B., 2008. Centrifuges, Sedimentation, Alfa Laval Separation AB, Sweden. www.alfalaval.com.

Beniuk, V.G., C.A. Vadeikis and J.N. Enraght-Moony, 1994. Centrifugal Jigging at Gravity Concentrates and Tailings at Renison Limited, Minerals Engineering, 7, 577-589

Boylu, F., 2013. Modelling and optimisation of ageing characteristics of soda activated Na^+ bentonites, Applied Clay Science, 83-84, 300-307.

Boylu, F., 2014. Effect of fluidizing characteristics on upgrading of lignitic coal in gravity based air jig, International Journal of Mineral Processing, 129, 27-35.

Brewis, T., 1995. Gravity separation, Mining Magazine, 5, 279-292.

Burt, R.O., 1984. Gravity Concentration Technology. Elsevier Science Publishers B.V. pp. 80–107 and 352–372.

Burt, R.O., Korinek, G., Young, S.R., Deveau, C., 1995. Ultrafine tantalum recovery strategies, Minerals Engineering, 8 (8), 859-870.

Campatelli, G., Lorenzini, L., Scippaet, A., 2014. Optimization of process parameters using a Response Surface Method for minimizing power consumption in the milling of carbon steel, Journal of Cleaner Production, 66, 309-316.

Canning, E., 1980. Dry mineral sand separation plants of associated mineral consolidated Ltd., New South Wales and Queensland. Australasian Mining and Metallurgical Operating Practices, 10, 758–761.

Cavalcante, K.S.B., Penha, M.N.C., Mendonça, K.K.M., Louzeiro, H.C., Vasconcelos, A.C.S., Maciel, A.P., de Souza, A.G., Silva, F.C., 2010. Optimization of transesterification of castor oil with ethanol using a central composite rotatable design (CCRD), Fuel, 89, 1172-1176.

Chan, S.K., Mozley, R.H., Childs, G.J.C., 1991. Extended trials with the high tonnage multi-gravity separator. Minerals Engineering, 4 (3–4), 489–496.

Chen, Y., Parlar, H., 2013. Enrichment behavior of immunoglobulin by foam fractionation using response surface methodology, Separation and Purification Technology, 107, 102-108.

Coulter, T., Subasinghe, G.K.N., 2005. A mechanistic approach to modelling Knelson concentrators, Minerals Engineering, 18, 9-17.

Crozier, R.D., 1992. Flotation Theory, Reagents and Ore Testing. Pergamon Press, New York.

Djoudi, W., Aissani-Benissad, F., Bourouina-Bacha, S., 2007. Optimization of copper cementation process by iron using central composite design experiments, Chemical Engineering Journal, 133, 1-6.

Dodbiba, G., Haruki, N., Shibayama, A., Miyazaki, T., Fujita, T., 2002. Combination of sink–float separation and flotation technique for purification of shredded PET-bottle from PE or PP flakes. International Journal of Mineral Processing. 65, 11–29.

Dodbiba, G., Fujita, T., 2015. Progress in Filtration and Separation, Chapter 12 – Air tabling, 527-555.

Dwari, R.K., Rao, K.H., 2007. Dry beneficiation of coal - a review, Mineral Processing and Extractive Metallurgy Review, 28, 177-234.

El-Midany, A.A., Ibrahim, S.S., 2011. Does calcite content affect its separation from celestite by Falcon concentrator? Powder Technology, 213 (1-3), 41-47.

Falconer, A., 2003. Gravity separation – old technique/new methods. Physical Separation in Science and Engineering, 12 (1), 31–48.

Fisher, R. A., 1966. The design of experiments, Eighth ed. Oliver and Boyd, Edinburgh.

Franks, G.V., Firdaus, M., Oshitani, J., 2013. Copper ore density separations by float/sink in a dry sand fluidised bed dense medium, International Journal of Mineral Processing, 121, 12–20.

Greenwood, M., Langlois, R., Waters, K.E., 2013. The potential for dry processing using a Knelson Concentrator, Minerals Engineering, 45, 44–46.

Gunaraj, V., Murugan, N., 1999. Application of response surface methodology for predicting weld bead quality in submerged arc welding of pipes, Journal of Materials Processing Technology, 88, 266-275.

Haldar, S.K., 2013. Mineral Exploration Principles and Applications, Chapter 12–Mineral Processing, 223-250.

Hamzah, M.O., Golchin, B., Tye, C.T., 2013. Determination of the optimum binder content of warm mix asphalt incorporating Rediset using response surface method, Construction and Building Materials, 47, 1328-1336.

Honaker, R.Q., Wang, D., Ho, K., 1996. Application of the Falcon concentrator for fine coal cleaning, Mineral Engineering, 9 (11), 1143-56.

Hudson, S.B., 1962. Air tabling of beach sand non-conductors for zircon recovery. Proceedings - Australasian Institute of Mining and Metallurgy. 204, 81–108.

Jaman, W., 1985. Pneumatic concentration. In: Weiss, N.L. (Ed.), SME Mineral Processing Handbook. Published Society of Mining Engineers. 4 (7), 4-51 to 4-52.

Kincl, M., Turk, S., Vrecer, F., 2005. Application of experimental design methodology in development and optimization of drug release method, International Journal of Pharmaceutics, 291, 39-49.

Knapp, E.A., 1953. Concentrating Ores by Pneumatic Tables. Recent Development in Mineral Dressing. A symposium arranged by IMM, held on September 23–25, 1952 at the Huxley building, Imperial College of science and technology, London, 299–311.

Knelson, B., 1992. The Knelson concentrator: Metamorphosis from crude beginning to sophisticated worldwide acceptance, Minerals Engineering, 5 (10-12), 1091-1097.

Knelson, B., Edwards, R., 1990. Development and economic application of Knelson concentrator in low grade alluvial gold deposits, The AusIMM Annual Conference, Rotorua, New Zeeland, March 18-21, 123-128.

Kökkılıç. O., Langlois, R., Waters, K.E., 2015. A design of experiments investigation into dry separation using a Knelson Concentrator, Minerals Engineering, 72, 73–86

Kroll-Rabotin, J., Bourgeois, F., Climent, E., 2010. Fluid dynamics based modelling of the Falcon concentrator for ultrafine particle beneficiation, Minerals Engineering, 23, 313–320.

Laplante, A.R., 1993. A Comparative Study of Two Centrifugal Concentrators, Proceedings of 24th Annual Meeting of Canadian Mineral Processors, Ottawa, Paper No. 5.

Laplante, A.R., Huang, L., Harris, B.G., 1999. The Upgrading of Primary Gold Gravity Concentrates, Proceedings of 31th Annual Meeting of Canadian Mineral Processors, Ottawa, 211-226.

Laplante, A.R., Huang, L., Noaparast, M., Nickoletopoulos, N., 1995. A philosopher's stone: Turning tungsten and lead into gold-The use of synthetic ores to study gold gravity separation, Proceedings of 27th Annual Meeting of Canadian Mineral Processors, Ottawa, 379-394.

Laplante, A.R., Nickoletopoulos, N., 1997. Validation of a Falcon model with a synthetic ore, Canadian Metallurgical Quarterly, 36 (1) 7-13.

Laplante, A.R., Spiller, D.E., 2002. Bench-scale & Pilot plant testwork for gravity concentration circuit design, Society for Mining, Metallurgy and Exploration Inc., Mineral Processing Plant Design, Practice, and Control Proceedings, 1, 160-175.

Laplante, A.R., Woodcock, F., Noaparast, M., 1995. Predicting gravity separation gold recovery, Minerals and Metallurgical Processing, 74-49.

Laplante, A.R., Dunne, R., 2002. The gravity-recoverable gold test and flash flotation, Proceedings of the 34th Annual Meeting of Canadian Mineral Processors, Ottawa. Canadian Institute of Mining, Metallurgy and Petroleum, Montréal, paper 7, 105–124.

Lazarkiewicz, S., and Troskolanski, A.T., 1965. Impeller pumps, Pergamon press, Oxford, New York, 7-9.

Ling, J., 1998. A study of a variable speed 3-in Knelson Concentrator, Ph.D. Thesis, Department of Mining and Metallurgical Engineering, McGill University, Montreal.

Lins, F.F., Veiga, M.M., Stewart, J.A., Papalia, A., Papalia, R., 1992. Performance of new centrifuge (Falcon) in concentrating a gold ore from Texada Island, B.C., Canada, Minerals Engineering, 5 (10-12), 1113-1121.

Llewellyn, R.L., 1977. Pneumatic Cleaning of Fine Coal for Sulfur Reduction, 3rd Symposium on Coal Preparation, NCA/BCR conference, October 1977, 123–136.

Lockhart, N.C., 1984. Powder Technology, 40, 17–42.

Louis, H., 1894. A Handbook of Gold Milling, London: Macmillan and Co., 319-320.

MacPherson, S.A., Galvin, K.P., 2010. The effect of vibration on dry coal beneficiation in the reflux classifier, International Journal of Coal Preparation and Utilization, 30, 283–294.

MacPherson, S.A., Iveson, S.M., Galvin, K.P., 2010. Density based separations in the Reflux Classifier with an air–sand dense–medium and vibration, Minerals Engineering, 23, 74-82.

MacPherson, S.A., Iveson, S.M., Galvin, K.P., 2011. Density-based separation in a vibrated Reflux Classifier with an air-sand dense-medium: Tracer studies with simultaneous underflow and overflow removal, Minerals Engineering, 24, 1046-1052.

Mak, C., Choung, J., Beauchamp, R., Kelly, D.J.A., Xu, Z., 2008. Potential of air dense medium fluidized bed separation of mineral matter for mercury rejection from Alberta sub-bituminous coal, International Journal of Coal Preparation and Utilization, 28, 115-132.

Montgomery, D.C., 2004. Design and analysis of experiments, Fifth ed. John Wiley and Sons, New Jersey.

Montgomery, D.C., 2009. Design and analysis of experiments, Seventh ed. John Wiley and Sons, New Jersey.

Oruç, F., Özgen, S., Sabah, E., 2010. An enhanced-gravity method to recover ultra-fine coal from tailings: Falcon Concentrator, Fuel, 89, 2433-2437.

Osborn, W.X., 1927. Tabling tungsten ore without water, Engineering and Mining Journal. 123 (7), 287–289.

Oshitani, J., Franks, G.V., Griffin, M., 2010. Dry dense medium separation of iron ore using a gas–solid fluidized bed, Advanced Powder Technology, 21, 573-577.

Oshitani, J., Kajimoto, S., Yoshida, M., Franks, G.V., Kubo, Y., Nakatsukasa, S., 2013a. Continuous float/sink density separation of lump iron ore using a dry sand fluidized bed dense medium, Advanced Powder Technology, 24, 468-472.

Oshitani, J., Kawahito, T., Yoshida, M., Gotoh, K., Franks, G.V., 2011. The influence of the density of a gas–solid fluidized bed on the dry dense medium separation of lump iron ore, Minerals Engineering, 24, 70-76.

Oshitani, J., Ohnishi, M., Yoshida, M., Franks, G.V., Kubo, Y., Nakatsukasa, S., 2013b. Dry separation of particulate iron ore using density-segregation in a gas-solid fluidized bed, Advanced Powder Technology, 24, 554-559.

Popa, O., Babeanu, N., Vamanu, A., Vamanu, E., 2007. The utilization of the response surface methodology for the optimization of cultivation medium and growth parameters in the cultivation of the yeast strain S. cerevisiae 3.20 on ethanol, African Journal of Biotechnology, 6 (23), 2700-2707.

Rose, T.K., 1898. The Metallurgy of gold. London: Charles Griffin and Company, Limited, 183-184.

Ryan, T.P., 2007. Modern experimental design. John Wiley and Sons, New Jersey.

Sahu, A.K., Biswal, S.K., Parida, A., 2009. Development of Air Dense Medium Fluidized Bed Technology For Dry Beneficiation of Coal - A Review, International Journal of Coal Preparation and Utilization, 29, 216-241.

Sampaio, C.H., Aliagaa, W., Pachecoa, E.T., Pettera, E., Wotrubab, H., 2008. Coal beneficiation of Candiota mine by dry jigging, Fuel Processing Technology, 89, 198-202.

Singh, R.K., Das, A., 2013. Analysis of separation response of Kelsey centrifugal jig in processing fine coal, Fuel Processing Technology, 115, 71-78

Sivamohan, R., Forssberg, E., 1985. Principle of tabling, International Journal of Mineral Processing, 15, 281–295.

Söderlund, J. and Johansson, B., 2005. Knelson Concentrator - New Gravity Equipment at the Boliden Concentrator, (http://www.flsmidth.com/~/media/PDF%20Files/FLSmidth%20Knelson/Papers/20051104BolidenMineralABTechnicalPaper.ashx)

Taggart, A.F., 1945. Handbook of Mineral Processing, 11-136.

Torrades, F., Saiz, S., García-Hortal, J.A., 2011. Using central composite experimental design to optimize the degradation of black liquor by Fenton reagent, Desalination, 268, 97-102.

Traore, A., Conil, P., Houot, R., and Save, M., 1995. An evaluation of the Mozley MGS for fine particle gravity separation, Minerals Engineering, 8 (7), 767-778.

Tripathy, S.K., Murthy, Y.R., 2012. Modeling and optimization of spiral concentrator for separation of ultrafine chromite, Powder Technology, 221, 387-394.

Truscott, S.J., 1923. A Text-book of Ore Dressing. Macmillan and Co. Ltd., 570–590.

Tucker, P., 1995. Modeling the Kelsey centrifugal jig, Minerals Engineering, 8, 333-336.

Turner, J.F., 1991. Gravity Concentration, Past, Present and Future, Minerals Engineering, 4, 213-223.

Wang, Q., Lu, J., Yin, W., Yang, H., Wei, L., 2013. Numerical study of gas–solid flow in a coal beneficiation fluidized bed using kinetic theory of granular flow, Fuel Processing Technology, 111, 29-41.

Wills, B.A., Atkinson K., 1991. The development of minerals engineering in the 20th century, Minerals Engineering, 4 (7-11), 643–652

Wills, B.A., Finch, J., 2016. Mineral Processing Technology, Eighth ed. Elsevier, Boston.

Wyslouzil, H.E., 1990. Evaluation of the Kelsey Centrifugal Jig at Rio Kemptville Tin, Proceedings of 22nd Annual Meeting of the Canadian Mineral Processors, CIM, 461-472.

Yang, X., Zhao, Y., Luo, Z., Song, S., Chen, Z., 2013. Fine coal dry beneficiation using autogenous medium in a vibrated fluidized bed, International Journal of Mineral Processing, 125, 86-91.